

7-2015

# Peptoid-Based KLVFF Mimics: A Unique Approach to Alzheimer's Disease

James Phillip Turner

*University of Arkansas, Fayetteville*

Follow this and additional works at: <http://scholarworks.uark.edu/etd>



Part of the [Biochemical and Biomolecular Engineering Commons](#)

---

## Recommended Citation

Turner, James Phillip, "Peptoid-Based KLVFF Mimics: A Unique Approach to Alzheimer's Disease" (2015). *Theses and Dissertations*. 1255.

<http://scholarworks.uark.edu/etd/1255>

This Dissertation is brought to you for free and open access by ScholarWorks@UARK. It has been accepted for inclusion in Theses and Dissertations by an authorized administrator of ScholarWorks@UARK. For more information, please contact [scholar@uark.edu](mailto:scholar@uark.edu), [ccmiddle@uark.edu](mailto:ccmiddle@uark.edu).

Peptoid-Based KLVFF Mimics: A Unique Approach to Alzheimer's Disease

Peptoid-Based KLVFF Mimics: A Unique Approach to Alzheimer's Disease

A dissertation submitted in partial fulfillment  
of the requirements for the degree of  
Doctorate of Philosophy in Chemical Engineering

by

James Phillip Turner  
University of Arkansas  
Bachelor of Science in Chemical Engineering, 2010

July 2015  
University of Arkansas

This dissertation is approved for recommendation to the Graduate Council.

---

Dr. Shannon Servoss  
Dissertation Director

---

Dr. Robert Beitle  
Committee Member

---

Dr. Christa Hestekin  
Committee Member

---

Dr. Suresh Kumar Thallapuranam  
Committee Member

---

Dr. Kartik Balachandran  
Committee Member

©2015 by James Phillip Turner  
All Rights Reserved

## **ABSTRACT**

Alzheimer's disease (AD) is the leading form of dementia worldwide. AD patients experience a slow, gradual cognitive decline that includes loss of memory and behavioral stability as the disease progresses. Surprisingly, AD is the sixth leading cause of death in the United States and has had a profound impact on the U.S. economy. Though there are medications to help improve the quality of life of diagnosed patients for a period of time, there is still no cure for AD. AD is characterized by the build-up of amyloid plaques that develop from the aggregation of the amyloid beta protein ( $A\beta$ ) in the body. Current treatment options for AD has been the development of compounds that can target and either inhibit or modulate the formation of  $A\beta$  aggregates.

Several small molecules and peptides have been studied for their ability to interact and inhibit or modulate  $A\beta$  aggregation. However, despite promising results *in-vitro*, none of these compounds have led to a therapeutic treatment. In this study, we demonstrate five novel peptoid modulators of  $A\beta$  aggregation. These peptoids were the first to be designed from the hydrophobic core of  $A\beta$ . Results have indicated that inclusion of aromatic side chains, peptoid secondary structure, side chain placement, and inclusion of charged sequences have a profound impact on  $A\beta$  aggregation. Overall, this study provides insight to the potential of novel peptoids as a therapeutic option for AD.

## **ACKNOWLEDGEMENTS**

I would like to thank Dr. Srinivas Jayanthi, Dr. Rohana Liyanage, and Dr. Mourad Benamara for valuable training. I would like to thank Dr. Bob Beitle for use of and consultation regarding FPLC and fluorometer, I would like to thank Dr. Suresh Kumar for use of and consultation regarding FPLC and CD. I want to acknowledge the Arkansas Statewide Mass Spectrometry Facility and the Arkansas Nano & Bio Materials Characterization Facility for use of equipment.

I would like to thank my friends Dhaval Shah, Alex Lopez, and German Perez. Your friendship, companionship, and lightheartedness made this time of my life truly memorable. I will greatly miss our time together. I would like to thank my grandmother and grandfather Sara and Jerry Hart for teaching me to always believe in myself. I would like to thank my father Phillip Turner Sr. You taught me life always takes more than it gives, but seeing the humor in life helps find happiness even in the most stressful situations. I would like to thank Dr. Tammy Rehtin for always being around to discuss research and bounce wacky ideas off of. I would like to thank the members of my thesis committee for their valued input and direction as I have worked towards this degree. I would like to thank my mentor, Dr. Shannon Servoss for taking a chance on me. I've never been anywhere near the perfect student, but she has always been patient and encouraging. She taught me to be critical, analytical, and precise. I cannot imagine pursuing this goal with anyone else as my adviser. Finally, I would like to thank my wife Meagan. Her support and faith in me has been truly amazing. Her strength and wisdom have helped guide me through this process. Without her constant encouragement, I do not believe I would have had the energy to complete this goal.

## **DEDICATIONS**

This dissertation titled *Peptoid-Based KLVFF Mimics: A Unique Approach to Alzheimer's Disease* is dedicated in loving memory of my mother Kathy Lynn Turner.

## TABLE OF CONTENTS

Chapter 1 Introduction .....	1
1.1 Alzheimer's Disease .....	1
1.2 Diseases Associated with Amyloids .....	2
1.3 Amyloid Beta Protein.....	2
1.3.1 Implications of Amyloid Precursor Protein .....	2
1.3.2 A $\beta$ Nucleation Process .....	3
1.3.3 A $\beta$ Aggregate Associated Toxicity .....	5
1.4 Techniques to Investigate A $\beta$ Aggregation .....	6
1.5 Alzheimer's Disease Therapeutic Approach .....	8
1.5.1 Targeting A $\beta$ Aggregation.....	8
1.5.2 Small Molecule Inhibitors of A $\beta$ Aggregation .....	9
1.6 The Peptide KLVFF.....	10
1.6.1 Utilization of the A $\beta$ Hydrophobic Core .....	10
1.6.2 Notable KLVFF Variants .....	11
1.7 Non-Natural Polymers for Biomedical Applications.....	13
1.8 Poly-N-Substituted Glycines (Peptoids) .....	14
1.8.1 Peptoids Advantages .....	14
1.8.2 Peptoid Secondary Structure.....	15
1.8.3 Peptoid Synthesis .....	16
1.8.4 Peptoids Biomimetics.....	17
1.8.5 Peptoids in the Neurodegenerative Field.....	18
1.9 Purpose and significance of research .....	19
Chapter 2 Methods and Improvements .....	20
2.1 Peptoid Synthesis .....	20
2.2 Peptoid Purification.....	21
2.3 Characterization of Peptoid Mass and Purity .....	23
2.4 Analysis of Peptoid Secondary Structure via Circular Dichroism .....	23
2.5 A $\beta$ 40 Monomer Purification.....	24
2.6 A $\beta$ 42 Monomer Preparation .....	27
2.7 Preparation of A $\beta$ 40 Fibrils .....	27
2.8 A $\beta$ Monomer Aggregation .....	28



2.9	Analysis of A $\beta$ Monomer Aggregation with ThT .....	28
2.10	Analysis of A $\beta$ Monomer Aggregation by Dot Blot .....	29
2.11	Analysis of A $\beta$ Monomer Aggregation .....	30
2.12	Transmission Electron Microscopy .....	32
2.13	Atomic Force Microscopy .....	32
Chapter 3 Rationally Designed Peptoids Modulate Aggregation of Amyloid-Beta 40 .....		33
Abstract .....		33
3.1	Introduction .....	33
3.2	Results and Discussion .....	35
3.2.1	Peptoid Sequence, Rationale, and Characterization .....	35
3.2.2	Aggregation Studies .....	38
3.2.3	Dot Blot Analysis .....	40
3.3	Conclusions .....	42
3.4	Methods .....	44
3.4.1	Materials .....	44
3.4.2	Peptoid Synthesis and Purification .....	44
3.4.3	Circular Dichroism .....	46
3.4.4	Preparation of A $\beta$ Peptide Solution .....	46
3.4.5	Binding Competition Assay .....	47
3.4.6	A $\beta$ 40 Monomer Aggregation Assay .....	48
3.4.7	Dot Blot .....	48
3.4.8	Statistical Analysis .....	50
Funding Sources .....		50
Chapter 4 Modulating A $\beta$ 40 Aggregation: The Effects of Peptoid Helicity and Side Chain Placement .....		51
Abstract .....		51
4.1	Introduction .....	51
4.2	Results and Discussion .....	54
4.2.1	Peptoid Sequence, Rationale, and Characterization .....	54
4.2.2	Aggregation Assays .....	55
4.2.3	Dot Blot Analysis .....	56
4.2.4	Morphology Studies .....	58
4.3	Conclusions .....	59

4.4	Methods .....	62
4.4.1	Materials .....	62
4.4.2	Peptoid Synthesis and Purification.....	63
4.4.3	Preparation of A $\beta$ Peptide Solution.....	66
4.4.4	A $\beta$ 40 Aggregation Assay.....	66
4.4.5	Transmission Electron Microscopy.....	67
Chapter 5 The Effects of Incorporating Charged Side Chain Groups within KLVFF-based Peptoid Mimics on A $\beta$ 42 Aggregation Species and Morphology .....		68
	Abstract .....	68
5.1	Introduction .....	68
5.2	Results .....	71
5.2.1	Circular Dichroism Spectroscopy .....	71
5.2.2	ThT Aggregation Assays .....	72
5.2.3	Dot Blot Analysis .....	73
5.2.4	TEM Studies .....	75
5.2.4	AFM Studies .....	77
5.3	Discussion.....	77
5.4	Conclusions .....	81
5.5	Materials and Methods.....	81
5.5.1	Materials .....	81
5.5.2	Peptoid Synthesis and Purification.....	82
5.5.3	Preparation of A $\beta$ 42 Peptide Solution.....	85
5.5.4	A $\beta$ 42 Aggregation Assay.....	85
5.5.5	Transmission Electron Microscopy.....	86
5.5.6	Atomic Force Microscopy .....	86
Chapter 6 Future Directions and Conclusion .....		87
6.1	Future Directions .....	87
6.1.1	In-Vivo Studies in Transgenic Mouse Models .....	87
6.1.2	Peptoid Biocompatibility .....	87
6.1.3	Investigation of peptoids creating unique pathways of A $\beta$ aggregation .....	88
6.2	Conclusion.....	88
REFERENCES .....		92
Chapter 2 Appendices .....		106

Appendix A: Submonomer structures .....	106
Appendix B: Effects of Reduced Peptoid Length on A $\beta$ 40 Aggregation.....	107
Appendix C: Investigation of Unique Pathways Associated with Peptoid-Based KLVFF Mimics .....	110

## Table of Figures

<b>Figure 1.1</b> A $\beta$ occurs as a polypeptide ranging in 37-42 amino acid residues long. $\gamma$ -secretase cleavage of APP dictates the length of A $\beta$ , while either $\beta$ -Secretase or $\alpha$ -secretase activity dictates amyloidogenic pathway. ....	3
<b>Figure 1.2</b> A $\beta$ aggregation: A) A $\beta$ aggregation progresses from a simple monomer to high weight oligomer species through a rate-limiting nucleation lag phase, growth phase where soluble aggregates grow in length and radius, and a plateau phase where monomer, soluble aggregates, and insoluble fibrils are in equilibrium. B) Monomeric A $\beta$ begins to aggregate into low weight oligomers during the lag phase. The growth phase occurs either by elongation or association of aggregates until fibrils are formed. ....	4
<b>Figure 1.3</b> Residues 16-20 of A $\beta$ (KLVFF) are essential for fibril formation. During aggregation, A $\beta$ forms an anti-parallel $\beta$ -sheet that results in ordered side chain stacking of F19 and I32, L34, and V36. Research has shown that KLVFF mimics can specifically bind to this hydrophobic region for targeted therapeutic potential ....	11
<b>Figure 1.4</b> A schematic for a peptoid that has adopted a polyproline type-I-like helix with three monomers per turn. Side chain pitch on each face of the helix is $\sim 6$ Å. ....	15
<b>Figure 1.5</b> Submonomer process of constructing peptoid scaffold. ....	17
<b>Figure 2.1</b> Purification of a peptoid that did not properly bind to the C18 column. The peptoid eluted in the solvent flow through and resulted in decreased target peaks. ....	22
<b>Figure 2.2</b> Purification of peptoid that properly bound to the C18 column. Proper care of the HPLC system and C18 column along with dissolving the peptoid in the proper percentage acetonitrile allowed for improved purification. ....	22
<b>Figure 2.3</b> A $\beta$ 40 monomer monomeric species is separated from larger aggregates using SEC on a Superdex 75 10/300 GL column. A $\beta$ 40 aggregates elute from the column at 8-10 mL, while A $\beta$ 40 monomer elutes between 12-15 mL. ....	25
<b>Figure 2.4</b> Comparison of the two methods of preparation for A $\beta$ 40 monomer from dried peptide. SEC purified monomer yields a lag time of 90 min with a plateau phase ranging from 165 to 285 min, while the HFIP treated monomer yields a lag time of 60 with a plateau phase ranging from 135 to 255 min. ....	26
<b>Figure 2.5</b> Representation of how larger aggregates settle at the bottom of the reaction vial during agitation. Prior to removing sample for ThT fluorescence measurement, samples should be gently mixed and immediately removed from the vial by drawing aliquot from the top of the sample solution. ....	29
<b>Figure 2.6</b> Schematic representation of lag extension and percent inhibition of control (solid line) versus inhibitor (dash line). ....	31
<b>Figure 3.1</b> Structure and characterization of peptoid JPT1. (A) Chemical structure of JPT1. (B) Circular dichroism spectra for JPT1. The spectra depict a polyproline type-I-like helical secondary structure. ....	37
<b>Figure 3.2</b> JPT1 does compete competitively with ThT for binding of fibrillar A $\beta$ . 2.5 $\mu$ M A $\beta$ 40 fibrils were incubated for 15 min with 10 $\mu$ M ThT in the presence and absence of 12.5 $\mu$ M JPT1, and ThT fluorescence was measured following gentle mixing. Parameters are expressed as mean $\pm$ SEM, n = 3. ....	38

**Figure 3.3** ThT analysis shows that peptoid JPT1 does not aggregate in the absence of A $\beta$ 40. The presence of  $\beta$ -sheet aggregates was detected by ThT fluorescence. Aggregation assays were in 40 mM Tris-HCl (pH 8.0) and 150 mM NaCl. Peptoid JPT1 was dissolved in DMSO and added at 100  $\mu$ M such that the final DMSO concentration was 1.25% (v/v). Assays were performed at 25 °C under agitation on an orbital shaker at 800 RPM. ....39

**Figure 3.4** ThT analysis shows that peptoid JPT1 modulates A $\beta$ 40 aggregation. JPT1 decreases lag time to A $\beta$ 40 aggregation and decreases the quantity of  $\beta$ -sheet aggregates formed. JPT1 was added to 20  $\mu$ M A $\beta$ 40 monomer at concentrations of 0 (control), 20, 50, 100, and 200  $\mu$ M and the presence of fibrillar aggregates was detected by ThT fluorescence. Normalized fluorescence values are calculated as a percentage of the control plateau. Lag extension, or the fold decrease in lag time, and percent inhibition, or percentage decrease in the plateau, are shown below the graph. Parameters are expressed as mean  $\pm$  SEM, n =2. \*p < 0.05; \*\*\*p < 0.0001. ....40

**Figure 3.5** Dot blot analysis shows that peptoid JPT1 modulates A $\beta$ 40 aggregation. JPT1 decreases lag time to A $\beta$ 40 aggregation and decreases the quantity of aggregates formed. JPT1 was added to 20  $\mu$ M A $\beta$ 40 monomer at a concentration of 0 (control) or 100  $\mu$ M, and the presence of fibrillar structure was detected by dot blot with antibody OC. Detection with antibody 6E10 was performed as a parallel control for detection of total protein. (A) Dot blot results. (B) Quantification of antibody OC. Normalized values are calculated as percentage of the control plateau. Parameters are expressed as mean $\pm$ SEM, n=3. \*\*p<0.005. ....41

**Figure 3.6** Peptoids were confirmed to be >98% pure via analytical HPLC (Waters 2695 Separations Module) equipped with a Duragel G C18 150 x 2.1 mm column (Peeke Scientific) using a linear gradient of 5 to 95% solvent D in C (solvent D: acetonitrile, 0.1% TFA; solvent C: water, 0.1% TFA) over 30 min. ....44

**Figure 3.7** MALDI-TOF mass spectrometry was used to confirm that the purified peptoid mass matched the theoretical mass. Peptoid JPT1 theoretical mass was 1130.48 Da. ....45

**Figure 3.8** SEC monomer purification of A $\beta$ 40. Monomer purification of A $\beta$ 40 typically results in elution of larger aggregates at ~8-10 mL and then followed by elution of A $\beta$ 40 monomer at ~13-15 mL. Percent recovery of monomer was calculated for specific A $\beta$ 40 lot. Ideally, quality lots provide >65% recovery. ....47

**Figure 3.9** Dot blot analysis shows that peptoid JPT1 does not bind to sequence-specific antibody 6E10 or conformation-specific antibody OC in the absence of A $\beta$ 40. Samples were spotted at 0 min and 285 min, respectively. ....49

**Figure 4.1** ThT analysis shows that peptoid JPT1, JPT1a, and JPT1s modulate A $\beta$ 40 aggregation similarly. Peptoids were added to 20  $\mu$ M A $\beta$ 40 monomer at concentrations of 0 or 100  $\mu$ M and  $\beta$ -sheet aggregates were detected via ThT fluorescence. Normalized fluorescence values are calculated as a percentage of the control plateau. Parameters are expressed as mean  $\pm$  SEM, n =7. ....56

**Figure 4.2** Dot blot analysis confirms peptoids JPT1, JPT1a, and JPT1s modulate A $\beta$ 40 aggregation and decrease fibrillar aggregates. Peptoids were added to 20  $\mu$ M A $\beta$ 40 monomer at concentrations of 0 or 100  $\mu$ M and fibrillar aggregates were detected via primary antibody OC. Peptoids JPT1 and JPT1s extend lag time by 2.67 $\pm$ 0.83 and 2.22 $\pm$ 0.28 times that of the control, respectively. Peptoid JPT1a decreased lag time extension to <0.42 times that of the control.

Normalized values are calculated as a percentage of the control plateau. Parameters are expressed as mean  $\pm$  SEM, n = 3. Data above is a graphical representation of all experiments...58

**Figure 4.3** Morphology of A $\beta$ 40 aggregates formed in the absence and presence of peptoid with varying side chain placement and helicity. 20  $\mu$ M A $\beta$ 40 monomer in 40 mM Tris-HCl (pH 8.0) was aggregated alone (control, A) or in the presence of 100  $\mu$ M peptoid (B) JPT1, (C) JPT1a, or (D) JPT1s. The control reaction was monitored via ThT fluorescence and upon plateau equilibrium was observed, samples were gridded and visualized by TEM at 255 min. Results are representative of 3 independent experiments and imaged grids were randomly selected. Scale bars are 500 nm. ....59

**Figure 4.4** Proposed mechanistic representation on how peptoids may create off-pathway A $\beta$  higher ordered aggregates. Future work will focus on utilizing atomic force microscopy (AFM) to quantitate the size of early aggregates in the lag phase associated with A $\beta$  aggregation. ....61

**Figure 4.5** Peptoids ( A: JPT1, B: JPT1a, and C: JPT1s) were confirmed to be >98% pure via analytical HPLC (Waters 2695 Separations Module) equipped with a Duragel G C18 150 x 2.1 mm column (Peeke Scientific) using a linear gradient of 5 to 95% solvent D in C (solvent D: acetonitrile, 0.1% TFA; solvent C: water, 0.1% TFA) over 30 min. ....64

**Figure 4.6** MALDI-TOF mass spectrometry was used to confirm that the purified peptoid mass matched the theoretical mass. A) Peptoid JPT1 theoretical mass was 1130.48 Da, B) Peptoid JPT1a theoretical mass was 1073.4 Da, and C) peptoid JPT1s theoretical mass was 1130.48 Da. ....65

**Figure 5.1** Circular dichroism spectra for JPT1+ and JPT1-. The spectra depicts a polyproline type-I-like helical secondary structure. ....72

**Figure 5.2** ThT analysis shows that peptoid JPT1, JPT1+, and JPT1- modulate A $\beta$ 42 aggregation. Peptoids JPT1 and JPT1+ reduce the formation of  $\beta$ -sheet aggregates, whereas JPT1- enhances the formation of  $\beta$ -sheet containing aggregates. Peptoids were added to 20  $\mu$ M A $\beta$ 42 monomer at concentrations of 100  $\mu$ M and  $\beta$ -sheet aggregates were detected via ThT fluorescence. Normalized fluorescence values are calculated as the percentage of the control plateau. Parameters are expressed as mean  $\pm$  SEM, n = 4. ....73

**Figure 5.3** Dot blot analysis confirms peptoids JPT1, JPT1+, and JPT1- modulate A $\beta$ 42 aggregation. A) Dot blot analysis with the primary antibody OC, which has been shown to bind to both fibrils and higher order A $\beta$  aggregates.<sup>156</sup> JPT1 and JPT1+ both reduce signal intensity as compared to the control. JPT1- does not decrease signal intensity compared to the control, indicating no reduction in higher ordered A $\beta$  aggregates. Parameters are expressed as mean  $\pm$  SEM, n = 3. B) Dot blot analysis with the primary antibody LOC, which has been shown to be more specific to A $\beta$  fibrils than OC.<sup>156</sup> Both JPT1 and JPT1+ have a significant reduction in signal intensity compared to the control, indicating a drastic reduction in fibrillar aggregates. Interestingly, JPT1- increases signal intensity for fibrillar aggregate detection, which corroborates ThT data. Parameters are expressed as mean  $\pm$  SEM, n = 2. ....74

**Figure 5.4** Representative figure of dot blot analysis with primary antibody 6E10. 20  $\mu$ M A $\beta$ 42 was incubated in the presence and absence of 100  $\mu$ M peptoids. The amino terminus is widely believe to play a role in conformational changes during oligomerization.<sup>13,46</sup> JPT1 and JPT1+ result in a decreased signal intensity compared to the control and JPT1-, indicating a JPT1- does not alter the A $\beta$  conformational state. ....75

<b>Figure 5.5</b> Morphology of A $\beta$ 42 aggregates formed in the presence and absence of peptoid with varying side chain charge. 20 $\mu$ M A $\beta$ 42 monomer in 40 mM Tris-HCl (pH 8.0) was aggregated alone (control, A-E) or in the presence of 100 $\mu$ M peptoid (F-J) JPT1, (K-P) JPT1+, or (Q-U) JPT1-. Samples were gridded at 3, 5, 9, 12, and 30 h time points (right to left) and visualized by TEM. Results are representative of 3 independent experiments and imaged grids were randomly selected. ....	76
<b>Figure 5.6</b> 20 $\mu$ M A $\beta$ 42 monomer was aggregated at 200 RPM at 25 $^{\circ}$ C in 40 mM Tris HCl buffer with 50 mM NaCl. Samples were taken at 3, 12, and 30 h and incubated on ruby muscovite mica for 10 min and was then rinsed with 0.2 $\mu$ m filtered water and then dried under nitrogen for 3 h. Control groups (A-C) display a typical A $\beta$ 42 aggregation that contains: A) low molecular weight species, B) large aggregates, C) fibrils. In the presence of JPT1 (D-F), A $\beta$ 42 aggregates to form: D) ordered branched aggregates, E) small, circular aggregates, and F) off pathway aggregates. In the presence of JPT1+ (G-I), A $\beta$ 42 aggregates to form: G) ordered aggregates, H) packed aggregates, and I) high ordered aggregates. In the presence of JPT1- (J-L), A $\beta$ 42 aggregates to form J) small molecular weight oligomers, K) low molecular weight species, and L) small and large aggregates.....	78
<b>Figure 5.7</b> Peptoids ( A: JPT1, B: JPT1a, and C: JPT1s) were confirmed to be >98% pure via analytical HPLC (Waters 2695 Separations Module) equipped with a Duragel G C18 150 x 2.1 mm column (Peeke Scientific) using a linear gradient of 5 to 95% solvent D in C (solvent D: acetonitrile, 0.1% TFA; solvent C: water, 0.1% TFA) over 30 min. ....	83
<b>Figure 5.8</b> MALDI-TOF mass spectrometry was used to confirm that the purified peptoid mass matched the theoretical mass. A) Peptoid JPT1 theoretical mass was 1130.48 Da, B) Peptoid JPT1+ theoretical mass was 1073.4 Da, and C) peptoid JPT1- theoretical mass was 1130.48 Da. ....	84
<b>Figure B.1</b> ThT analysis shows that peptoid JPT1 modulates A $\beta$ 40 aggregation. JPT15 did not reduce the formation of $\beta$ -sheet aggregates. Peptoids were added to 20 $\mu$ M A $\beta$ 40 monomer at concentrations of 100 $\mu$ M and $\beta$ -sheet aggregates were detected via ThT fluorescence. Normalized fluorescence values are calculated as the percentage of the control plateau. Parameters are expressed as mean $\pm$ SEM, n = 7. ....	108
<b>Figure C.1</b> Dot blot analysis of known small molecules that work on unique A $\beta$ aggregation pathways. Peptoid JPT1 and small molecules were added to 20 $\mu$ M A $\beta$ 40 monomer at concentrations of 100 $\mu$ M and fibrillar aggregates were detected via primary antibody OC. Normalized values are calculated as a percentage of the control plateau. Parameters are expressed as mean $\pm$ SEM, n = 2. Data above is a graphical representation of all experiments.....	113
<b>Figure C.2</b> Morphology studies of A $\beta$ 40 aggregates formed in the presence (control; A) and absence of B) JPT1, C) Congo Red, D) Orange G, and E) Rhodamine B. 20 $\mu$ M A $\beta$ 40 monomer was aggregated in the presence and absence of 100 $\mu$ M small molecules at 800 RPM in 40 mM Tris-HCl (pH 8.0) in the presence of 150 mM NaCl.....	114

## List of Tables

<b>Table 4.1</b> Peptoid sequence, theoretical MW (Da), and percent acetonitrile elution (HPLC).....	53
<b>Table 5.1</b> Peptoid structures, molecular weights (MW), and percent acetonitrile elution from analytical HPLC (% elution).....	71
<b>Table B.1</b> Peptoids corresponding 1 letter amino acid code and molecular weight.....	108
<b>Table C.1</b> Small compounds and their respective class of compound.....	112



## Chapter 1 Introduction

### 1.1 Alzheimer's Disease

Alzheimer's disease (AD) is the leading form of dementia and sixth leading cause of death in the United States.<sup>1</sup> AD is a slow, degenerative disease that takes many years to develop. While there is no cure for AD, medications are available for patients to alleviate symptoms. However, these medications work for a brief period of time and only for ~50% of the patients.<sup>1</sup> One of the rising concerns with AD is the associated cost to the economy. Among the top ten causes of death in the United States, AD is the only cause that cannot be treated or cured. Combining this with the aging baby boomer generation, an economic burden is resulting in ~\$220 billion dollars lost due to treatment, research, and lost productivity from patients and caregivers every year.<sup>1,2</sup>

AD is a neurodegenerative disease that is characterized by the cultivation of amyloid plaques and overt neurofibrillary tangles (NFTs), more commonly known as tau protein tangles, in the brain.<sup>2-4</sup> The amyloid plaques are the result of the amyloid beta protein ( $A\beta$ ) aggregating,<sup>5</sup> while the presence of NFT's are the result of dysregulation of the phosphorylation cascade of the tau protein.<sup>6</sup> In its native form, the tau protein exists as an unfolded monomer.<sup>7</sup> Tau is essential for microtubule dynamics in the brain and is believed to play a role with neuronal cell functions.<sup>8</sup> Although tau pathology has been attributed to neurodegenerations such as familial frontotemporal dementia, thus leading to fatal neurodegeneration, alteration to the amyloid precursor protein (APP) is believed to preclude the formation of NFTs.<sup>3,8</sup> This has been supported by observations of mouse hippocampal primary neuronal cultures demonstrating  $A\beta$  toxicity is dependent of the formation of NFTs.<sup>3,9</sup> While NFTs are a concern for neuronal health in the brain, the defining cause of AD is widely accepted to be the aggregation of  $A\beta$ .

## 1.2 Diseases Associated with Amyloid Formations

The deposition of amyloid plaques in the brain are considered a hallmark of AD.<sup>2</sup> Amyloid plaques are insoluble fibrous protein aggregates that share specific structural states. However, AD is not the only disease in which amyloid formations are believed to contribute to the progression of the disease. There are at least eighteen misfolded proteins and polypeptides that are known to be the cause of disease-associated amyloid deposits.<sup>10</sup> Some of the more notable proteins associated with amyloid deposits include A $\beta$  (Alzheimer's Disease & Cerebral amyloid angiopathy),<sup>11-13</sup> the islet-associated polypeptide (type II diabetes),<sup>14,15</sup> the prion protein (Transmissible spongiform encephalopathy),<sup>16</sup> and alpha-synuclein (Parkinson's disease).<sup>12</sup> While there are some sequence and structural similarities between some of the individual amyloid proteins, there is no similarity that crosses through all the different proteins. The symptoms associated with each amyloid disease presents unique clinical challenges, yet all of these diseases have implications from amyloid formations. Surprisingly, the fibrils that form as a result of aggregation are all long, straight, unbranched fibers 40-120 Å in diameter and adopt a cross  $\beta$ -sheet structure.<sup>17,18</sup> While recent evidence has shown that fibrils may not be the toxic species resulting in neurodegeneration, fibril formation is still an important area of investigation in preventing advanced forms of neurodegenerative diseases such as AD.

## 1.3 Amyloid Beta Protein

### 1.3.1 Implications of Amyloid Precursor Protein

A $\beta$  occurs in isoforms ranging from 37-42 amino acids residues long. The two most common polypeptides are 40 or 42 amino acid residues long, denoted as A $\beta$ 40 and A $\beta$ 42, respectively. A $\beta$  polypeptides are derived by proteolytic cleavage from the larger APP.<sup>19,20</sup> Cleavage of APP occurs at two sites and can occur via two pathways (Figure 1.1). Both pathways have carboxy-

terminus cleavage by  $\gamma$ -secretase, resulting in the formation of either A $\beta$ 40 (the more abundant species) or A $\beta$ 42 (the more pathogenic species).<sup>21</sup>  $\gamma$ -secretase cleavage of APP occurs due to a protease complex of components that contain presenilin 1 and presenilin 2.<sup>22–24</sup> Amino terminus cleavage occurs by  $\beta$ -Secretase activity, which has been attributed to a single protein, BACE-1.<sup>25</sup> Amino terminus cleavage can also occur via  $\alpha$ -secretase activity, which is involved in the non-amyloidogenic pathway by cleaving APP within the A $\beta$  domain and thus precluding A $\beta$  formation.<sup>26</sup>

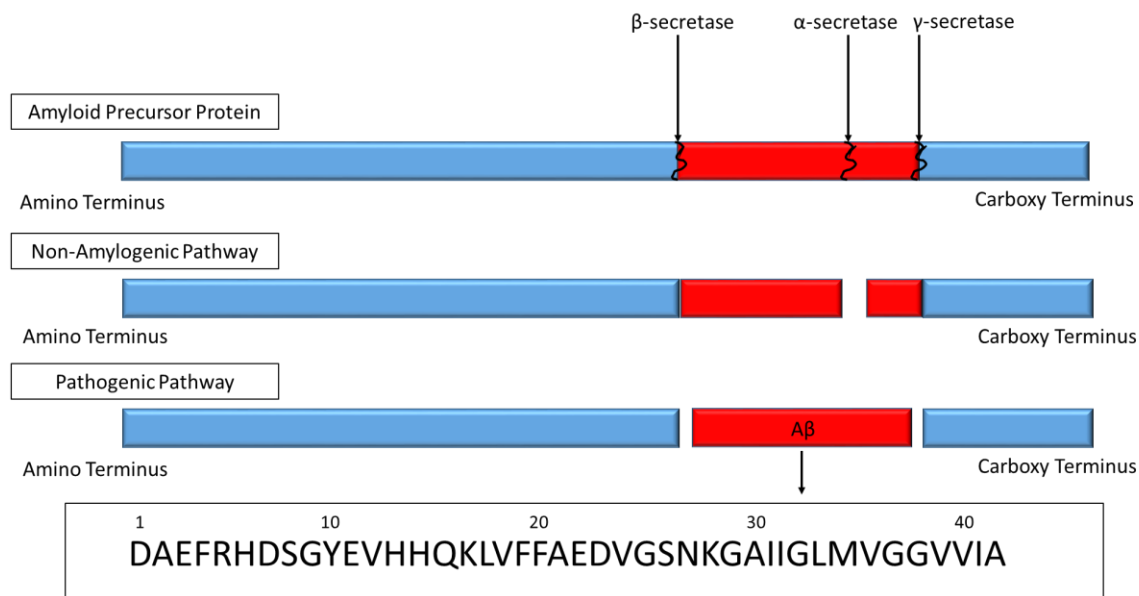


**Figure 1.1** A $\beta$  occurs as a polypeptide ranging in 37-42 amino acid residues long.  $\gamma$ -secretase cleavage of APP dictates the length of A $\beta$ , while either  $\beta$ -Secretase or  $\alpha$ -secretase activity dictates amyloidogenic pathway.<sup>159</sup> Adapted with permission.<sup>160</sup>

### 1.3.2 A $\beta$ Nucleation Process

The formation of plaques associated with AD brains are primarily composed of insoluble amyloid fibrils that form due to A $\beta$  aggregation. A $\beta$  aggregation results in the transformation of the simple, harmless monomer species that is predominately random coil to oligomer intermediates (dimers, trimers, heptamers, etc.) that begin to form  $\beta$ -sheet aggregates and finally

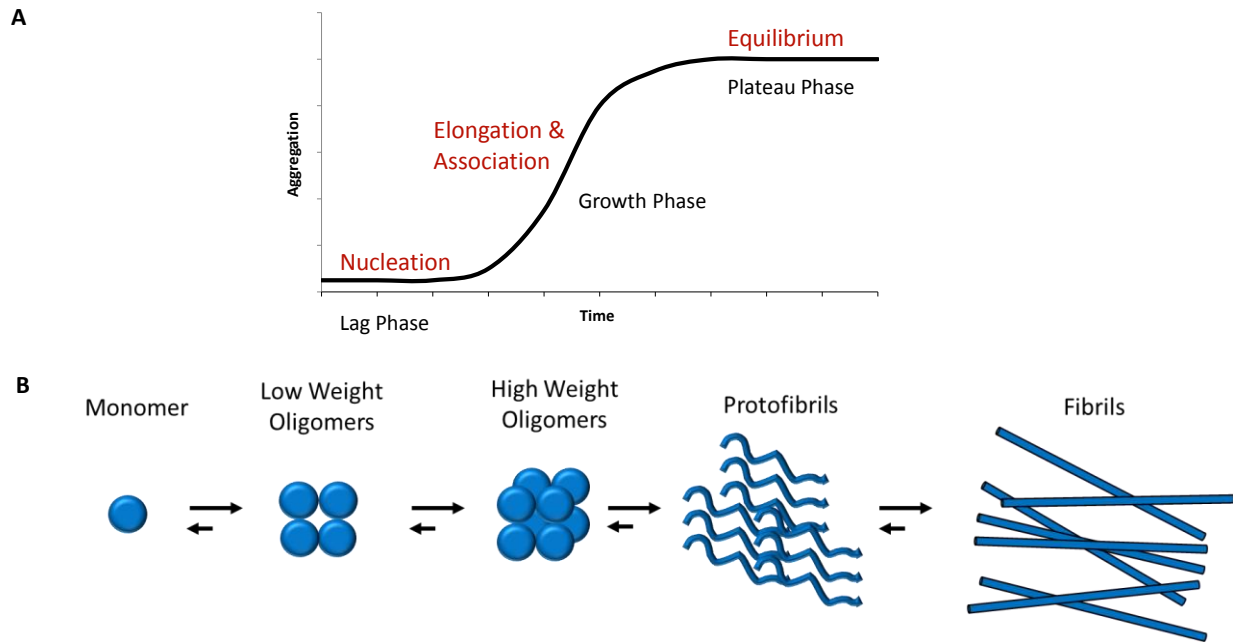


**Figure 1.2** A $\beta$  aggregation: A) A $\beta$  aggregation progresses from a simple monomer to high weight oligomer species through a rate-limiting nucleation lag phase, growth phase where soluble aggregates grow in length and radius, and a plateau phase where monomer, soluble aggregates, and insoluble fibrils are in equilibrium. B) Monomeric A $\beta$  begins to aggregate into low weight oligomers during the lag phase. The growth phase occurs either by elongation or association of aggregates until fibrils are formed.<sup>161</sup>

form insoluble amyloid fibrils that accumulate to create plaques that deposit in the brain.<sup>27,28</sup> The A $\beta$  aggregation pathway is the result of a rate-limiting nucleation of the monomer (lag phase) that allows for rapid growth of soluble aggregates (growth phase) either by elongation or association until insoluble fibrils are formed.<sup>29–33</sup> Once equilibrium is reached, all A $\beta$  species are in equilibrium with one another (plateau phase; Figure 1.2A). Fibril formation (Figure 1.2B) can occur via elongation or association. Aggregate elongation is the result of monomeric A $\beta$  attaching to the ends of soluble aggregates while aggregate association occurs when two or more soluble aggregates bind laterally, resulting in the increase in aggregate size. The growth phase of soluble aggregates results in intermediates termed oligomers,<sup>34</sup> micelles,<sup>35</sup> amyloid derived diffusible ligands (ADDLs),<sup>36,37</sup>  $\beta$ amy balls,<sup>38</sup> amylospheroids (ASPDs),<sup>39</sup> and protofibrils.<sup>40,41</sup> These intermediates are typically placed in one of two classes: low molecular weight or high

molecular weight species. Low molecular weight species are typically referred to as oligomers, whereas high molecular weight species are typically referred to as protofibrils and fibrils. In addition to the low and high molecular weight species that are formed during A $\beta$  aggregation, off pathway oligomers and higher order assemblies have been identified.<sup>42,43</sup> Interestingly, these higher order assemblies fail to form an organized fibrillar structure. Another instance of off pathway aggregation is the induced fibrillation due to fibrillar seeds.<sup>44</sup> When A $\beta$  monomer is exposed to fibrillar A $\beta$  seeds, the growth phase is accelerated, resulting in the formation of fibrils that have a reduction in size and branching.<sup>44</sup>

### *1.3.3 A $\beta$ Aggregate Associated Toxicity*

The A $\beta$  proteins that aggregate to form insoluble fibrils that will lead to the deposition of plaques in the brain are comprised of either A $\beta$ 40 or A $\beta$ 42.<sup>2</sup> The accumulation of insoluble fibrils or plaques were believed to be the cause for disease severity early on. However, research has shown that soluble aggregates of A $\beta$  may have a more direct impact on neurodegeneration than the monomers or insoluble fibrils.<sup>30,45,46</sup> This hypothesis is further supported by *in vitro* cell studies that implicate that A $\beta$ 40 and A $\beta$ 42 soluble aggregates can induce cellular dysfunction and toxicity in cultured cells.<sup>37,40,47</sup> Similarly, *in vivo* A $\beta$  dodecamers have been shown to induce memory deficits in AD mice.<sup>48</sup> Soluble A $\beta$  aggregates generated in cell culture models have been shown to inhibit nerve impulses in the hippocampal region of rats.<sup>34</sup> Furthermore, insoluble A $\beta$  fibrils have poor correlation with disease severity in AD mouse models.<sup>49</sup> Currently, there is limited knowledge on the aggregation mechanism of A $\beta$ , thus adding to the complexity of developing a therapeutic treatment for AD.

## 1.4 Techniques to Investigate A $\beta$ Aggregation

Monitoring potential inhibitors and modulators of A $\beta$  is a difficult task. Several techniques are available; however, each of these techniques can have a varying set of challenges, bias, and implication. Even more problematic, preparation of synthetic A $\beta$  can result in varying biological activity.<sup>50</sup> Predissolution of synthetic A $\beta$  is required due to limited solubility in physiological buffers.<sup>51</sup> Predissolution of synthetic A $\beta$  usually comes in the form of using one of two solvents: sodium hydroxide or 1,1,1,3,3,3-Hexafluoro-2-propanol (HFIP). Following predissolution, monomerization can occur via size exclusion chromatography (SEC) or organic dissolution. SEC is typically considered the optimal purification technique, whereas organic dissolution is faster and allows for longer shelf life of A $\beta$  monomer. While some have argued SEC produces superior aggregation kinetics that simulate physiological conditions, little work has been performed to confirm this. More importantly, when solid phase synthesis of A $\beta$  is paired with purification techniques such as high pressure liquid chromatography (HPLC), the production of trifluoroacetic acid salts can occur.<sup>52</sup> This can slightly alter the biophysical activity of A $\beta$  and result in a change in aggregation kinetics.

The detection of  $\beta$ -sheet aggregates typically utilize a benzothiazole salt known as ThT that binds to  $\beta$ -sheet-rich structures to yield a shifted and enhanced fluorescent signal.<sup>53-55</sup> Specifically, when ThT binds to  $\beta$ -sheets formed from A $\beta$  aggregation assays, dramatic increases in fluorescent signaling occurs at 485 nm, when excited at 440 nm.<sup>56</sup> ThT aggregation assays are considered a valuable, straight-forward approach to not only monitor the aggregation of A $\beta$ , but also determine the capabilities of specific molecules to act as an inhibitor or modulator. However, precaution must be taken when assessing data from ThT assays. Many molecules that are designed to inhibit A $\beta$  aggregation are designed to specifically bind to A $\beta$ , thus disrupting

the folding of the cross- $\beta$ -sheet structure.<sup>55</sup> Small molecules have the propensity to disrupt the bindings of ThT to  $\beta$ -sheet structures, which can render a false positive.<sup>57</sup> Nonetheless, ThT assays prove to be valuable in initial inhibitor studies for small molecules. These assays are easy to use, allow for qualitative analysis, and can help narrow the IC<sub>50</sub> of small molecules for A $\beta$  aggregation. More importantly, percent inhibition and lag time can be determined for small molecule inhibitors. Percent inhibition is a measurement of the ability of a small molecule to reduce the  $\beta$ -sheet content of A $\beta$  aggregation, compared to the control. Lag time is correlated as the time it takes for A $\beta$  to nucleate and begin the growth phase. A positive increase in lag time correlates a small molecules ability to delay nucleation. Percent inhibition and lag time are often reported for small molecules that may serve as a therapeutic option for AD.<sup>53,58-60</sup>

Immunoblotting techniques offer a straight-forward, rapid approach to determine the presence of specific A $\beta$  species. Conformation-specific antibodies such as A11, OC, and LOC allow for the detection of aggregate species such as oligomers and fibril,<sup>61-63</sup> whereas sequence-specific antibodies such as 6E10 allow for the detection of all A $\beta$  species.<sup>61,62</sup> However, immunoblotting does not allow for the determination of aggregate size.<sup>64,65</sup> Percent inhibition and lag time can still be observed, similar to ThT assays. By utilizing software packages such as Image J, a quantitative analysis of the mean density can be utilized to correlate percent inhibition and lag time of fibrillar aggregates from OC and LOC detection.

Transmission electron microscopy (TEM) and atomic force microscopy (AFM) imaging allows for visualization of A $\beta$  species. TEM is typically used as a method to visualize and confirm the presences of A $\beta$  fibrils, though visualization of protofibrils have been reported.<sup>29,66</sup> TEM can also be used to estimate the size of fibrils. However, one of the drawbacks to TEM is the inability to distinguish between A $\beta$  oligomeric species. By pairing TEM with AFM,

characterization of oligomers is possible, thus allowing for a full spectrum of the morphological changes to A $\beta$ .<sup>54,66</sup> AFM can be utilized to visualize small and high molecular weight oligomers. Some of the reported intermediates have been globular oligomers, protofibrils, and even fibrils.<sup>54,66</sup> However, measurement of fibrils with AFM can be challenging, resulting in varied results. To allow for a full assessment of A $\beta$  aggregate species, pairing TEM and AFM improves the shortcomings of both techniques.

Other techniques have been utilized to investigate A $\beta$  aggregation. Electrophoresis techniques have been utilized to monitor the size of A $\beta$  aggregates. Specifically, sodium dodecyl sulfate polyacrylamide gel electrophoresis (SDS-PAGE) and western blotting can be used to determine the size and quantity of A $\beta$  oligomers.<sup>34,67</sup> Capillary electrophoresis (CE) has also been employed with A $\beta$ 40 and A $\beta$ 42 at monitoring A $\beta$  nucleation in solution and has shown promising results.<sup>68</sup> Investigation on the effects of A $\beta$  secondary structure in the presence of small molecules and peptides have been studied with circular dichroism (CD).<sup>27,69</sup> These studies allow for the qualitative analysis of changes to  $\beta$ -sheet formation of A $\beta$  aggregates in the presence of small molecules and peptides. Overall, these techniques allow for the determination of size, structure, and nucleation. Combining these techniques with the development of small molecules or peptides can help in finding a therapeutic treatment for AD.

## **1.5 Alzheimer's Disease Therapeutic Approach**

### *1.5.1 Targeting A $\beta$ Aggregation*

Multiple treatment strategies have been considered due to the complex A $\beta$  biology.<sup>3</sup> AD is believed to be an imbalance of A $\beta$  production and A $\beta$  clearance.<sup>67</sup> One approach to this problem is to investigate the factors that cause these imbalances. For instance, A $\beta$  is derived from APP due to proteolytic cleavage. Inhibition of either of the proteases was thought to potentially lead to



fewer A $\beta$  plaques deposited in the brain.<sup>3,25</sup> Another approach has been to prevent the nucleation of monomeric A $\beta$  species, thus reducing accumulation of  $\beta$ -sheet and fibrillar aggregates.<sup>70,71</sup> Inhibition can occur by preventing the growth of soluble oligomers either by association or elongation mechanisms. Design of inhibitors to bind to the carboxy terminus of aggregate species can prevent elongation whereas developing inhibitors to bind laterally to A $\beta$  can prevent association. Other approaches include anti-inflammatory strategies,<sup>72-74</sup> modulating cholesterol homeostasis,<sup>75,76</sup> and the prevention of neurodegenerative effects triggered by A $\beta$  accumulation.<sup>3</sup> Modulation of the A $\beta$  aggregation pathway has recently been considered a potential therapeutic approach to AD.<sup>53,77,78</sup> This approach was considered when A $\beta$  aggregation occurred off pathway, resulting in higher ordered assemblies that did not form fibrils.<sup>42,43</sup>

### *1.5.2 Small Molecule Inhibitors of A $\beta$ Aggregation*

Numerous small molecule inhibitors have been developed to target and inhibit A $\beta$  aggregates at various stages of aggregation. This includes selectively halting the formation of mature A $\beta$  fibrils from monomers without stopping the formation of soluble aggregates,<sup>79</sup> allowing fibril formation but preventing fibril growth,<sup>60</sup> and even inhibiting select pathways of soluble aggregate growth.<sup>58</sup> Some small molecules have shown the capability to block specific aggregation pathways of A $\beta$ , thus remodeling soluble oligomers.<sup>80</sup> Specifically, Tessier and colleagues reported three classes of molecules that created unique pathways of A $\beta$  aggregation.<sup>80</sup> Class I molecules are capable of converting soluble oligomers into large, unstructured aggregates, class II molecules selectively convert soluble oligomers into fibrils, and class III molecules have the capability to disaggregate fibrils. One key feature of several potential therapeutic small molecules is that they all contain aromatic groups. These aromatic groups are believed to initiate pi-pi stacking in the between the polyphenols and aromatics in amyloid

formations.<sup>81</sup> Pi-pi stacking between small molecules and the aromatics in A $\beta$  aggregates are believed to allow for a stabilization of the aggregates, thus allowing for a remodeling of toxic, soluble oligomers into non-toxic forms.<sup>80,82</sup>

Work with small molecules has demonstrated the effects of utilizing aromatic compounds that are capable of either altering the A $\beta$  aggregation pathway or simply stabilizing toxic, soluble oligomers to yield stable, non-toxic oligomers. Many of these compounds have even shown the capability to bypass the blood-brain barrier (BBB), thus making these molecules an interesting therapeutic option.<sup>80</sup> Unfortunately, lack of bioavailability has prevented the emergence of these technologies as a viable therapeutic option.<sup>83</sup>

## 1.6 The Peptide KLVFF

### 1.6.1 Utilization of the A $\beta$ Hydrophobic Core

The peptide KLVFF (residues 16-20 of A $\beta$ ) has been utilized to create a class of peptidomimetics to serve as a potential therapeutic treatment for AD. KLVFF is recognized as the essential amino acid sequence for fibril formation due to the hydrophobic interactions (Figure 3).<sup>84,85</sup> By utilizing the KLVFF sequence, researchers have created variants that are capable of specifically binding to A $\beta$ , resulting in either inhibiting or modulating aggregation *in vitro*.<sup>59,78,85-91</sup> One notable compound was a five residue peptide with a proline point substitution called iA $\beta$ 5 that had the corresponding amino acid sequence LPFFD. iA $\beta$ 5 was capable of interfering with A $\beta$  self-assembly, resulting in a reduction of  $\beta$ -sheet containing aggregates.<sup>92,93</sup> However, proteolytic degradation was a major concern with iA $\beta$ 5 *in vivo*. To increase bioavailability and blood-brain permeability, the N-terminus of the peptide was acetylated and the C-terminus was modified with an amide group to create the peptide iA $\beta$ 5p.<sup>94</sup> Though iA $\beta$ 5p

did improve upon the lack of bioavailability of iA $\beta$ 5, activity towards inhibiting A $\beta$  aggregation was greatly reduced.<sup>93</sup>

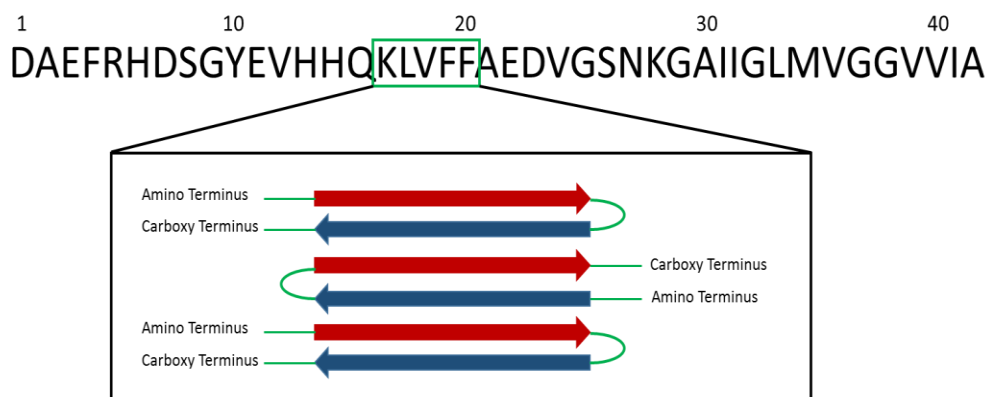


**Figure 1.3** Residues 16-20 of A $\beta$  (KLVFF) are essential for fibril formation. During aggregation, A $\beta$  forms an anti-parallel  $\beta$ -sheet that results in ordered side chain stacking of F19 and I32, L34, and V36.<sup>32</sup> Research has shown that KLVFF mimics can specifically bind to this hydrophobic region for targeted therapeutic potential.

### 1.6.2 Notable KLVFF Variants

Another notable KLVFF compound, KLVFF-K<sub>6</sub>, was developed by Murphy and colleagues.<sup>95</sup> This peptide consisted of the KLVFF recognition element to specifically bind to A $\beta$  and a hexalysine (K<sub>6</sub>) disruption element.<sup>78,88,95</sup> KLVFF-K<sub>6</sub> was designed to disrupt A $\beta$  self-assembly; however, this peptide was reported to increase the rate of A $\beta$  fibril formation with an alteration to the fibrillar morphology. Surprisingly, this change was reported to have a decrease in A $\beta$  toxicity by MTT reduction assay.<sup>78,88,95</sup> Further work with KLVFF-K<sub>6</sub> demonstrated that the peptide altered A $\beta$  assembly by selectively altering protofibril elongation and inhibiting monomer aggregation.<sup>59</sup> This suggested that ligand binding to varying surfaces in the A $\beta$  peptide could greatly affect the formation and morphology of protofibrils and fibrils.

Another class of novel KLVFF molecules consisted of the recognition element and a hydrophilic disruption element consisting of aminoethoxy ethoxy acetic acid (AEEA) possessing

an ethylene glycol skeleton and aspartate.<sup>89</sup> This peptide was designed to have varying lengths of AEEA for study of A $\beta$  activity and self-assembly disruption. The group reported varying results of inhibitors that were capable of either inhibiting fibril formation and cytotoxicity or accelerating fibril formation but not inhibiting cytotoxicity. Based on the results of the study, it was concluded that two factors (conformational flexibility and degree of hydration) were necessary in evaluating disruption elements. The group also noted the charge of the disruption element seemed to effect the capabilities of inhibiting fibril formation and cytotoxicity.

Finally, another group investigated the intervention of A $\beta$ 42 aggregation by utilizing a multivalent KLVFF variant.<sup>96</sup> This work compared the efficacy of a monomeric KLVFF variant and a dendritic variant that exhibited a branched structure. The rationale for comparison of these two structures was that A $\beta$  has different species that are known to contribute to the pathogenesis of AD. Similar to other KLVFF variants, the dendritic variant did not exhibit self-aggregation, which is vital for therapeutic applications. Results demonstrated that the dendritic variant was more potent at inhibiting A $\beta$ 42 aggregation, specifically at preventing low molecular weight species compared to the monomeric variant.

Even more problematic is that many of the small molecules that have had success at selectively halting A $\beta$  progression have pitfalls. Failure typically results from either failure to cross the BBB and/or proteolytic degradation.<sup>97-99</sup> While there are numerous examples of small molecules that act on A $\beta$  aggregates in different ways, it is important to note that these studies demonstrate that small molecule inhibitors can be created in a variety of ways to act on various aggregation pathways.<sup>84</sup>

## 1.7 Non-Natural Polymers for Biomedical Applications

Proteins are incredible structures that have desirable therapeutic capabilities. Protein therapeutic agents, such as peptides, are currently in a variety of applications including the treatment of diabetes, cancer, and helping fight infection. Small molecules and antibodies are often utilized as therapeutics; however, peptides offer several key advantages such as size and bioavailability. Peptides have generated great interest in medical therapies due to their high biological activity, low toxicity, and high specificity. Peptides can interact specifically with desired targets with lower cytotoxicity effects compared to small molecules. Peptides have the improved stability and immunogenicity compared to antibodies. However, peptide-based therapeutics do not see the same wide spread use that small molecules and antibodies do. This in part is due to the degree of difficulty in purification steps and proteolytic degradation *in vivo*.<sup>100</sup>

There is much interest in the use of synthetic peptides in medical settings. The majority of synthetic peptide therapeutics are based upon sequences utilized in nature.<sup>91,100</sup> Furthermore, engineered peptides have generated great interest in medical therapies due to their high biological activity, low toxicity, and high specificity. Peptides can form a wide array of three-dimensional structures based on the specific sequence of the amino acids. As a result of the vast amount of amino acid combinations, a multitude of three-dimensional structures are possible. This endless combination of amino acid sequences not only yields new and interesting structures, but also allows specific functions often determined by three-dimensional structure. In terms of the pharmaceutical industry, this multitude of naturally assumed functions and ease of synthesis through the use of automated machinery has led to the consideration of synthetic peptides for therapeutic use. However, peptides have a short half-life *in vivo* due to protease degradation,

which decreases their effectiveness clinically.<sup>83</sup> Furthermore, since peptides are prone to degradation there is a lack of biological function and specificity, or bioavailability.

Much effort has gone into the development of peptidomimetics, non-natural polymers that are designed to mimic natural peptides. Peptidomimetics often mimic the secondary and/or tertiary structure of peptides, and therefore produce the same biological effect while maintaining bioavailability.<sup>101</sup> Examples of such molecules include  $\beta$ -peptides,<sup>102,103</sup> oligopyrrolinones,<sup>104</sup> and poly-N-substituted glycines (or peptoids).<sup>105,106</sup> These compounds increased bioavailability and are resistant to proteolysis compared to peptides. Many of these compounds have been shown to adopt secondary structures that are vital for protein dynamics. In the case of AD, extending the half-life of therapeutic treatments *in-vivo* would greatly enhance the potential for a viable treatment option. Advances in peptidomimetics could prove to be beneficial towards combatting neurodegenerative diseases such as AD, Huntington's disease (HD), and Parkinson's disease.

## **1.8 Poly-N-Substituted Glycines (Peptoids)**

### *1.8.1 Peptoids Advantages*

Poly-N-substituted glycines (peptoids) are an interesting class of peptidomimetics due to their ease of synthesis, low cost, availability of diverse side chains, and improved bioavailability.<sup>97,105</sup> Peptoids have a structure that resembles that of a peptide, but with the side chain appended to the amide nitrogen rather than the  $\alpha$ -carbon (Figure 1.4). This modification renders peptoids resistant to proteolytic attack, making them more stable than peptides.<sup>107</sup> Furthermore, studies have shown peptoids elicit only a slight antibody response, thus demonstrating peptoids can be nontoxic and nonimmunogenic.<sup>107-109</sup> Peptoids have a lack in both backbone chirality and hydrogen bond donors, both of which are required for the formation

of secondary structures in peptides.<sup>110–112</sup> However, peptoids that include chiral, bulky groups can adopt a helical secondary structure due to steric and electronic repulsions between adjacent residues.<sup>106,113–116</sup>

### 1.8.2 Peptoid Secondary Structure

Extensive work has gone into the investigation of peptoid secondary structure formation. Helical structures were noted to occur when minimal N-substitution were performed with peptoids.<sup>117</sup> Early molecular modeling by Armand *et al.* predicted that fully N-substituted glycines with chiral, aromatic side chain groups could successfully form stable helical structures.<sup>113</sup> This was later confirmed by nuclear magnetic resonance.<sup>114</sup> Peptoid helices as short as five monomers have been shown to form helices, which have a periodicity of three monomers per turn and exhibit a helical pitch of  $\sim 6$  Å between the side chains (Figure 1.4).<sup>106</sup> Peptoids that adopt a polyproline type-I-like helix have been shown to have a signature circular dichroism (CD) spectra that is similar to that of a peptide  $\alpha$ -helix.<sup>118</sup> This includes two exhibited minima at 205 and 220 nm, respectively, and a maxima at 190 nm.<sup>118–120</sup> Blackwell and colleagues were the

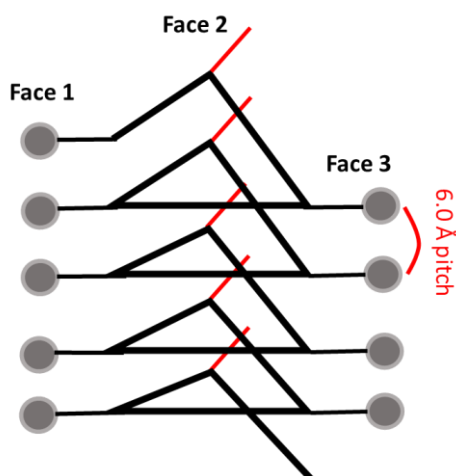


**Figure 1.4** A schematic for a peptoid that has adopted a polyproline type-I-like helix with three monomers per turn. Side chain pitch on each face of the helix is  $\sim 6$  Å.

first to utilize x-ray crystallography on peptoids.<sup>121</sup> Their work confirmed N-substituted oligomers with chiral, aromatic side chains formed stable, right-handed helices that had repeating cis-amide bonds with an average of three monomers per turn and ~6 Å pitch, similar to  $\alpha$ -peptides.<sup>121</sup>

Further investigation of peptoid helices led to some general rules for the formation of robust helical structures: (1) at least 50% of the side chains must be chiral and aromatic, (2) a chiral, aromatic side chain should be included at the C-terminus of the peptoid structure, and (3) one helical face should be composed of chiral, aromatic side chains.<sup>115,116</sup> Finally, because peptoids are stabilized by steric and electronic repulsions of the side chains rather than hydrogen bonds, they are stable in extreme conditions, including 8 M urea at 70 °C.<sup>122</sup>

### *1.8.3 Peptoid Synthesis*

When compared to other peptidomimetics, peptoids are relatively easy to synthesize due to the ability to be constructed on solid support using either an automated peptide synthesizer or by manual additions of side chains. By utilizing a submonomer protocol, diverse side chains can be incorporated as primary amines.<sup>110</sup> The submonomer protocol (Figure 1.5) is a two-step process: (1) bromoacetic acid is used to acylate a secondary amine on the resin, leaving an S<sub>N</sub>2 reaction substrate and (2) a primary amine is added to the oligomer via an S<sub>N</sub>2 reaction. These steps are repeated until the desired oligomer chain length is achieved. The submonomer method approach allows for high coupling efficiencies (99% per added residue) that has been used to produce peptoids over 100 residues in length.<sup>123</sup> Peptoids are cleaved from the resin using a cocktail that contains an acid and scavenger reagent. Furthermore, a large diversity of side chain moieties can be incorporated due to the large number of primary amines available commercially.<sup>124</sup>



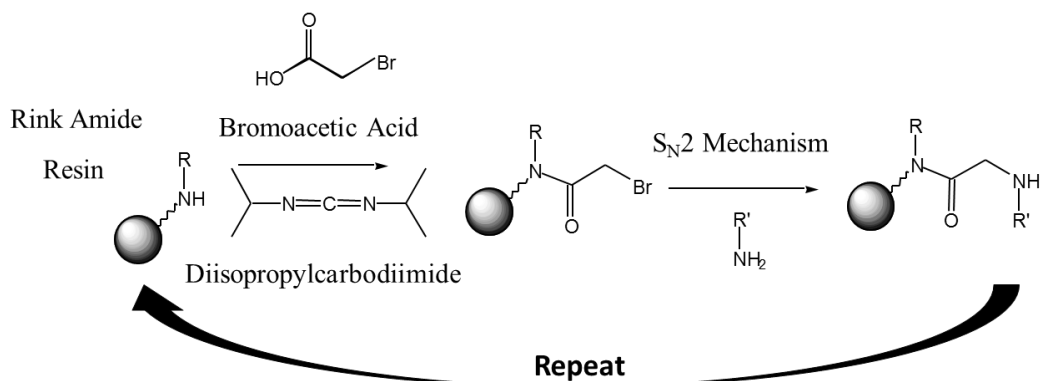


**Figure 1.5** Submonomer process of constructing peptoid scaffold.<sup>110</sup>

#### 1.8.4 Peptoids Biomimetics

Peptoids are ideal candidates that offer the development of new, interesting molecules that have vast functionality due to incorporation of near limitless side-chain possibilities.<sup>105</sup> The submonomer process has allowed for a rapid manufacturing process that is inexpensive.<sup>110</sup> Finally, peptoid secondary structure leads to tertiary structure functionality that are seen with peptides.<sup>106,115,116,122,125,126</sup> Peptoids have been proposed for use in a number of biomimicry proteins.<sup>118</sup> Biomimetic peptoids have been utilized for lung surfactant protein B and C, both of which have been considered suitable replacements for the natural lung surfactant of patients with respiratory distress syndrome.<sup>127-132</sup> Peptoids have also been designed to mimic the characteristics of antimicrobial agents to yield protease-resistant structures that have an increased bioavailability.<sup>107,108</sup> Researchers have also taken advantage of utilizing the protease-resistant characteristics of peptoids to create a lipid-peptoid structure for DNA transfer.<sup>133</sup> These structures hold promise as a potential replacement for traditionally used viruses in the transport of DNA to cells for undergoing gene therapy.<sup>133</sup> Finally, peptoid microspheres have been proposed as a means to improve slide coatings for disease detection via ELISA microarray.<sup>119,120</sup>

### 1.8.5 Peptoids in the Neurodegenerative Field

While peptoids offer several advantages over traditional peptidomimetics, only a small percentage have been shown to bypass the blood-brain barrier (BBB). This is a major concern with creating molecules intended to treat neurodegenerative diseases such as Huntington's disease (HD) and AD. To circumvent this problem, intranasal administration demonstrated the capability of peptoids to bypass the BBB. Specifically, CHIR5585 was delivered to the brain and spine by delivery through the olfactory bulb into the central nervous system (CNS) of five Harlan Sprague-Dawley rats.<sup>99</sup> CHIR5585 is an antagonist of the urokinase plasminogen activator receptor and was designed to have anti-tumor effects as seen previously with peptide variants.<sup>134,135</sup> Interestingly, even though peptoids are immune to proteolytic degradation, a high concentration of CHIR5585 was found in the kidneys of the rodents. This suggests the kidneys play a pivotal role in elimination of peptoids.

The development of diagnostics for the early detection of misfolded protein diseases (MFP) such as AD has been challenging. Typical reagents that are used for detection of MFP's, such as Thioflavin T and Congo Red, only detect larger aggregated species of MFPs. This is an issue in early detection of MFPs due to the smaller, oligomeric species believed to be the causative agent for neurodegeneration. To address this, peptoid ASR1 was developed as part of a diagnostic tool.<sup>136</sup> The positively charged ASR1 was designed to bind to the negatively charged epitope of MFP's, which is widely believed to be a common characteristic in cross  $\beta$ -sheets that are commonly associated with MFP's.<sup>136,137</sup> ASR1 was then used to demonstrate A $\beta$ 40 oligomers in CSF can serve as a biomarker for AD.<sup>138</sup>

Peptoid library screens are often used to target sequences with potential to specifically bind to proteins as a potential therapeutic agent. Chen *et al.* utilized a mutant Huntingtin protein (Htt-

N-82Q) to identify peptoid HQP09 from a library of 60,000 peptoids.<sup>139</sup> This 6mer peptoid showed promise at specifically binding to polyQ-expanded forms of mHtt.<sup>139</sup> HQP09 and a 4mer derivative (HQP09\_9) both showed promise at inhibiting aggregation of Htt-N-53Q *in vitro* and exerted Ca<sup>2+</sup> stabilizing effects in HD mice.<sup>139</sup> The HD mice had improved motor behavioral functions, suggesting these peptoids may hold promise as a therapeutic treatment of HD.

Developing peptide inhibitors to target A $\beta$  as a means to treat AD has been challenging due to proteolytic degradation. To address this pitfall, a peptoid was identified by utilizing an on bead peptoid library with biotinylated A $\beta$ 42 in the presence of 20-fold molar excess of A $\beta$ 40. The peptoid IAM1 was identified as a potential therapeutic peptoid to inhibit A $\beta$ 42 aggregation.<sup>140</sup> IAM1 was compared to ASR1 to determine capabilities of inhibiting A $\beta$ 42 and exhibited superior activity in terms of A $\beta$  inhibition. However, both IAM1 and its dimer (IAM1)<sub>2</sub> inhibition activity required a 10-fold excess or greater to inhibit A $\beta$ 40 or A $\beta$ 42 aggregation by more than 70%.

## 1.9 Purpose and significance of research

Peptide KLVFF analogs have shown incredible promise *in vitro* as a potential therapeutic treatment for AD.<sup>59,78,86,88–91</sup> However, proteolytic degradation of these analogs *in vivo* has been a major pitfall.<sup>94,141,142</sup> To capitalize on the benefits associated with the recognition element of A $\beta$ , we have synthesized a series of peptoid sequences based on the peptide KLVFF. Peptoids are ideal candidates as a therapeutic treatment for AD since they are proteolytically stable.<sup>105,143</sup> In this study, a series of peptoid sequences were examined for their effects as novel A $\beta$  aggregation modulators. Peptoid sequence (Chapter 3), helicity and side chain placement (Chapter 4), and peptoid charge (Chapter 5) were altered throughout the extent of this project to determine the effects on A $\beta$  aggregation, morphology, size, and species growth.

## Chapter 2 Methods and Improvements

### 2.1 Peptoid Synthesis

Peptoids were synthesized via a two-step process using an Applied Biosystems 433A automated peptide synthesizer (Carlsband, CA) that was refurbished from a 431A synthesizer.<sup>110</sup> Rink amide resin was swelled with dimethylformamide (DMF) and the Fmoc protecting group was removed using 20% piperidine in DMF. The secondary amine was acylated by adding 1.2 M bromoacetic acid (BAA) in DMF and diisopropylcarbodiimide (DIC) at a ratio of 5.3:1 and vortexing for 60 min. The resin was then drained and rinsed three times with DMF to remove all traces of BAA and DIC prior to addition of side chain amines. Side chain amines were added to the resin at a concentration of 8 M via an  $S_N2$  reaction mechanism for a period of 60 min and then drained and rinsed three times with DMF. Following this step, the acylation and displacement steps were repeated until the desired oligomer length was reached. The resin was then immersed in dichloromethane three times and allowed to dry under nitrogen flow for 10 min and then stored in the -20 °C freezer.

Towards the end of this research project, an improved process for synthesizing peptoids was discussed at the annual ACS meeting by Modi Wetzler.<sup>123</sup> Wetzler proposed decreased coupling time and reduction of reagent waste by utilizing manual addition of peptoid oligomers. For manual addition, peptoids were synthesized in Torviq propylene syringes (Niles, MI) as previously utilized by Kirshenbaum and colleagues.<sup>144</sup> Rink amide resin was swelled with DMF and the Fmoc protecting group was removed using 20% piperidine in DMF. The secondary amines were acylated by adding 0.4 M BAA in DMF and DIC at a ratio of 5.3:1 and mixing for 1 min. The resin was drained and rinsed three times with DMF to remove all traces of BAA and

DIC. Side chain amines were added to the resin at a concentration of 1 M via an  $S_N2$  reaction mechanism for a period of 1 min. The acylation and displacement steps were repeated until desired oligomer length was reached. Finally, resin was rinsed three times with dichloromethane and allowed to dry under vacuum for 10 min prior to storing in the  $-20\text{ }^\circ\text{C}$  freezer. Utilization of this new protocol allowed for rapid synthesis of peptoid oligomers and drastically reduced synthesis time from 16 h to 1 h per 8 side chain couplings while significantly reducing the cost and associated waste of reagents during synthesis.

The peptoid was removed from the resin by using a cleavage solution containing 95% trifluoroacetic acid (TFA), 2.5% water, and 2.5% triisopropylsilane for 5 min. The acid was removed using a Heidolph Laboraota 4001 rotating evaporator (Elk Grove Village, IL) and the peptoid was diluted to a  $3\text{ mg mL}^{-1}$  solution of acetonitrile-water for purification.

## **2.2 Peptoid Purification**

Peptoids were purified using a Waters Delta 600 preparative high performance liquid chromatography unit (HPLC; Milford, MA) with a Duragel G C18 150 x 20 mm column (Peeke Scientific, Novato, CA). Gradients were run at  $\sim 1\%$  per minute with 5-95% solvent B in A (solvent A: water, 5% acetonitrile, 0.1% TFA; solvent B: acetonitrile, 5% water, 0.1% TFA).

During the early stages of this research project, all peptoids were dissolved in a 50:50 acetonitrile:water solution to a concentration of  $3\text{ mg mL}^{-1}$ . Early peptoid sequences designed did not have any issues regarding purification when dissolved in a 50:50 acetonitrile:water solution. However, it was discovered that peptoid charge, polarity, hydrophobicity, and hydrophilicity greatly impact ease of purification. Failed purification runs typically resulted in a high

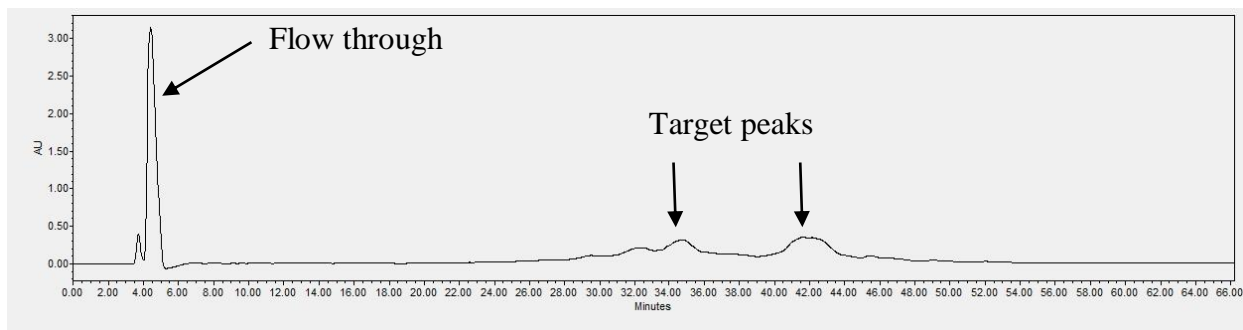


**Figure 2.1** Purification of a peptoid that did not properly bind to the C18 column. The peptoid eluted in the solvent flow through and resulted in decreased target peaks.

absorbance on the 214 nm wavelength in the solvent flow through with decreased absorbance for target peak (Figure 2.1). To improve peptoid purification, careful care was taken to prepare and degas solvents, equilibrate the C18 HPLC column, and clean the injection loop. To load peptoids onto the C18 column, the crude peptoids were dissolved in a solution containing 5-95% acetonitrile with the remaining solution consisting of deionized (DI) water at  $3 \text{ mg mL}^{-1}$ . The percent acetonitrile used to dissolve the crude peptoids were determined by analytical RP-HPLC of the crude peptoids. These steps helped ensure proper binding to the preparative HPLC C18 column prior to purification. This resulted in improved purification (Figure 2.2).

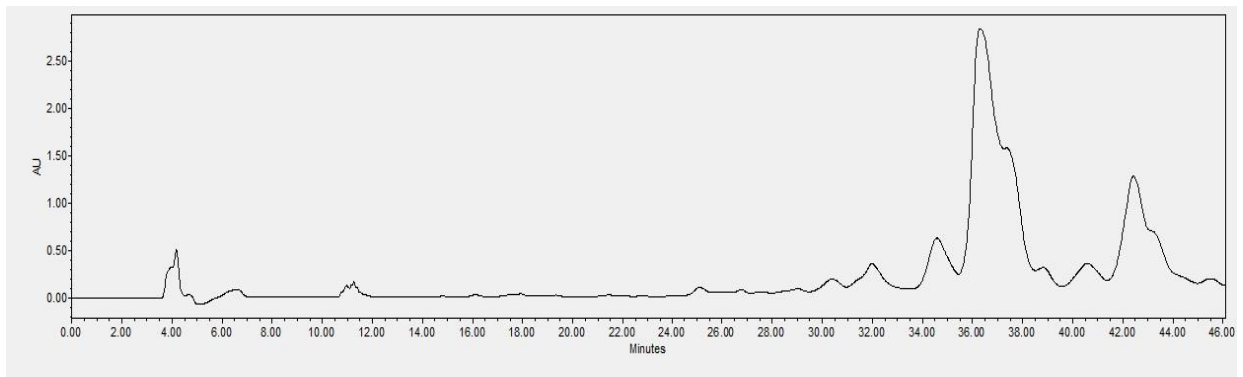


**Figure 2.2** Purification of peptoid that properly bound to the C18 column. Proper care of the HPLC system and C18 column along with dissolving the peptoid in the proper percentage acetonitrile allowed for improved purification.

### **2.3 Characterization of Peptoid Mass and Purity**

Peptoids were characterized via matrix-assisted laser desorption/ionization time of flight (MALDI-TOF) mass spectrometry and analytical HPLC. MALDI-TOF mass spectrometry was used to confirm that the purified peptoid mass matched the theoretical mass. Peptoids were mixed with 2,5-dihydroxy benzoic acid to allow for the co-crystallization of molecules onto the target plate. To confirm peptoids were >98% pure, purified peptoids were injected onto a Waters 2695 Separation Module equipped with a Duragel G C18 150 x 2.1 mm column (Peeke Scientific) using a linear gradient of 3 % per min. Gradients were 5 to 95 % solvent D in C (solvent D: acetonitrile, 0.1% TFA; solvent C: water, 0.1% TFA) over 30 min.

### **2.4 Analysis of Peptoid Secondary Structure via Circular Dichroism**

Peptoid secondary structure was confirmed via circular dichroism (CD) spectrometry analysis via a Jasco J-710 instrument (Easton, MD). Polyproline type-I like helix peptoid secondary structure exhibits two minima (205 and 220 nm, respectively) and a maxima (190 nm). Though peptoids do not contain a chiral backbone, the chiral centers of the side chains elicits the signal detected by CD. CD was operated using a scanning speed of 20 nm min<sup>-1</sup> at room temperature with a path length of 0.1 cm. All peptoids were measured at 100-120 μM concentration and CD spectra is the cumulative of 20 scans.

Characterization of peptoids via CD spectra allowed for all peptoids to be compared to know polyproline type-I-like CD spectra signals. Peptoids that resemble a peptide  $\alpha$ -helix have a CD spectra with a maxima at 190 nm and two minima at 205 and 220 nm.<sup>118-120</sup>

## 2.5 A $\beta$ 40 Monomer Purification

A $\beta$ 40 aggregation studies can vary widely depending on several factors, including the method of purification of the monomeric species. A $\beta$ 40 purchased from Anaspec, Inc. and other reputable peptide companies must be properly processed before aggregation studies can be initiated. If proper steps are not taken prior to aggregation studies, small aggregates may be present at the beginning of the assays that will affect aggregation kinetics. Two methods have been considered suitable for A $\beta$  monomer purification: (1) size exclusion chromatography (SEC) and (2) organic dissolution.

SEC purified monomer has long been believed to be considered the prime monomer purification method for A $\beta$ 40. SEC was performed on an AKTA Fast Protein Liquid Chromatography (FPLC) system that utilized a Superdex 75 10/300 GL column (GE Healthcare). Prior to monomer purification, the Superdex 75 column was rinsed with deionized (DI) water at a flowrate of 0.5 mL min<sup>-1</sup> for 60 min. The Superdex 75 column was then equilibrated with 40 mM Tris-HCl (pH 8.0) at a flowrate of 0.5 mL min<sup>-1</sup> for 60 min. To prevent the chance of nonspecific interactions with A $\beta$ 40 and the column matrix on the Superdex 75, the column was pre-treated with 2 mg/mL BSA dissolved in 40 mM Tris-HCl (pH 8.0) buffer prior to injection of solubilized A $\beta$ 40. A flowrate of 0.5 mL min<sup>-1</sup> using 40 mM Tris-HCl (pH 8.0) elution buffer for 60 min. To initiate the purification, A $\beta$ 40 peptide was re-suspended from a lyophilized state at a 2 mg/mL concentration in 50 mM NaOH to dissociate preformed aggregates. Monomer purification was performed using 40 mM Tris-HCl (pH 8.0) at a flowrate of 0.5 mL min<sup>-1</sup> for 60 min. Fractions were continuously collected throughout the run for 1 min intervals. Two significant peaks are noticed within the elution profile, an aggregate peak (8-10 mL) containing A $\beta$ 40 aggregates, followed by the monomer peak which elutes at 12-15 mL (Figure 1). The



fractions of eluted monomer were immediately analyzed using an ND-1000 Nanodrop Spectrophotometer to determine fraction concentration (277 nm,  $\epsilon = 1450 \text{ M}^{-1} \text{ cm}^{-1}$ ). Purified monomeric A $\beta$ 40 was stored at 4 °C for no longer than 5 days.

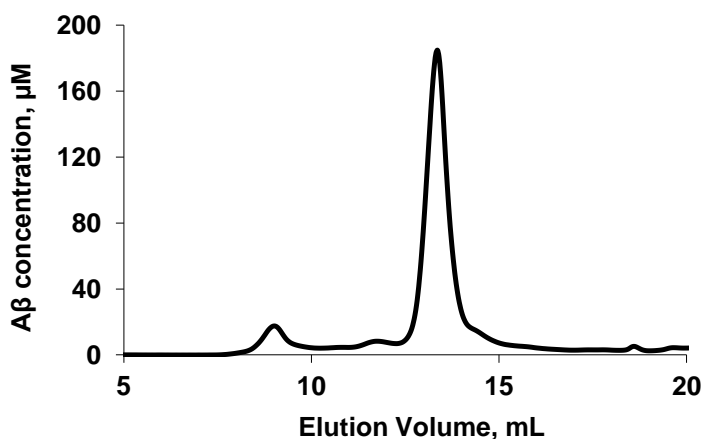


**Figure 2.3** A $\beta$ 40 monomer monomeric species is separated from larger aggregates using SEC on a Superdex 75 10/300 GL column. A $\beta$ 40 aggregates elute from the column at 8-10 mL, while A $\beta$ 40 monomer elutes between 12-15 mL.

Organic dissolution of A $\beta$ 40 is typically performed overnight to yield peptide films. To initiate this process, lyophilized A $\beta$ 40 was re-suspended in cold HFIP so that the final concentration of A $\beta$ 40 was 1 mM on ice for 60 min. Careful precautions must be taken to ensure A $\beta$ 40 solution is 1 mM. Reputable companies typically sell A $\beta$  in 1 mg vials. However, it was determined during the extent of this project that provided peptide content is needed to properly calculate and create a 1 mM solution of A $\beta$  in HFIP. After incubation, the peptide solution was aliquoted into individual non-siliconized micro-centrifuge tubes and left overnight at room temperature in the fume hood to evaporate and create thin peptide films. Once dry, peptide films were stored desiccated at -80 °C until use or for no longer than 12 months. Prior to experimentation, peptide films were rehydrated in 5 mM NaOH for 5 min followed by incubation in 40 mM Tris-HCl (pH 8.0) for 10 min. Following incubation, appropriate levels of

NaCl and inhibitor or DMSO (positive control) was added to yield a final working concentration of 20  $\mu$ M A $\beta$ 40.

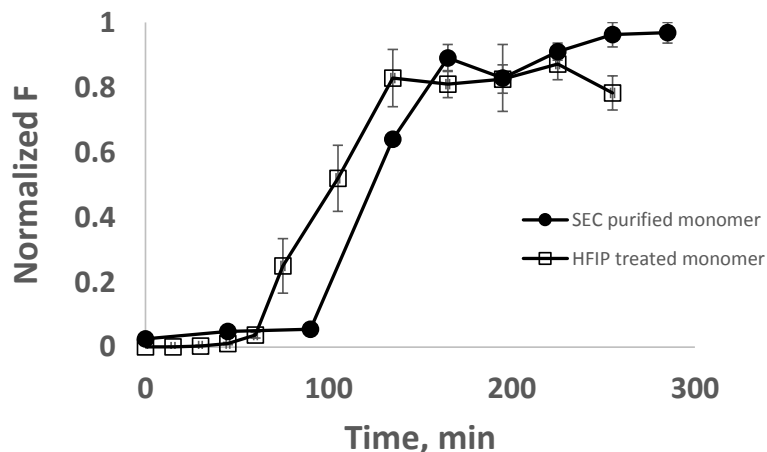


**Figure 2.4** Comparison of the two methods of preparation for A $\beta$ 40 monomer from dried peptide. SEC purified monomer yields a lag time of 90 min with a plateau phase ranging from 165 to 285 min, while the HFIP treated monomer yields a lag time of 60 min with a plateau phase ranging from 135 to 255 min.

As previously mentioned, it is widely believed that SEC purified A $\beta$ 40 monomer is the best method of preparation. However, one of the major downfalls to this method is the potential for varied product lots purchased from various peptide companies. Varied product lots increase the chance of purchasing a non-aggregating lot following SEC. The preparation of A $\beta$ 40 monomer via 1,1,1,3,3,3-Hexafluoro-2-propanol (HFIP) treatment allows a more consistent aggregation to occur from lot to lot, but is widely considered to give a reduced lag and plateau phase. This is most likely due to the increased presence of intermediates within HFIP treated A $\beta$ 40. Figure 2 compares the two methods of preparation for A $\beta$ 40 monomer. Lag time for the SEC purified monomer method is typically around 90 min with a plateau phase extending from 165 to 285 min. For the HFIP treated monomer method, lag time is decreased to 60 min and the plateau phase is from 135 to 255 min. Both methods yield reproducible results and allow for purified A $\beta$ 40 monomer to be easily obtained.

## **2.6 A $\beta$ 42 Monomer Preparation**

To prepare A $\beta$ 42 monomer, lyophilized A $\beta$ 42 was re-suspended in cold HFIP so that the final concentration of A $\beta$ 42 was 1 mM on ice for 60 min. To accurately ensure A $\beta$ 42 solution is 1 mM, purchased peptide weight was multiplied by the peptide content percentage to yield the actual weight of peptide minus the residual salt. After incubation, the peptide solution was aliquoted into individual non-siliconized micro-centrifuge tubes and left overnight at room temperature in the fume hood to evaporate and create thin peptide films. Once dry, peptide films were stored desiccated at -80 °C until use or for no longer than 12 months. Peptide films yield a 20  $\mu$ M A $\beta$ 42 solution with a total volume of 400  $\mu$ L when re-suspended prior to experiments. Prior to experimentation, peptide films were rehydrated in 5 mM NaOH for 5 min followed by incubation in 40 mM Tris-HCl (pH 8.0) for 10 min to help facilitate aggregates were unfolded. Following incubation, appropriate levels of inhibitor or DMSO (positive control) and NaCl (5-150 mM) was added to yield a final working concentration of 20  $\mu$ M A $\beta$ 42. The concentration of NaCl utilized during aggregation assays helped control the rate of A $\beta$  aggregation.

## **2.7 Preparation of A $\beta$ 40 Fibrils**

A $\beta$ 40 fibrils were prepared from SEC purified A $\beta$ 40 monomer. Fibrils were formed by agitating purified 50  $\mu$ M A $\beta$ 40 monomer in 40 mM Tris-HCl (pH 8.0) at 800 RPM on an orbital shaker at 25 °C for 20 hours in the presence of 250 mM NaCl. Fibrils were then separated via centrifugation at 15,000 RPM for 15 min until a visible pellet was observed. The fibril pellet was removed from solution and resuspended in 40 mM Tris-HCl (pH 8.0) at a concentration of 50  $\mu$ M that was calculated from the fraction of pelleted protein. Fibrils were stored at 4 °C for no longer than 5 days.

## **2.8 A $\beta$ Monomer Aggregation**

A $\beta$  (40 or 42 amino acid versions) monomer aggregation was carried out by aggregating 20  $\mu$ M SEC or HFIP purified A $\beta$  monomer in NaCl (5-150 mM), 40 mM Tris-HCl (pH 8.0), and 5 mM NaOH (HFIP treated monomer only). A $\beta$  monomer was incubated alone (positive control) or in the presence of peptoid inhibitors (experimental samples). Reactions were incubated at room temperature (25 °C) and agitated at 800 RPM on an orbital shaker. Total reaction volume was 400  $\mu$ L throughout all experiments.  $\beta$ -sheet or fibrillar content was used to assess the extent of aggregation via ThT fluorescence or dot blot analysis. Experiments were carried between 4-37 hours and were considered complete for all samples when an observed drop in ThT fluorescence from the control was observed.

## **2.9 Analysis of A $\beta$ Monomer Aggregation with ThT**

Fluorescence measurements were taken periodically to assess the extent of monomer aggregation. Measurements were recorded by taking a 25  $\mu$ L aliquot of A $\beta$  monomer and combining with 175  $\mu$ L of 14.29  $\mu$ M ThT. ThT is a benzathiole dye that has been shown extensively to bind to  $\beta$ -sheet rich structures of amyloid aggregates. Fluorescence measurements were taken on a Shimadzu RF-150 mini fluorometer (excitation at 440 nm  $\pm$  10 nm and emission at 490 nm  $\pm$  10 nm) with an average scan time of 4 seconds. Raw fluorescence values were subtracted from the ThT baseline (ThT alone) to yield the corrected fluorescence values. Fluorescence measurements are then normalized to the control to analyze quantitatively and plotted normalized F versus time.

Early work focused on optimizing assay conditions. Early work demonstrated the importance of the molar ratio of ThT to A $\beta$  monomer. The volume and concentrations of ThT and A $\beta$

monomer could be altered, though increasing A $\beta$  monomer (40 or 42 residue variants) concentration above 50  $\mu$ M would drastically reduce lag time to  $\beta$ -sheet formation. However, it was determined that there was an optimum molar ratio of ThT to A $\beta$  monomer that was required to ensure proper binding of ThT to  $\beta$ -sheet aggregates that would allow for a detectable increase in fluorescence. This molar ratio of ThT to A $\beta$  monomer is 5:1.

Proper care had to be taken assays to ensure experiments were repeatable and consistent. During A $\beta$  monomer aggregation on the orbital shaker, large aggregates can fall out of solution and settle on the bottom of the reaction vial (Figure 2.5). Improper pipetting techniques such as drawing the solution from the bottom will result in increased fluorescence signals, increased immunoblotting signal intensity, and false positive results when studying morphology. To ensure consistency, care should be taken to gently mix the solution prior to removing sample for ThT fluorescence measurement. Samples for measurement should only be drawn from the top of the sample solution.

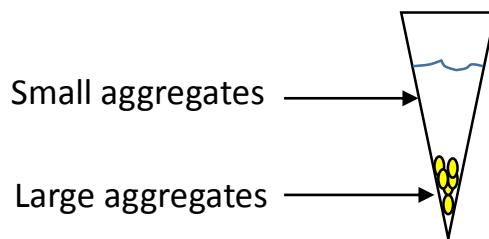


**Figure 2.5** Representation of how larger aggregates settle at the bottom of the reaction vial during agitation. Prior to removing sample for ThT fluorescence measurement, samples should be gently mixed and immediately removed from the vial by drawing aliquot from the top of the sample solution.

## 2.10 Analysis of A $\beta$ Monomer Aggregation by Dot Blot

To corroborate the measured extent of aggregation confirmed by ThT fluorescence, dot blot analysis was used. A 2  $\mu$ L sample was removed from each reaction and at designated times was spotted onto a 0.1  $\mu$ m nitrocellulose membrane (GE Healthcare), and allowed to dry for 15 min.

The nitrocellulose membrane was blocked in 5% non-fat milk solution in Tris Buffered Saline with Tween (TBS-T) at 4 °C until the aggregation was complete. Membranes were washed three times with TBS-T and then incubated with either primary antibody 6E10 (1:2000 dilution), primary antibody OC (1:5000 dilution), or primary antibody LOC (1:5000 dilution) for 1 hour at room temperature with gentle agitation. Membranes were washed three times with TBS-T. Protein detection for bound 6E10, OC, and LOC antibodies was performed by binding alkaline phosphatase-conjugated anti-mouse IgG (1:2000 dilution) or alkaline phosphatase-conjugated anti-rabbit IgG (1:3000 dilution), respectively, for 1 hour at room temperature with gentle agitation. Dot blots were developed using Nitro blue tetrazolium and 5-Bromo-4-chloro-3-indolyl phosphate in TBST-MgCl<sub>2</sub> until precipitate from the reaction was no longer forming. The developing reaction was halted by a 10% acetic acid solution. Dot blots were immediately imaged using a Canon CanoScan 9000F (Tokyo, Japan). Blots were analyzed using imageJ software provided by the NIH. Density values for each dot were calculated and then normalized to the control for comparison between blots and experiments.

## **2.11 Analysis of A $\beta$ Monomer Aggregation**

To evaluate the inhibition capabilities of peptoids, A $\beta$  aggregation in the presence or absence of all peptoids were quantitatively compared to the positive control of each reaction. Lag extension, which is the time period before an observed increase in signal (ThT fluorescence or OC detection) indicates the ability of an inhibitor to slow or accelerate nucleation. Lag time is defined as the period prior to an exponential signal increase for the sample. Lag extension was calculated as the ratio for the experimental sample (tE) relative to that of the control (tC) (Equation 2.1, Figure 2.6). A lag extension >1 indicated an inhibitor slows nucleation, whereas a lag extension 1< indicates an inhibitor accelerates nucleation.

$$LE = \frac{tE}{tC} \quad \text{Equation 2.1}$$

Reduction of fluorescence in the plateau phase, which occurs at the end of the aggregation reaction when all A $\beta$  species are in equilibrium with each other, indicates the ability of an inhibitor to decrease either the quantity of aggregates containing  $\beta$ -sheet structures (ThT fluorescence) or fibrillar aggregates (OC dot blot analysis). Percent inhibition was calculated as the percentage decrease in the average plateau signal observed for each experimental inhibitor (SE) compared to that observed with the control (SC) (Equation 2.2, Figure 2.6). A positive percent inhibition indicates that an inhibitor reduces either  $\beta$ -sheet or fibrillar aggregates.

$$\% \text{ Inhibition} = \frac{SC - SE}{SC} * 100\% \quad \text{Equation 2.2}$$

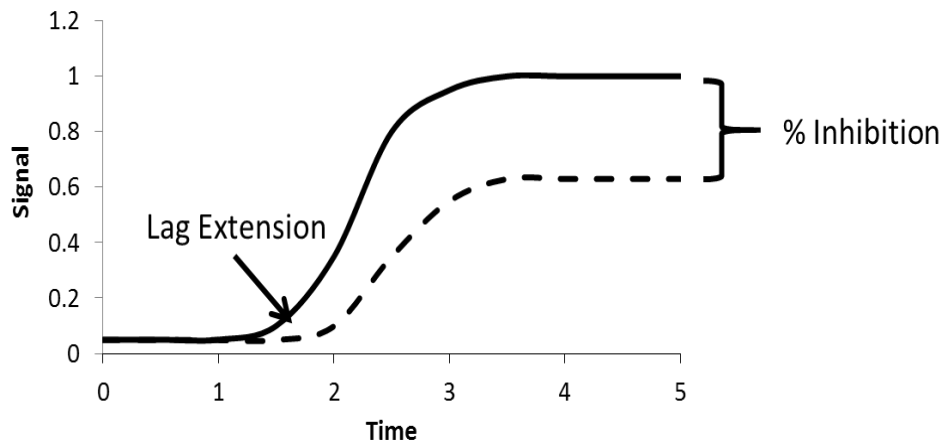


**Figure 2.6** Schematic representation of lag extension and percent inhibition of control (solid line) versus inhibitor (dash line).

## **2.12 Transmission Electron Microscopy**

Monomer aggregation reactions were gridded for Transmission Electron Microscopy (TEM) at various time points in the presence and absence of peptoids to monitor changes in A $\beta$  morphology. A 3  $\mu$ L sample was inverted onto a 300 square mesh formvar-carbon supported nickel grid. After 1 min, the sample was wicked away from the side of the grid using a piece of filter paper. Gridded samples were then inverted onto 3  $\mu$ L of 2% aqueous uranyl acetate for 45 seconds. Excess stain was wicked away from the side with a piece of filter paper. Grids were allowed to dry for a minimum of 24 h prior to imaging. Imaging was performed using a JEOL JEM-1011 TEM (JEOL Ltd., Tokyo, Japan) with an accelerating voltage of 100 kV.

## **2.13 Atomic Force Microscopy**

Monomer aggregation reactions were incubated onto a substrate for Atomic Force Microscopy (AFM) at various time points to monitor changes to A $\beta$  species in the presence and absence of peptoids. A 20  $\mu$ L sample was placed on ruby muscovite mica for a period of 10 min and then rinsed three times with 0.2  $\mu$ m filtered distilled water. After rinsing, substrates were gently dried under nitrogen for 3 h. Imaging was performed using a Bruker AFM Dimension 3100 (Billerica, MA) and HQ:NSC15/AL BS tip probes (MikroMasch USA; Lady's Island, SC). Scan area was 5  $\mu$ m x 5  $\mu$ m and the scan rate was set at 1.0 Hz. Analysis was performed using Nanoscope Software 5.1.



## Chapter 3 Rationally Designed Peptoids Modulate Aggregation of Amyloid-Beta 40

Reprinted with permission from *ACS Chem. Neurosci.*, **2014**, 5 (7), pp 552–558 DOI: 10.1021/cn400221u Publication Date (Web): April 1, 2014 Copyright © 2014 American Chemical Society

### Abstract

Alzheimer's disease (AD) is the most common form of dementia and the sixth leading cause of death in the United States. Plaques comprised of aggregated amyloid-beta ( $A\beta$ ) accumulate between neural cells in the brain and are associated with dementia and cellular death. Many strategies have been investigated to prevent  $A\beta$  self-assembly into disease-associated  $\beta$ -sheet amyloid aggregates; however, a promising therapeutic has not yet been identified. In this study, a peptoid-based mimic of the peptide KLVFF (residues 16-20 of  $A\beta$ ) was tested for its ability to modulate  $A\beta$  aggregation. Peptoid JPT1 includes chiral, aromatic side chains to induce formation of a stable helical secondary structure that allows for greater interactions between the aromatic side chains and the cross  $\beta$ -sheet of  $A\beta$ . JPT1 was found to modulate  $A\beta$ 40 aggregation, specifically decreasing lag time to  $\beta$ -sheet aggregate formation as well as the total number of fibrillar,  $\beta$ -sheet structured aggregates formed. These results suggest that peptoids may be able to limit the formation of  $A\beta$  aggregates that are associated with AD.

### 3.1 Introduction

Alzheimer's disease (AD) is the most prevalent form of dementia worldwide and is a leading cause of death among the elderly population.<sup>3</sup> AD is a neurodegenerative disorder that is classified by the build-up of aggregated amyloid-beta protein ( $A\beta$ ) as plaques in the brain, which are associated with cellular death and dementia.  $A\beta$  is generated as a result of proteolytic cleavage of the amyloid precursor protein and is typically 40 or 42 amino acid residues long

(A $\beta$ 40 and A $\beta$ 42, respectively).<sup>3</sup> Though the specific mechanism that causes AD is not clear, the deposition of aggregated A $\beta$  in the brain and the formation of tau tangles within neuronal cells are closely associated with disease progression.<sup>3</sup> A $\beta$  monomer typically has a random coil secondary structure, but in the case of AD it forms fibrils with a cross- $\beta$ -sheet pattern that ultimately deposit as plaques around the neural cells.<sup>27</sup> Amyloid plaques were originally thought to be directly involved in cellular death; however, recent studies suggest that smaller soluble oligomeric aggregates are the toxic species.<sup>30,45,46</sup>

While there is currently no cure for AD, many groups are working to develop small molecules and peptides that inhibit A $\beta$  aggregation. One such group of peptides is based upon KLVFF (residues 16-20 of A $\beta$ ), which was first identified by Tjernberg et al. and serves as the key recognition element that allows for aggregation due to hydrophobic interactions.<sup>86,87</sup> Variants of the peptide KLVFF bind to A $\beta$  and inhibit aggregation *in vitro*.<sup>59,85,87-90</sup> However, as with all peptides, KLVFF variants are rapidly degraded *in vivo* and have low bioavailability.<sup>141</sup>

In order to increase bioavailability, we are utilizing poly-N-substituted glycines (peptoids) to mimic the peptide KLVFF. Peptoids are a novel class of peptidomimetics that are resistant to protease degradation.<sup>97</sup> Peptoids are similar in structure to peptides, but with the side chain appended to the amide group rather than the  $\alpha$ -carbon.<sup>110</sup> This change in location of the side chain group leads to a lack of backbone chirality and hydrogen bond donors, both of which are required for secondary structure formation in peptides.<sup>110-112</sup> However, the inclusion of chiral side chains in the peptoid sequence leads to the formation of helical secondary structure.<sup>106,113-116,122</sup> Peptoids that include chiral, aromatic side chains form polyproline type-I-like helices with as little as five monomers.<sup>106</sup> Peptoid helices have a periodicity of three monomers per turn and exhibit a helical pitch of  $\sim 6$  Å.<sup>106</sup> Because peptoid helices are stabilized by steric interactions

rather than hydrogen bonds, they are stable under extreme conditions including 8 M urea at 70 °C.<sup>122</sup> The bioavailability of peptoids is favorable compared to peptides due to the change in backbone structure, which results in proteolytic stability and improved promise as a therapeutic.<sup>97</sup> Furthermore, peptoids can be synthesized using automated, solid-phase equipment via a two-step process.<sup>110</sup> Because the side chain group is added through the addition of a free amine, there are a multitude of available chemistries that can be included.<sup>105,110</sup>

Peptoids have only recently gained momentum for use as therapeutics and detection agents in protein misfolding diseases. The peptoid ligand HQP09 specifically binds to expanded polyglutamine proteins to inhibit aggregation of Htt-N-53Q *in vitro* and shows promise for the treatment of Huntington's disease (HD) by exerting Ca<sup>2+</sup> stabilizing and neuroprotective effects in HD mice.<sup>139</sup> The peptoid IAM1 and its dimer have been shown to selectively bind to both A $\beta$ 40 and A $\beta$ 42, as well as to inhibit A $\beta$  aggregation.<sup>140</sup> Peptoids have also been used to create an AD blood test that senses antibodies produced specifically in AD patients.<sup>136</sup> Peptoids are ideal therapeutic candidates for protein misfolding diseases, such as AD, due to increased bioavailability compared to peptides<sup>97,105</sup> and improved membrane permeability compared to small molecules.<sup>97,143,145</sup> In the present study, a novel peptoid-based mimic of the peptide KLVFF is reported to modulate A $\beta$ 40 aggregation.

## **3.2 Results and Discussion**

### *3.2.1 Peptoid Sequence, Rationale, and Characterization*

The pentapeptide KLVFF is known to be the minimum sequence required to bind to A $\beta$ 40.<sup>86</sup> The peptide KLVFF was later shown to stereospecifically bind to the homologous sequence in A $\beta$  via hydrophobic and electrostatic interactions.<sup>87</sup> As a result, a five residue peptide with a proline point substitution (LPFFD, iA $\beta$ 5) was designed to inhibit A $\beta$  aggregation by interfering

with A $\beta$  self-assembly.<sup>92,93</sup> However, iA $\beta$ 5 is susceptible to proteolytic degradation and has low bioavailability.<sup>94,141,142</sup> In order to reduce proteolytic degradation and increase blood-brain permeability, the N-terminus of the peptide was acetylated and the C-terminus was modified with an amide group (iA $\beta$ 5p).<sup>94</sup> While this chemical modification reduced the extent of proteolytic degradation, the ability of the peptide to inhibit A $\beta$  aggregation was also decreased.<sup>142</sup> Here, we propose to use a protease-resistance, peptoid-based mimic of KLVFF to modulate the aggregation of A $\beta$ . The peptoid JPT1 (Figure 3.1A) was designed to have a sequence similar to that of the peptide KLVFF. The sequence of JPT1 is KIIFFIFF, in terms of corresponding amino acids. This peptoid was designed to exhibit helical secondary structure such that the aromatic F groups align on two faces of the helix with  $\sim 6$  Å spacing between. The spacing between the F groups on the face of the helix corresponds to the spacing between backbone carbons  $i$  and  $i+2$  in a  $\beta$ -sheet, and may facilitate pi-pi stacking between the aromatic groups within the peptoid and A $\beta$  aggregates. In order to induce helical secondary structure in the peptoid, the aliphatic L and V groups have been replaced with the chiral I-like group and the aromatic F groups have been replaced with a chiral F-like group. An additional helical turn, composed of chiral I-like and F-like groups, was added at the C-terminus to create a more robust helical structure and to allow for more potential interactions between the aromatic side chains and A $\beta$  aggregates.

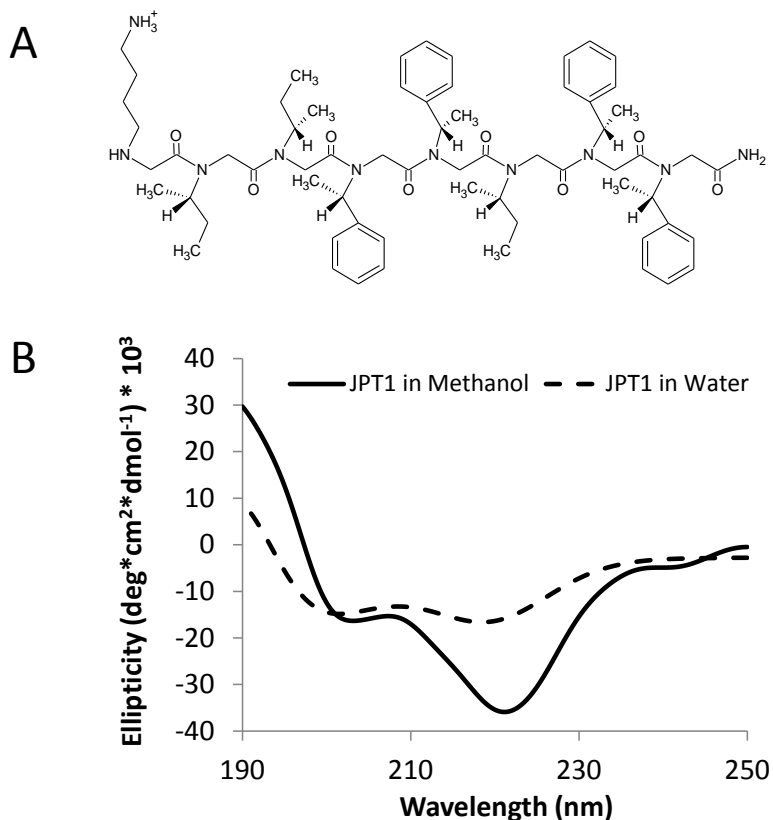


**Figure 3.1** Structure and characterization of peptoid JPT1. (A) Chemical structure of JPT1. (B) Circular dichroism spectra for JPT1. The spectra depict a polyproline type-I-like helical secondary structure.

The secondary structure of JPT1 was determined via circular dichroism (CD). The CD spectra for JPT1 (Figure 3.1B) in both methanol and water resemble that of a peptide  $\alpha$ -helix. This corresponds to a polyproline type-I-like helix for peptoids.<sup>106</sup> Specifically, the CD spectra exhibited a characteristic maximum near 190 nm and two minima near 205 and 220 nm.<sup>106,113,115,116</sup> In methanol, the increased intensity of the peak near 220 nm as compared to the peak near 205 nm indicates that the helical secondary structure is more stable.<sup>114</sup> In water, JPT1 continues to depict a polyproline type-I-like helical structure, though the helical structure is more loosely formed than in methanol.

### 3.2.2 Aggregation Studies

Thioflavin T (ThT) binds to  $\beta$ -sheet-rich structures to yield a shifted and enhanced fluorescent signal. As a result, it can be used to selectively detect  $\beta$ -sheet aggregates of A $\beta$ . Since inhibitors often also work by binding to A $\beta$  they have the potential to disrupt the binding of ThT to aggregate structure, which can render false positive results. Thus, it is important to first evaluate whether peptoid JPT1 competes for binding sites with ThT. A competitive ThT binding assay was performed by adding 12.5  $\mu$ M JPT1 to a solution of preformed 2.5  $\mu$ M A $\beta$ 40 fibrils and incubating for 15 min. These concentrations are representative of those within diluted samples used for ThT measurements. ThT fluorescence results show no significant competitive binding for JPT1 (Figure 3.2), confirming that ThT detection of A $\beta$  aggregates within the aggregation reaction will yield reliable results. Likewise, no ThT signal was observed when JPT1 was incubated alone, eliminating the possibility of aberrant interactions between the peptoid and ThT (Figure 3.3).

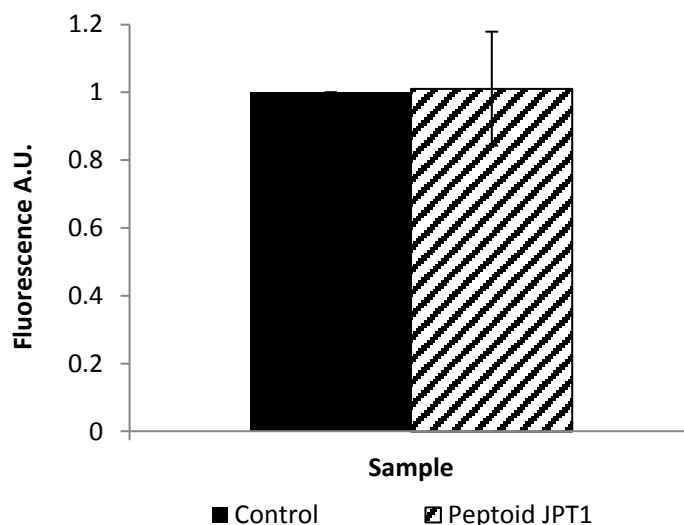


**Figure 3.2** JPT1 does not compete competitively with ThT for binding of fibrillar A $\beta$ . 2.5  $\mu$ M A $\beta$ 40 fibrils were incubated for 15 min with 10  $\mu$ M ThT in the presence and absence of 12.5  $\mu$ M JPT1, and ThT fluorescence was measured following gentle mixing. Parameters are expressed as mean $\pm$ SEM, n = 3.

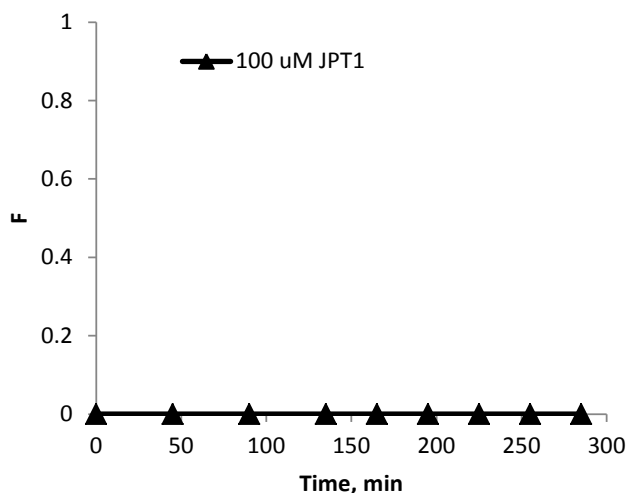


**Figure 3.3** ThT analysis shows that peptoid JPT1 does not aggregate in the absence of A $\beta$ 40. The presence of  $\beta$ -sheet aggregates was detected by ThT fluorescence. Aggregation assays were in 40 mM Tris-HCl (pH 8.0) and 150 mM NaCl. Peptoid JPT1 was dissolved in DMSO and added at 100  $\mu$ M such that the final DMSO concentration was 1.25% (v/v). Assays were performed at 25  $^{\circ}$ C under agitation on an orbital shaker at 800 RPM.

Aggregation assays were used to assess the ability of the peptoid JPT1 to modulate A $\beta$ 40 aggregation.<sup>57</sup> Assays were performed with 20  $\mu$ M purified A $\beta$ 40 monomer in the absence (control) and presence of JPT1 at concentrations of 20, 50, 100, and 200  $\mu$ M. Aggregation was initiated via agitation on an orbital shaker. ThT fluorescence measurements (excitation at 440 $\pm$ 10 nm and emission at 490 $\pm$ 10 nm) were taken every 30 to 45 min to monitor aggregate formation. In the absence of peptoid, A $\beta$ 40 aggregation exhibited a lag time, the time at which ThT fluorescence begins to increase, followed by a rapid growth, and ending in a plateau, the point where the ThT fluorescence no longer increases and aggregates are in equilibrium with monomer (Figure 3). In the presence of peptoid JPT1 the lag time is shortened, indicating a more rapid formation of aggregates, and the plateau intensity is reduced, indicating the formation of fewer  $\beta$ -sheet aggregates at equilibrium (Figure 3.4). To quantify these effects, a lag extension is calculated as the ratio of the lag time to that of the control and a plateau reduction is calculated as the percentage decrease in the plateau fluorescence as compared to the control. A lag

extension less than one was observed for all concentrations of JPT1, indicating that A $\beta$ 40 aggregates are forming more quickly in the presence of the peptoid (Figure 3.4). Further, a dose-dependence was observed up to 100  $\mu$ M, where ThT fluorescence was increased at the first data point taken. A dose dependence was also observed for reduction of the equilibrium plateau, with inhibition increasing from 46.5 $\pm$ 4.9% to 81.2 $\pm$ 4.4% as the peptoid concentration is increased from 20 to 100  $\mu$ M JPT1 (Figure 3.4). Higher concentrations exhibited similar inhibition to 100  $\mu$ M JPT1, indicating that saturation of the inhibitory effect was achieved.

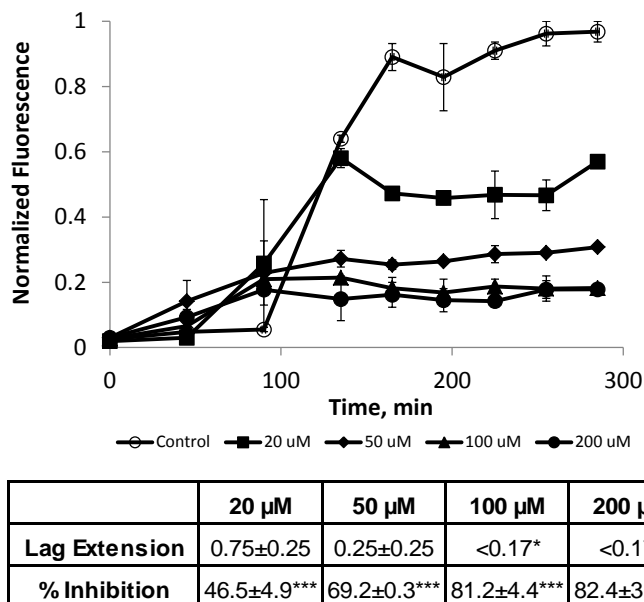


**Figure 3.4** ThT analysis shows that peptoid JPT1 modulates A $\beta$ 40 aggregation. JPT1 decreases lag time to A $\beta$ 40 aggregation and decreases the quantity of  $\beta$ -sheet aggregates formed. JPT1 was added to 20  $\mu$ M A $\beta$ 40 monomer at concentrations of 0 (control), 20, 50, 100, and 200  $\mu$ M and the presence of fibrillar aggregates was detected by ThT fluorescence. Normalized fluorescence values are calculated as a percentage of the control plateau. Lag extension, or the fold decrease in lag time, and percent inhibition, or percentage decrease in the plateau, are shown below the graph. Parameters are expressed as mean  $\pm$  SEM, n =2.\*p < 0.05; \*\*\*p < 0.0001.

### 3.2.3 Dot Blot Analysis.

Dot blot analyses were performed in conjunction with ThT fluorescence measurements to confirm the presence of the fibrillar species of A $\beta$ 40, as detected by a conformation-specific



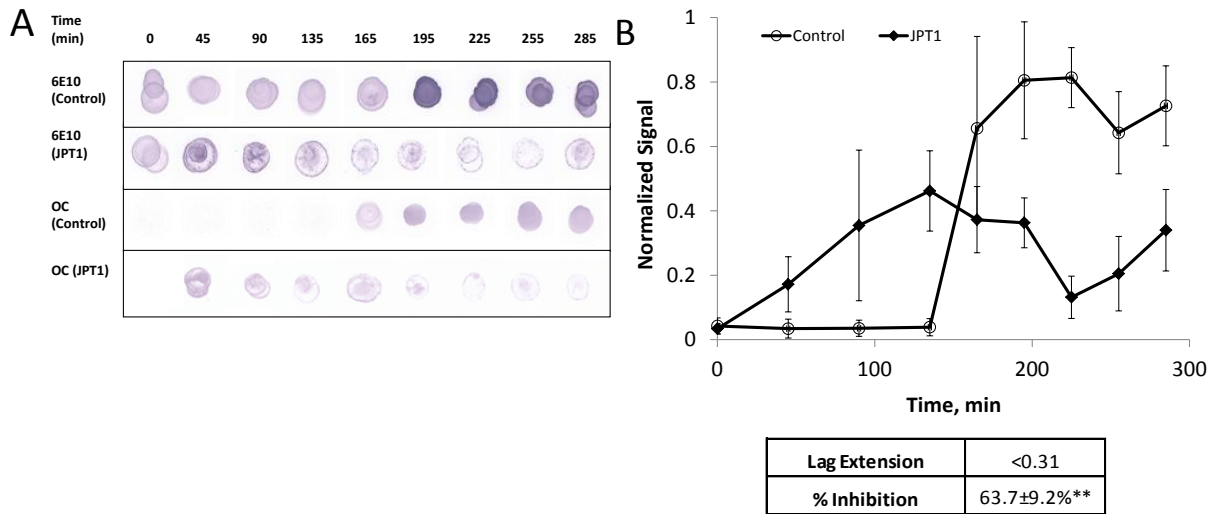


**Figure 3.5** Dot blot analysis shows that peptoid JPT1 modulates A $\beta$ 40 aggregation. JPT1 decreases lag time to A $\beta$ 40 aggregation and decreases the quantity of aggregates formed. JPT1 was added to 20  $\mu$ M A $\beta$ 40 monomer at a concentration of 0 (control) or 100  $\mu$ M, and the presence of fibrillar structure was detected by dot blot with antibody OC. Detection with antibody 6E10 was performed as a parallel control for detection of total protein. (A) Dot blot results. (B) Quantification of antibody OC. Normalized values are calculated as percentage of the control plateau. Parameters are expressed as mean $\pm$ SEM, n=3. **\*\***p<0.005.

antibody. Figure 3.5A shows the dot blot analysis for the time course of 20  $\mu$ M A $\beta$ 40 aggregation in the absence (control) and presence of peptoid JPT1 at 100  $\mu$ M. The dots were first probed with sequence-specific antibody 6E10, which recognizes residues 1-16 of A $\beta$ , as a positive control to indicate that A $\beta$  is present.<sup>35</sup> The amino terminus has been implicated in playing a role in conformational changes during oligomerization.<sup>61,62</sup> The ability of 6E10 to recognize A $\beta$  in the presence of peptoid JPT1 is dramatically decreased compared to the control (Figure 3.5A). This difference may be due in part to a masking of the amino terminus due to conformation changes, a result that has been observed in other studies.<sup>98,146</sup> Replicate dots were probed with the conformation-specific antibody OC, which binds fibrillar structures, to detect the presence of fibrillar A $\beta$  aggregates.<sup>36</sup> Dot blot analysis with the antibody OC confirms fibril formation of A $\beta$ 40 in the control beginning at 165 min, just slightly later than that observed via ThT fluorescence. In the presence of 100  $\mu$ M JPT1, fibrils were observed at 45 min resulting in a lag

extension of  $<0.31$ , also consistent with the decreased lag time observed using ThT fluorescence. Quantification of the dot blot assays showed that in the presence of JPT1 there is a plateau reduction of  $63.7 \pm 9.2\%$  (Figure 3.5B). Although this is slightly lower than the inhibition detected by ThT, this difference is likely due to differing sensitivities between the assays. This data confirms that JPT1 is able to decrease lag time for A $\beta$  aggregation as well as reduce the amount of fibrillar A $\beta$  aggregates formed.

### 3.3 Conclusions

In this study, for the first time a novel peptoid mimic of the peptide KLVFF was shown to modulate A $\beta$ 40 aggregation. Specifically, addition of the peptoid JPT1 to A $\beta$ 40 monomer results in a decreased time to aggregate formation and a reduction in the amount of fibrillar structured aggregates formed at equilibrium. Both effects were found to be dose dependent, with little change when the concentration of JPT1 was increased beyond 100  $\mu$ M.

Experimental evidence suggests that the A $\beta$  hydrophobic core plays a pivotal role in aggregation. Thus, the peptoid JPT1 was designed for optimal interaction with the hydrophobic regions of the A $\beta$  cross  $\beta$ -sheet via incorporation of aromatic groups with  $\sim 6$  Å spacing on the peptoid helix to match that within the  $\beta$ -sheet backbone. The observed promotion of A $\beta$ 40 aggregation by JPT1 may occur along a different pathway that bypasses the formation of toxic soluble oligomers, as observed with “fibrillar seeds.”<sup>44</sup> These “fibrillar seeds” propagated fibril formation while at the same time significantly inhibiting total aggregate levels, similar to the peptoid JPT1.

Previous studies have shown that variants of the peptide KLVFF can act to inhibit or accelerate A $\beta$  aggregation.<sup>59,89,90,140</sup> However, little progress toward a viable therapeutic has been made with these peptides due to issues with proteolytic degradation *in vivo*.<sup>59,86,87</sup> One variant of the peptide KLVFF (iA $\beta$ 5p) was chemically modified to reduce the extent of proteolytic

degradation. However, the ability of the peptide to inhibit A $\beta$  aggregation was also decreased.<sup>94,142</sup>

Since peptoids can mimic peptide structure, and sometimes activity, but are not susceptible to proteolytic degradation, they are ideal candidates for treatment of neurological diseases that are associated with misfolded proteins.<sup>97,99,105,118,137</sup> Luo et al. used a combinatorial library to identify peptoids that bind to A $\beta$ 40 and A $\beta$ 42. The peptoid IAM1 was shown to inhibit the aggregation of both A $\beta$ 40 and A $\beta$ 42 by roughly one half at a molar ratio of 100:1 and 20:1 (peptoid to A $\beta$ ), respectively. The dimer of the peptoid, (IAM1)<sub>2</sub>, was shown to be more effective in inhibiting A $\beta$ 42 aggregation, with complete inhibition at a 10:1 molar ratio (peptoid to A $\beta$ 42). However, it did not inhibit A $\beta$ 40 aggregation effectively at any ratio tested.

Our studies with peptoid JPT1 have shown ~84% inhibition of  $\beta$ -sheet containing aggregates during A $\beta$ 40 aggregation at a ratio of 5:1 (peptoid to A $\beta$ 40). Our results indicate that the peptoid JPT1 holds promise as a therapeutic agent for AD. In comparison of the efficacy of peptoid JPT1 to the peptide KLVFF, at a concentration equimolar with A $\beta$  monomer peptoid JPT1 inhibits fibrillar structured aggregates at ~46%, while at this same stoichiometry peptide KLVFF either has no effect or slightly enhances the presence of  $\beta$ -sheet containing structures.<sup>70,147</sup> Further studies will focus on modifications to the sequence that allow for greater than 80% reduction of A $\beta$  aggregation at equimolar concentration or lower. In addition, the size and morphology of the aggregates formed in the presence of peptoid will be characterized and the effect that peptoid-induced changes in A $\beta$  aggregation have upon the physiological activity of aggregates will be assessed.

### 3.4 Methods

#### 3.4.1 Materials

(N)-(S)-sec-Butylamine (I-like group), (S)-(-)- $\alpha$ -methylbenzylamine (F-like group), piperidine, bovine serum albumin (BSA), and ThT were purchased from Sigma-Aldrich (St. Louis, MO). *Tert*-Butyl N-(4-aminobutyl) carbamate (K-like group) was purchased from CNH Technologies Inc. (Woburn, MA). MBHA rink amide resin was purchased from NovaBiochem (Gibbstown, NJ). A $\beta$ 40 was purchased from Anaspec, Inc. (Fremont, CA). Primary antibody OC was purchased from EMD Millipore (Billerica, MA). Primary antibody 6E10, alkaline phosphatase-conjugated anti-mouse IgG, and alkaline phosphatase-conjugated anti-rabbit IgG were purchased from Thermo Scientific (Rockford, IL). All other reagents used during synthesis, purification, and sample preparation were purchased from VWR. All chemicals were used without further modification unless otherwise indicated.

#### 3.4.2 Peptoid Synthesis and Purification

Peptoids were synthesized *via* a two-step process using an Applied Biosystems 433A automated peptide synthesizer (Carlsband, CA) that was refurbished from a 431A synthesizer.<sup>110</sup> Rink amide resin was swelled with dimethylformamide (DMF) and the Fmoc protecting group

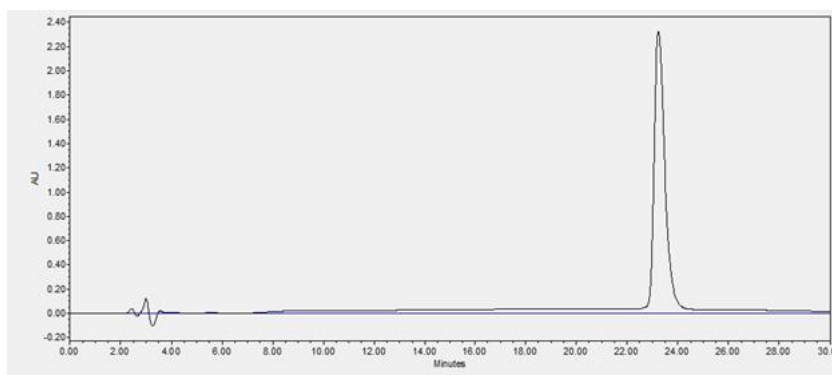


**Figure 3.12** Peptoids were confirmed to be >98% pure via analytical HPLC (Waters 2695 Separations Module) equipped with a Duragel G C18 150 x 2.1 mm column (Peeke Scientific) using a linear gradient of 5 to 95% solvent D in C (solvent D: acetonitrile, 0.1% TFA; solvent C: water, 0.1% TFA) over 30 min.

was removed using 20% piperidine in DMF. The secondary amine was acylated by adding 1.2 M bromoacetic acid in DMF and diisopropylcarbodiimide at a ratio of 5.3:1 and vortexing for 60 min. Side chain amines were added to the resin *via* an S<sub>N</sub>2 reaction mechanism. The peptoid was removed from the resin by bathing it in a cleavage cocktail consisting of 95% trifluoroacetic acid (TFA), 2.5% triisopropylsilane, and 2.5% water for 5 min. The acid was removed using a Heidolph Laborota 4001 rotating evaporator (Elk Grove Village, IL) and the peptoid was diluted to a concentration of ~3 mg mL<sup>-1</sup> in a 35:65 solution of acetonitrile-water. Peptoids were purified using a Waters Delta 600 preparative high performance liquid chromatography unit (HPLC; Milford, MA) with a Duragel G C18 150 x 20 mm column (Peeke Scientific, Novato, CA). Gradients were run at ~1% per minute with 5-95% solvent B in A (solvent A: water, 5% acetonitrile, 0.1% TFA; solvent B: acetonitrile, 5% water, 0.1% TFA). Peptoids were confirmed to be >98% pure via analytical HPLC (Waters 2695 Separations Module) equipped with a Duragel G C18 150 x 2.1 mm column (Peeke Scientific) using a linear gradient of 5 to 95% solvent D in C (solvent D: acetonitrile, 0.1% TFA; solvent C: water, 0.1% TFA) over 30 min (Figure 3.6). MALDI-TOF mass spectrometry was used to confirm that the purified peptoid mass

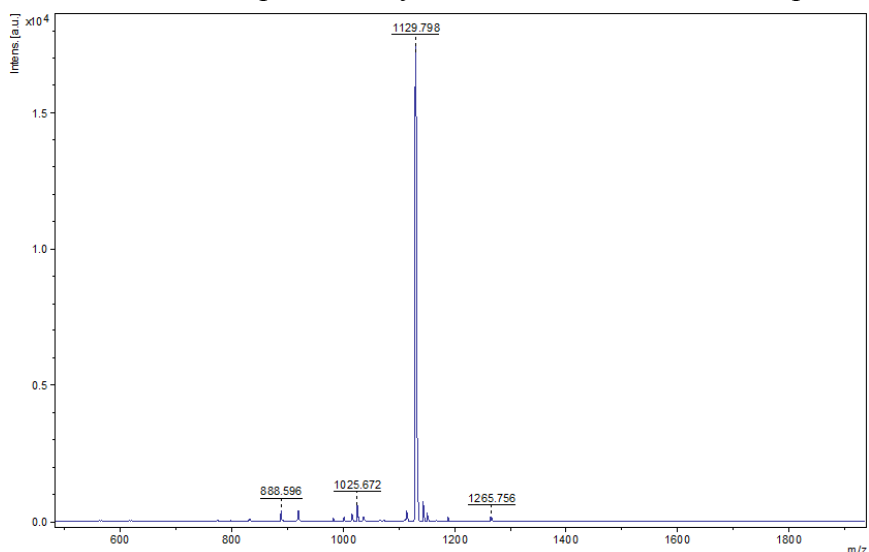


**Figure 3.7** MALDI-TOF mass spectrometry was used to confirm that the purified peptoid mass matched the theoretical mass. Peptoid JPT1 theoretical mass was 1130.48 Da.

matched the theoretical mass (Figure 3.7). Purified peptoid solutions were dried to powder using a Labconco lyophilizer (Kansas City, MO) and stored at -20 °C.

### 3.4.3 Circular Dichroism

Circular dichroism (CD) spectrometry analysis was performed using a Jasco J-710 instrument (Easton, MD) at room temperature with a scanning speed of 20 nm min<sup>-1</sup> and a path length of 0.1 mm. JPT1 was measured in pure methanol and water at a concentration of 120 μM. CD spectra is the cumulative average of twenty scans.

### 3.4.4 Preparation of Aβ Peptide Solution

Aβ<sub>40</sub> (1 mg) was dissolved in 0.5 mL of 50 mM NaOH for 5 min prior to separation of aggregates from monomer *via* size exclusion chromatography on a Superdex 75 10/300 GL column (GE Healthcare, Pittsburg, PA). Size exclusion chromatography was performed using an AKTA FPLC in a running buffer of 40 mM Tris-HCl (pH 8.0) and at a flow 0.5 mL min<sup>-1</sup> and 25 °C. The column was pre-treated with 2 mg mL<sup>-1</sup> BSA to optimize yield by reducing nonspecific interactions between Aβ and the column matrix. Fractions were eluted in 0.5 mL increments and

immediately analyzed *via* an ND-1000 Nanodrop Spectrophotometer to determine fraction concentration (Figure 3.8, 277 nm,  $\epsilon = 1450 \text{ M}^{-1} \text{ cm}^{-1}$ ).

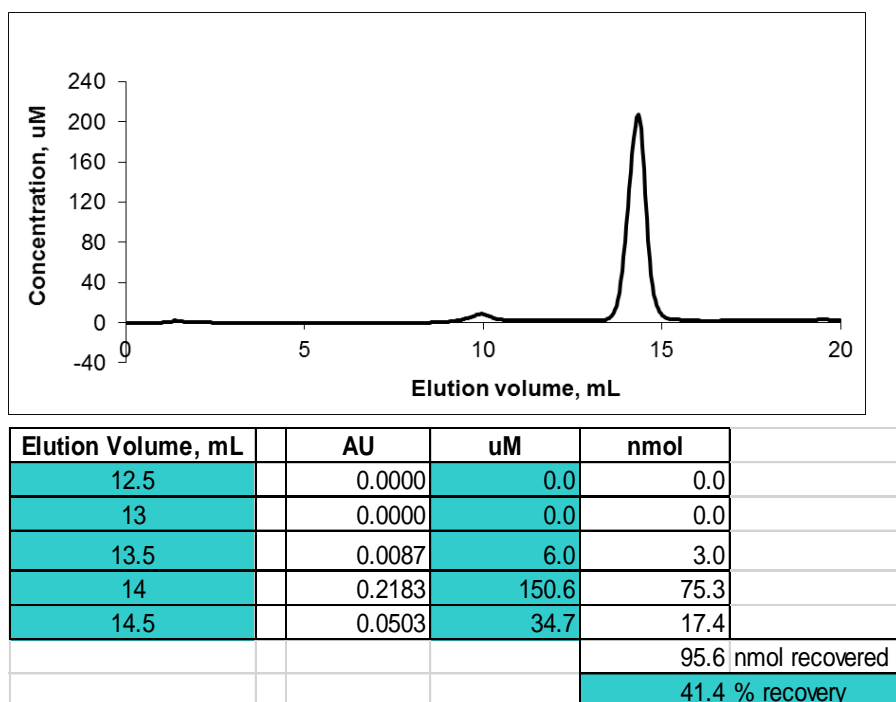


**Figure 3.8** SEC monomer purification of A $\beta$ 40. Monomer purification of A $\beta$ 40 typically results in elution of larger aggregates at ~8-10 mL and then followed by elution of A $\beta$ 40 monomer at ~13-15 mL. Percent recovery of monomer was calculated for specific A $\beta$ 40 lot. Ideally, quality lots provide >65% recovery.

### 3.4.5 Binding Competition Assay

Assays to assess binding competition between JPT1 and ThT were performed by incubating A $\beta$ 40 fibrils in the presence and absence of JPT1. Fibrils were formed prior to the assay by agitating purified 50  $\mu\text{M}$  A $\beta$ 40 in 40 mM Tris-HCl (pH 8.0) at 800 RPM on an orbital shaker at 25  $^{\circ}\text{C}$  for 20 hours. Fibrils were then separated via centrifugation at 15,000 RPM for 15 min until a visible pellet was observed. The fibril pellet was removed from solution and resuspended in 40 mM Tris-HCl (pH 8.0) at a concentration of 50  $\mu\text{M}$ . Competition assay solutions were prepared by gently mixing 0 (control) or 2.5  $\mu\text{M}$  A $\beta$ 40 with 12.5  $\mu\text{M}$  JPT1, 10  $\mu\text{M}$  ThT, 1.25% (v/v) dimethyl sulfoxide (DMSO), and 40 mM Tris-HCl (pH 8.0). Solutions were allowed to incubate

for 15 min to ensure binding. Fluorescence measurements were then taken on a Shimadzu RF-150 mini fluorometer (excitation at 440 nm and emission at 490 nm) with an average scan time of 4 seconds.

#### *3.4.6 A $\beta$ 40 Monomer Aggregation Assay*

Aggregation assays were performed with 20  $\mu$ M purified A $\beta$ 40 in 40 mM Tris-HCl (pH 8.0) and 150 mM NaCl. Peptoid JPT1 was dissolved in DMSO and added at 0, 20, 50, 100, or 200  $\mu$ M such that the final DMSO concentration was 1.25% (v/v). Assays were performed at 25 °C under agitation on an orbital shaker at 800 RPM. For ThT measurements, an aliquot was taken every 45 min and combined with ThT at a 5:1 molar ratio (ThT to A $\beta$  monomer unit). Samples were well mixed for 8 seconds and then scanned with a Shimadzu RF-150 mini fluorometer (excitation at 440 $\pm$ 10 nm and emission at 490 $\pm$ 10 nm) with an average scan time of 4 seconds. ThT fluorescence with background (ThT alone) subtraction was normalized for the fluorescence detected at equilibrium for the control reaction and plotted against time. Lag time was noted for both the control and peptoid JPT1 as the time point before a significant increase in fluorescence was observed (5% of the plateau). Lag extension was calculated as the ratio of the lag time for peptoid JPT1 to that of the control. Equilibrium plateau was determined for both the control and peptoid JPT1 and percent inhibition was calculated for all peptoid JPT1 concentrations as the percentage decrease of the equilibrium relative to the control.

#### *3.4.7 Dot Blot*

In parallel with ThT fluorescence, aggregation assays were also assessed with dot blot analysis. Every 30 to 45 min, samples were spotted onto 0.1  $\mu$ m nitrocellulose membrane (GE Healthcare, Pittsburg, PA) and immediately blocked with 5% skim milk in Tris buffered saline containing 0.2% Tween20 (TBS-T) at 4 °C overnight. Membranes were washed three times with



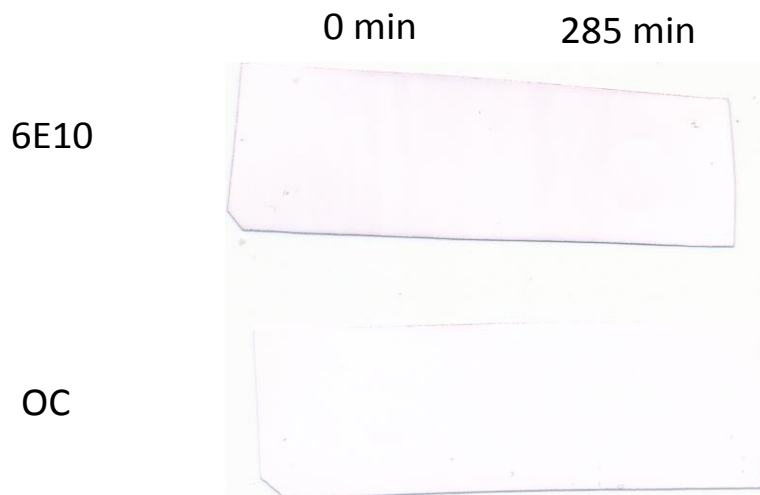


**Figure 3.9** Dot blot analysis shows that peptoid JPT1 does not bind to sequence-specific antibody 6E10 or conformation-specific antibody OC in the absence of A $\beta$ 40. Samples were spotted at 0 min and 285 min, respectively.

TBS-T and then incubated with either A $\beta$ 1-16 specific 6E10 antibody (1:2000 dilution) or A $\beta$  fibril specific OC antibody (1:5000 dilution) for 1 hour at room temperature with gentle agitation. Membranes were washed three times with TBS-T. Protein detection for bound 6E10 and OC antibodies was performed by binding alkaline phosphatase-conjugated anti-mouse IgG (1:2000 dilution) or alkaline phosphatase-conjugated anti-rabbit IgG (1:3000 dilution), respectively, for 1 hour at room temperature with gentle agitation. Dot blots were developed using Nitro blue tetrazolium and 5-Bromo-4-chloro-3-indolyl phosphate in TBST-MgCl<sub>2</sub> until precipitate from the reaction was no longer forming. The developing reaction was halted by a 10% acetic acid solution. Dot blots were immediately imaged using a Canon CanoScan 9000F (Tokyo, Japan). Controls performed by dotting with JPT1 alone confirmed an absence of signal for the peptoid (Figure 3.9). Images were analyzed with ImageJ software using the gel lane analysis tool. Dot density was normalized to the density detected at equilibrium for the control

and plotted against time. Lag extension and percent inhibition were assessed as described for ThT fluorescence.

#### *3.4.8 Statistical Analysis*

Data were analyzed using Prism 5 software (GraphPad Software Inc., La Jolla, CA). Differences in lag extension and percent inhibition were assessed using a one-way analysis of variance (ANOVA) or t-test for ThT fluorescence and dot blot analysis, respectively. For ANOVA, Dunnett's post-test was used to identify groups with means significantly different from control.

#### *Funding Sources*

This publication was made possible by Grant Number P30 GM103450-03 from the National Institute of General Medical Sciences, a component of the National Institutes of Health (NIH) (SLS), Arkansas Bioscience Institute (SLS), NIH Grant Number P20 RR-016461 from the National Center for Research Resources (MAM), and NSF/EPSCoR Grant Number EPS-0447660 (MAM).

## **Chapter 4 Modulating A $\beta$ 40 Aggregation: The Effects of Peptoid Helicity and Side Chain Placement**

### **Abstract**

Alzheimer's disease (AD) is characterized by the buildup of insoluble aggregated amyloid-beta proteins (A $\beta$ ) into plaques that accumulate between the neural cells in the brain. AD is the sixth leading cause of death in the United States and is the only cause inside the top ten causes of death that cannot be treated or cured. Researchers have focused on developing small molecules and peptides to prevent A $\beta$  self-assembly; however, little progress has been made at finding a viable therapeutic treatment. We previously reported a peptoid-based mimic (JPT1) of the peptide KLVFF (residues 16-20 of A $\beta$ ) that was capable of modulating A $\beta$ 40 aggregation, specifically decreasing lag time to  $\beta$ -sheet aggregate formation as well as the total number of fibrillar,  $\beta$ -sheet structured aggregates formed. In this study, we designed two new variants of JPT1 that tested the importance of peptoid helical secondary structure (JPT1a) and side chain placement (JPT1s). All three peptoids were found to modulate A $\beta$ 40 aggregation while reducing total  $\beta$ -sheet and fibrillar aggregates. Interestingly, all peptoids allowed for an altered morphological formation of A $\beta$  in the plateau phase of A $\beta$ 40 aggregation. These results suggest that the A $\beta$ 40 aggregation pathway may be different in the presence of each peptoid. Furthermore, peptoids may be able to limit the formation of A $\beta$  aggregates and alter aggregation pathways associated with AD.

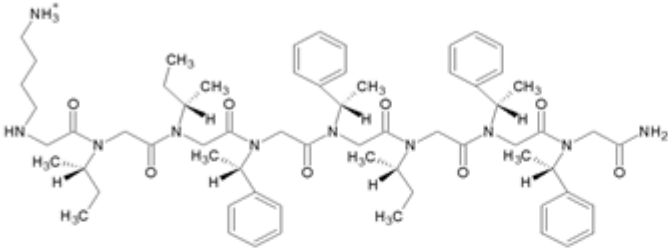
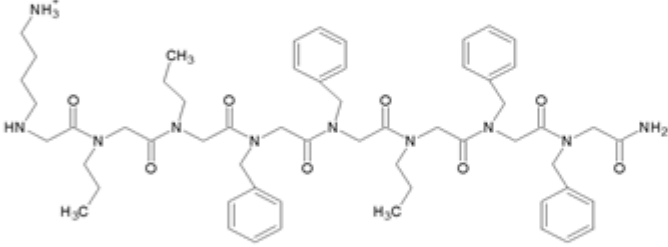
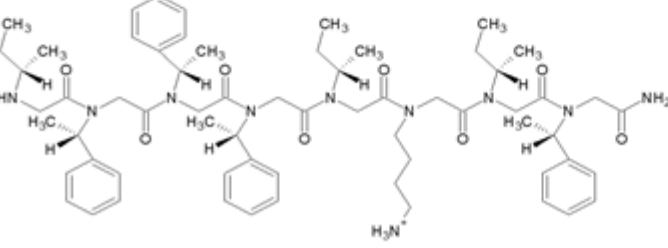
### **4.1 Introduction**

Alzheimer's disease (AD) is a neurodegenerative disease that is characterized by the buildup of aggregated amyloid-beta protein (A $\beta$ ) and the formation of tau tangles within neuronal cells.<sup>3</sup> A $\beta$  results from the proteolytic cleavage of the amyloid precursor protein and typically contains 40 or 42 amino acid residues (A $\beta$ 40 and A $\beta$ 42, respectively).<sup>3</sup> AD affects more than 40% of

individuals over 65 years of age and results in billions of dollars lost due to patient care every year.<sup>1</sup> While the specific mechanism that causes AD is not clearly understood, research has focused on the development of small molecules and peptides to modify A $\beta$  aggregation. One such group of peptides is based on the hydrophobic sequence KLVFF, which has been shown to either inhibit or accelerate A $\beta$  aggregation.<sup>59,85-90</sup> Peptide KLVFF variants are modeled after the key recognition element within A $\beta$  (residues 16-20). As a result, KLVFF variants self-recognize and stereospecifically bind to this core, thereby acting as a disruption element to A $\beta$  aggregation. Previous work showed promise for these compounds *in vitro*; however, protease degradation *in vivo* has been a deterrent for further development of therapeutic agents with these compounds.<sup>59,86,87,141</sup>

We have previously published the design and characterization of a novel, protease-resistant peptoid-based mimic of KLVFF, referred to as JPT1.<sup>53</sup> Peptoids are a novel class of peptidomimetics that are resistant to protease degradation and elicit a low immune response, making them ideal candidates for use as therapeutics and detection agents in protein misfolding diseases.<sup>97</sup> Peptoids have a backbone similar to peptides with the side chains attached to the amide nitrogen rather than the alpha-carbon. While this small change results in an achiral backbone, inclusion of chiral side chains within the peptoid sequence leads to a helical secondary structure.<sup>106,113-116,122</sup> Peptoids adopt a polyproline type-I like helix exhibiting a helical pitch of  $\sim 6$  Å and 3 monomers per turn when chiral, aromatic side chains are included.<sup>106</sup> Peptoid helices are extremely stable and can withstand denaturation in 8 M urea at 70 °C.<sup>122</sup> Furthermore, peptoids have increased bioavailability compared to peptides due to the change in backbone structure, resulting in a protease resistant structure that can improve therapeutics.<sup>97</sup>

**Table 4.1** Peptoid sequence, theoretical MW (Da), and percent acetonitrile elution (HPLC).

	Structure	MW (Da)	% Elution
JPT1	 <p>The structure of JPT1 is a peptoid with a backbone of four secondary amide bonds. The N-terminus is a protonated primary amine (NH<sub>3</sub><sup>+</sup>). The side chains are: a 4-aminobutyl group, a 1-phenylethyl group, a 1-phenylethyl group, and a 1-phenylethyl group. The backbone is shown in a helical conformation.</p>	1130	72
JPT1a	 <p>The structure of JPT1a is a peptoid with a backbone of four secondary amide bonds. The N-terminus is a protonated primary amine (NH<sub>3</sub><sup>+</sup>). The side chains are: a 1-phenylethyl group, a 1-phenylethyl group, a 1-phenylethyl group, and a 1-phenylethyl group. The backbone is shown in a helical conformation.</p>	1032	73
JPT1s	 <p>The structure of JPT1s is a peptoid with a backbone of four secondary amide bonds. The N-terminus is a protonated primary amine (NH<sub>3</sub><sup>+</sup>). The side chains are: a 1-phenylethyl group, a 1-phenylethyl group, a 1-phenylethyl group, and a 1-phenylethyl group. The backbone is shown in a helical conformation.</p>	1130	72

JPT1 was designed to mimic the peptide KLVFF and exhibits a helical secondary structure with chiral aromatic (F-like) side chains on two faces of the helix with  $\sim 6$  Å spacing. This spacing of the F-like side chains should allow for optimum interaction with  $\beta$ -sheet backbone carbons  $i$  and  $i+2$  within  $A\beta$  and correspond to pi-pi stacking of the aromatic groups in the peptoid and  $A\beta$  aggregates. Aggregation assays showed that JPT1 effectively modulated  $A\beta_{40}$  aggregation by reducing the time for aggregate formation as well as the overall number of  $\beta$ -sheet containing aggregates formed at equilibrium.<sup>53</sup> This indicated JPT1 may potentially serve as a therapeutic option for AD.

We originally hypothesized that JPT1 would have favorable interactions with  $A\beta$  due to the spacing of chiral, aromatic side chain groups and the potential for pi-pi stacking. To test the

validity of this hypothesis, two additional novel peptoid-based mimics of KLVFF have been designed to investigate the effect of peptoid helicity and side chain arrangement within the peptoid sequence. The ability of these sequences to modulate A $\beta$ 40 aggregation has been compared to that of JPT1. We demonstrate that although all three peptoids modulate A $\beta$ 40 aggregation, side chain placement and secondary structure play a crucial role in better understanding the mechanism by which peptoids interact with A $\beta$ .

## 4.2 Results and Discussion

### 4.2.1 Peptoid Sequence, Rationale, and Characterization

The peptoid JPT1 (Table 4.1) was designed to have a similar sequence to that of the peptide KLVFF. JPT1 exhibits a helical secondary structure in both methanol and water, as indicated by circular dichroism.<sup>53</sup> JPT1 has chiral, aromatic F-like groups aligned on two faces of the helix with ~6 spacing between. This spacing corresponds to that between backbone carbons *i* and *i*+2 in a  $\beta$ -sheet, facilitating pi-pi stacking between the aromatic groups within the peptoid and A $\beta$  aggregates.

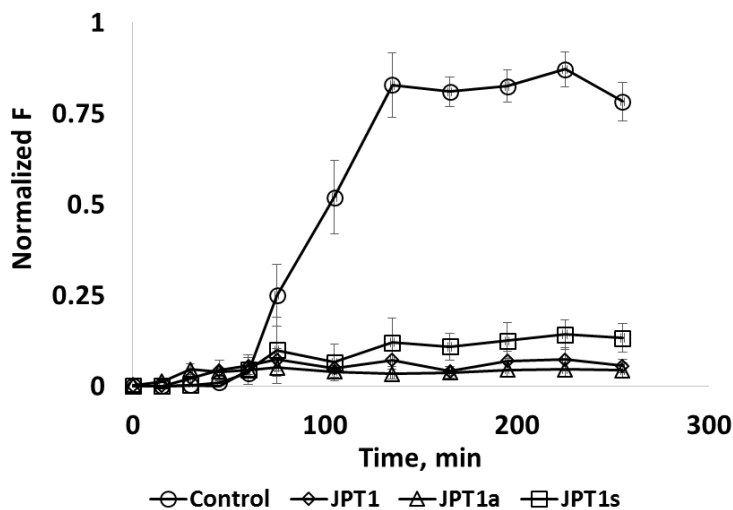
To determine the importance of peptoid helicity in the modulation of A $\beta$ 40 aggregation, a peptoid that maintains the side chain chemistry and sequence of JPT1, but lacks chirality and hence helical secondary structure was designed (JPT1a; Table 4.1). Given the lack of secondary structure, it is possible peptoid JPT1a may improve A $\beta$  modulation due to the increased flexibility of the peptoid backbone.

To determine the importance of spacing between F-like side chains, a rationally scrambled variant of JPT1 was created to yield peptoid JPT1s (Table 4.1). The ‘scrambled’ peptoid was designed to avoid the placement of two F-like side chains on the same helical face with ~6 Å spacing. Because JPT1 contains only eight side chain groups, four of which are F-like side

chains, JPT1s contains two faces of the helix with one F-like side chain and one face of the helix with two F-like side chains. The spacing of these two F-like side chains on the same face is  $\sim 12$  Å. As a result, we anticipate JPT1s to have decreased activity towards A $\beta$  as compared to JPT1.

#### 4.2.2 Aggregation Assays

Thioflavin T (ThT) aggregation assays were used to assess the ability of peptoids JPT1, JPT1a, and JPT1s to modulate A $\beta$ 40 aggregation. ThT is a benzothiazole dye that binds to  $\beta$ -sheet rich structures, resulting in an increased fluorescent signal.<sup>57</sup> Assays were performed with 20  $\mu$ M A $\beta$ 40 monomer in the absence (control) and presence of 100  $\mu$ M JPT1, JPT1a, or JPT1s. Aggregation was initiated via agitation on an orbital shaker at 800 RPM and 25°C in the presence of 150 mM NaCl in 40 mM Tris-HCl (pH 8.0). ThT fluorescence measurements (excitation at  $440\pm 10$  nm and emission at  $490\pm 10$  nm) were taken every 15 min until an increase in fluorescence was observed. After initial fluorescence was detected, measurements were taken every 30 min. In the control, A $\beta$ 40 aggregation exhibited a lag time of 60 min (the time at which fluorescence begins to increase), followed by rapid  $\beta$ -sheet growth for 75 min, and ending in a plateau, where aggregates are in equilibrium, for 120 min as previously observed.<sup>29,33,53,77,148,149</sup> In the presence of JPT1, JPT1a, or JPT1s the plateau intensity is drastically reduced, indicating that fewer  $\beta$ -sheet aggregates are present at equilibrium (Figure 4.1). We previously reported that JPT1 reduced the number of  $\beta$ -sheet aggregates at equilibrium by  $81.2\pm 4.4$  % of the control, which is consistent with the  $83.07\pm 4.84$  % presented here. This indicates JPT1a and JPT1s both reduce the formation of  $\beta$ -sheet aggregates similar to JPT1.



	JPT1	JPT1a	JPT1s
<b>% Inhibition</b>	83.07 ± 4.84	85.57 ± 4.82	76.93 ± 4.77

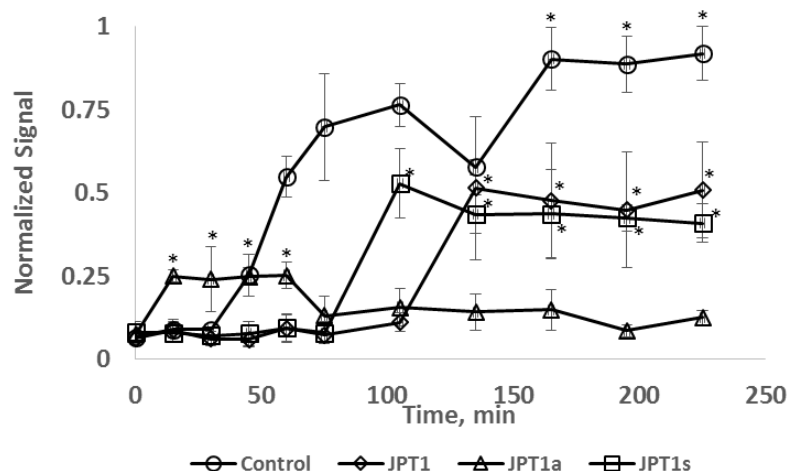
**Figure 4.1** ThT analysis shows that peptoid JPT1, JPT1a, and JPT1s modulate A $\beta$ 40 aggregation similarly. Peptoids were added to 20  $\mu$ M A $\beta$ 40 monomer at concentrations of 0 or 100  $\mu$ M and  $\beta$ -sheet aggregates were detected via ThT fluorescence. Normalized fluorescence values are calculated as a percentage of the control plateau. Parameters are expressed as mean  $\pm$  SEM, n =7.

#### 4.2.3 Dot Blot Analysis

To assess the presence of fibrillar species of A $\beta$ 40, immunoblotting techniques were performed in conjunction with the A $\beta$ 40 monomer aggregation assays. A $\beta$  aggregates can be detected via antibodies which fall into one of two categories: (i) sequence-specific and (ii) conformation-specific. Sequence-specific antibodies, such as 6E10, bind to A $\beta$  in both monomeric and aggregated forms.<sup>62</sup> In contrast, conformation-specific antibodies, such as OC, recognize specific fibrillar aggregates.<sup>61</sup> Dot blot analysis with the antibody OC confirms fibril formation of A $\beta$ 40 in the control beginning at 45 min (Figure 4.2), which is slightly earlier than the data obtained via ThT fluorescence. This difference in lag time is not unexpected since ThT and OC are specific for different A $\beta$ 40 conformations. In the presence of 100  $\mu$ M JPT1, fibrils



were observed at 135 min, a lag extension of  $2.67 \pm 0.83$  times that of the control. Interestingly, this is different from the results previously published with JPT1.<sup>53</sup> This is most likely the result of varying lots from the A $\beta$  peptide supplier. Specifically, solid phase synthesis of A $\beta$  coupled with high pressure liquid chromatography can result in producing trifluoroacetic acid salts.<sup>52</sup> This in turn will yield stock peptides that can have a varying biophysical and biological behavior from lot to lot. The addition of 100  $\mu$ M JPT1a and JPT1s resulted in lag extensions of  $<0.42$  and  $2.22 \pm 0.28$ , respectively. Similar to ThT results, the addition of all peptoids reduced the quantity of fibrils formed. Specifically, JPT1 resulted in a decrease in fibrillar aggregates of  $47.8 \pm 11.4\%$ , which is slightly less than data previously reported on JPT1. This is likely due to the change in A $\beta$  lots, which have been shown to differ in quality of monomer preparation and aggregation.<sup>27,52</sup> The addition of JPT1a and JPT1s resulted in  $75.0 \pm 4.5\%$  and  $57.3 \pm 9.0\%$  reduction of fibrillar aggregates, respectively. According to ThT analysis, JPT1, JPT1a, and JPT1s reduced the overall number of  $\beta$ -sheet aggregates similarly. Interestingly, JPT1a appears to reduce significantly more fibrillar aggregates compared to JPT1 and JPT1s by dot blot analysis. JPT1s had a slightly greater reduction of fibrillar aggregates compared to JPT1, suggesting side chain placement is crucial for reducing fibrillar aggregates.



	JPT1	JPT1a	JPT1s
<b>% Inhibition</b>	46.0 ± 11.4	72.6 ± 4.5	50.5 ± 9.0
<b>Lag Extension</b>	2.67 ± 0.83	ND	2.22 ± 0.28

**Figure 4.2** Dot blot analysis confirms peptoids JPT1, JPT1a, and JPT1s modulate A $\beta$ 40 aggregation and decrease fibrillar aggregates. Peptoids were added to 20  $\mu$ M A $\beta$ 40 monomer at concentrations of 0 or 100  $\mu$ M and fibrillar aggregates were detected via primary antibody OC. Peptoids JPT1 and JPT1s extend lag time by 2.67±0.83 and 2.22±0.28 times that of the control, respectively. Peptoid JPT1a decreased lag time extension to <0.42 times that of the control. Normalized values are calculated as a percentage of the control plateau. Parameters are expressed as mean ± SEM, n = 3. Data points used for % inhibition measurements are signified with a \*.

#### 4.2.4 Morphology Studies

To confirm the inhibition of A $\beta$ 40 aggregates via peptoids and investigate the morphology of aggregates, transmission electron microscopy (TEM) images were acquired at equilibrium. In the absence of the peptoids, A $\beta$ 40 formed thick fibrillar-like aggregates (Figure 4.3A), as observed previously.<sup>33,77,149</sup> The addition of JPT1, JPT1a, or JPT1s resulted in a reduction in the overall number of aggregates, agreement with ThT fluorescence and dot blot data, as well as the size of the aggregates formed (Figures 4.3B-D). Interestingly, the morphology of A $\beta$ 40 aggregates in the presence of the different peptoids varies significantly. The addition of JPT1 resulted in small aggregates with no extensive branching (Figure 4.3B). When A $\beta$ 40 is aggregated in the presence

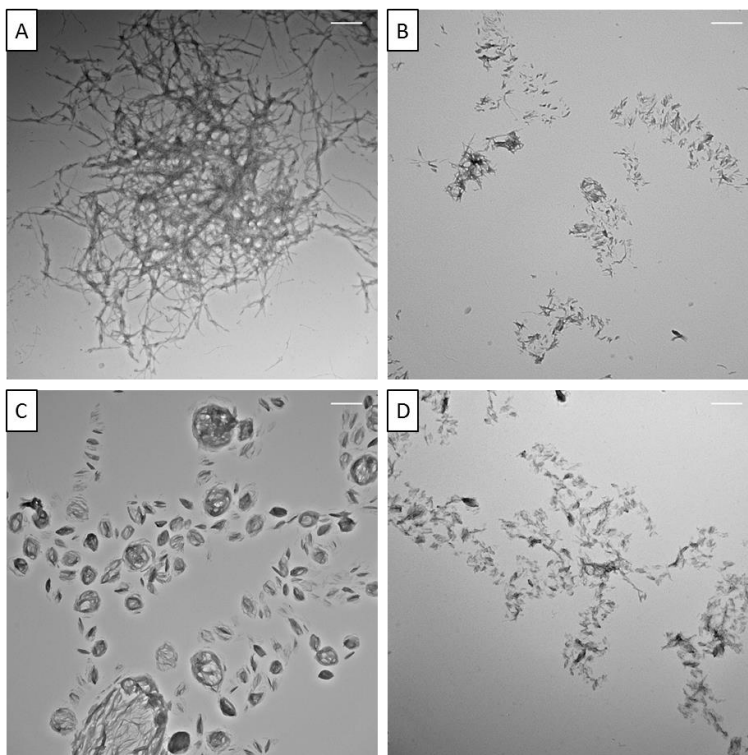


**Figure 4.3** Morphology of A $\beta$ 40 aggregates formed in the absence and presence of peptoid with varying side chain placement and helicity. 20  $\mu$ M A $\beta$ 40 monomer in 40 mM Tris-HCl (pH 8.0) was aggregated alone (control, A) or in the presence of 100  $\mu$ M peptoid (B) JPT1, (C) JPT1a, or (D) JPT1s. The control reaction was monitored via ThT fluorescence and upon plateau equilibrium was observed, samples were gridded and visualized by TEM at 255 min. Results are representative of 3 independent experiments and imaged grids were randomly selected. Scale bars are 500 nm.

of JPT1a, the aggregates adopt a circular morphology that do not have external branching (Figure 4.3C). Compared to the morphology of JPT1, JPT1a has a similar number of aggregates that are larger in size and vary by morphology. In the presence of JPT1s, A $\beta$ 40 aggregates are reduced compared to the control and display a similar morphology to that of JPT1 (Figure 4.3D). When compared to JPT1, JPT1s has a similar number of aggregates that are slightly larger in size, but share a similar morphology.

### 4.3 Conclusions

In this study, we have shown that three peptoids designed to mimic the sequence of the peptide KLVFF modulate A $\beta$ 40 aggregation. All three peptoids, regardless of changes in side

chain chirality and placement, had a similar effect on the formation of  $\beta$ -sheet containing aggregates as determined by ThT fluorescence. However, immunoblotting and TEM results suggest that A $\beta$ 40 follows a different aggregation pathway in the presence of each of the peptoids. By removing side chain chirality from JPT1 to create JPT1a, we see a significant reduction in the number of aggregates by immunoblotting. However, TEM images show that the addition of JPT1 results in smaller A $\beta$ 40 aggregates as compared to JPT1a. Interestingly, the larger aggregates formed with JPT1a appear less fibrillar than those formed in the presence of JPT1, which is likely why they are not detected by the fibril-specific antibody OC. Both JPT1 and JPT1a use the same corresponding amino acid, with the only difference being JPT1 utilizes a chiral version of I and F, respectively. As a result, JPT1 has shown to adopt a polyproline type-I like helix in both methanol and water.<sup>53</sup> The removal of chirality from JPT1a will yield a secondary conformation that is not helical. As a consequence, peptoids utilizing side chains without chiral centers or steric bulk should have the propensity to adopt a trans conformation as previously reported by Laursen et al.<sup>150</sup> Considering JPT1a is more likely to form a trans conformation, we believe this peptoid is able to adopt a favorable conformation within the A $\beta$  environment. This results in a similar reduction of  $\beta$ -sheet and fibrillar aggregates compared to JPT1, but may result in a different aggregation pathway that forms different morphologies at equilibrium.

By rationally scrambling peptoid JPT1, JPT1s was created so that only one face of the helix contained two F-like groups spaced  $\sim 12$  Å apart. This sequence change results in a decrease in the number of fibrillar aggregates in the plateau phase of the aggregation curve as compared to JPT1 based on OC detection via dot blot analysis. Morphology studies confirm that both JPT1 and JPT1s work similarly in terms of altering the morphology of A $\beta$ 40. This indicates the

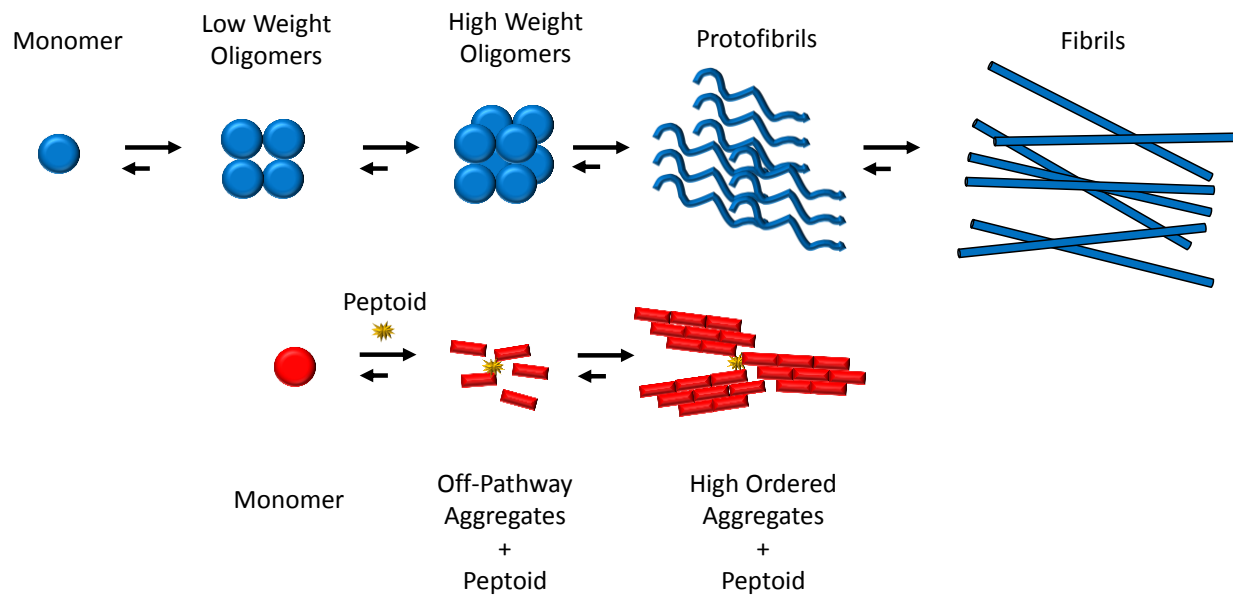


**Figure 4.4** Proposed mechanistic representation on how peptoids may create off-pathway A $\beta$  higher ordered aggregates. Future work will focus on utilizing atomic force microscopy (AFM) to quantitate the size of early aggregates in the lag phase associated with A $\beta$  aggregation.

spacing of F-like side chain groups within the peptoid backbone is an important feature to reducing the overall number of aggregates at equilibrium. While both peptoids will have a helical secondary conformation, the interaction with A $\beta$  appears to be greatly affected by the spacing of the F-like side chain groups on the face of the helix. This indicates pi-pi stacking between the F-like side chain groups and aromatic groups within the  $\beta$ -sheet is crucial for reducing the overall number of aggregates at equilibrium.

Our results indicate that peptoids may be creating an off-pathway formation of higher ordered aggregates for A $\beta$  (Figure 4.4), similar to the pathway observed when A $\beta$  is aggregated in the presence of “fibrillar seeds.”<sup>44</sup> These fibrillar seeds were shown to propagate fibril formation while significantly reducing total aggregate levels and reducing soluble oligomer toxicity. Specifically, all three peptoids have shown ~80% inhibition of  $\beta$ -sheet containing aggregates during A $\beta$ 40 aggregation at a ratio of 5:1 (peptoid to A $\beta$ 40) by ThT fluorescence.

However, immunoblotting and TEM images indicate that there are differences in the number and the morphology of the aggregates formed. This suggests side chain placement and cis-trans isomerization may play a key role in pi-pi stacking with the  $\beta$ -sheets within A $\beta$ .

Our studies indicate rationally designed peptoids from the hydrophobic core of A $\beta$  may hold promise as a therapeutic agent for the treatment of AD. Peptoid helicity and side chain placement play a crucial role in the aggregation pathway followed; however, all peptoids reduced  $\beta$ -sheet and fibrillar aggregates. Based on the results shown here, it is possible varying peptoid sequences may elicit different aggregation pathways and morphologies of A $\beta$ .

## 4.4 Methods

### 4.4.1 Materials

(N)-(S)-*sec*-Butylamine (I-like side chain), (S)-(-)- $\alpha$ -methylbenzylamine (F-like side chain), Benzylamine (achiral F-like side chain), propylamine (achiral I-like side chain) piperidine, and Thioflavin T (ThT) were purchased from Sigma-Aldrich (St. Louis, MO). *tert*-Butyl N-(4-aminobutyl) carbate (Boc protected K-like side chain) was purchased from CNH Technologies, Inc. (Wobrun, MA). MBHA rink amide resin was purchased from NovaBiochem (Gibbstown, NJ). A $\beta$ 40 was purchased from Anaspec, Inc. (Freemont, CA). Primary antibody OC was purchased from EMD Millipore (Billerica, MA). Primary antibody 6E10, alkaline phosphatase-conjugated anti-mouse IgG, and alkaline phosphatase-conjugated anti-rabbit IgG were purchased from Thermo Scientific (Rockford, IL). All other reagents used during synthesis, purification, and sample preparation were purchased from VWR or Fisher. All chemicals were used without further modification unless otherwise indicated.

#### 4.4.2 Peptoid Synthesis and Purification

Peptoids were synthesized *via* a two-step process using an Applied Biosystems 433A automated peptide synthesizer (Carlsband, CA) that was refurbished from a 431A synthesizer.<sup>110</sup> Rink amide resin was swelled with dimethylformamide (DMF) and the Fmoc protecting group was removed using 20% piperidine in DMF. The secondary amine was acylated by adding 1.2 M bromoacetic acid in DMF and diisopropylcarbodiimide at a ratio of 5.3:1 and vortexing for 60 min. Side chain amines were added to the resin *via* an S<sub>N</sub>2 reaction mechanism. The peptoid was removed from the resin by bathing it in a cleavage cocktail consisting of 95% trifluoroacetic acid (TFA), 2.5% triisopropylsilane, and 2.5% water for 5 min. The acid was removed using a

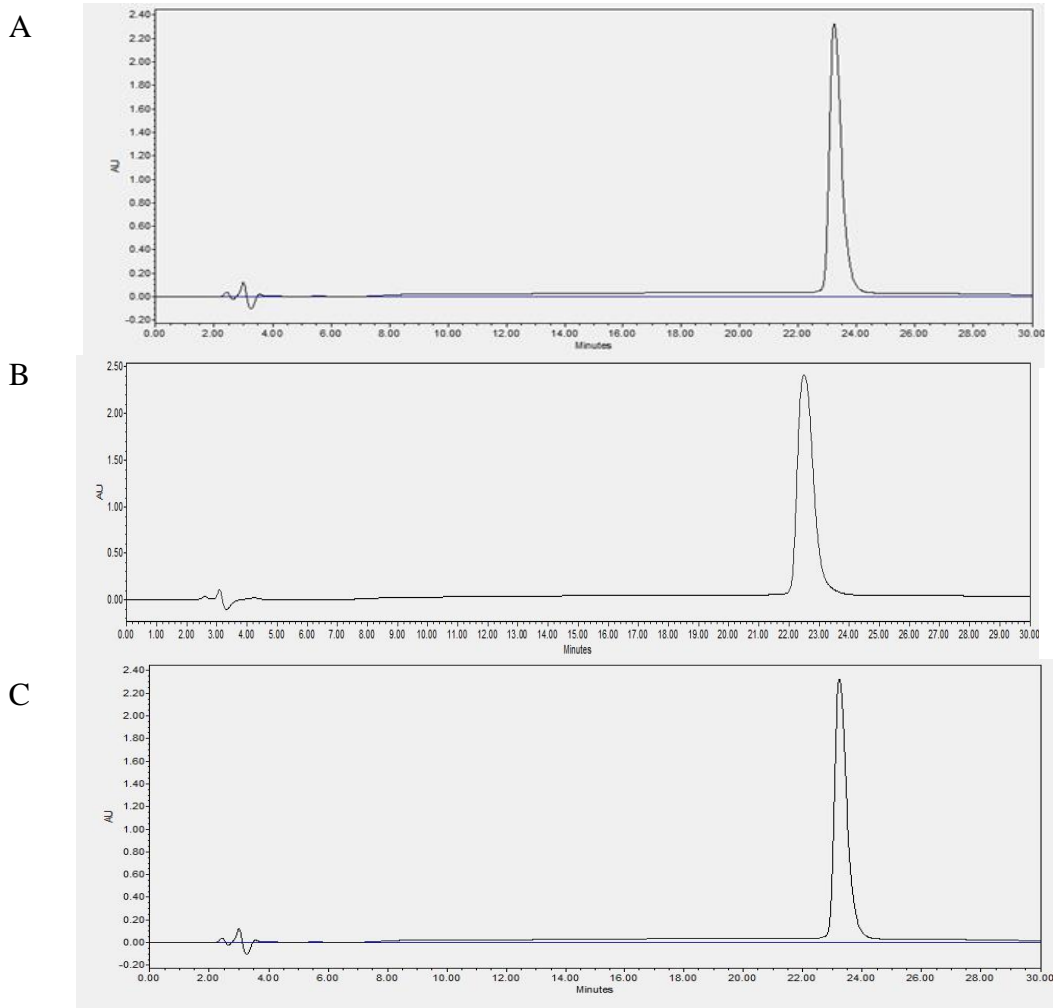


**Figure 4.5** Peptoids ( A: JPT1, B: JPT1a, and C: JPT1s) were confirmed to be >98% pure via analytical HPLC (Waters 2695 Separations Module) equipped with a Duragel G C18 150 x 2.1 mm column (Peeke Scientific) using a linear gradient of 5 to 95% solvent D in C (solvent D: acetonitrile, 0.1% TFA; solvent C: water, 0.1% TFA) over 30 min.

Heidolph Laborota 4001 rotating evaporator (Elk Grove Village, IL) and the peptoid was diluted to a concentration of  $\sim 3 \text{ mg mL}^{-1}$  in a 35:65 solution of acetonitrile-water. Peptoids were purified using a Waters Delta 600 preparative high performance liquid chromatography unit (HPLC; Milford, MA) with a Duragel G C18 150 x 20 mm column (Peeke Scientific, Novato, CA). Gradients were run at  $\sim 1\%$  per minute with 5-95% solvent B in A (solvent A: water, 5% acetonitrile, 0.1% TFA; solvent B: acetonitrile, 5% water, 0.1% TFA). Peptoids were confirmed



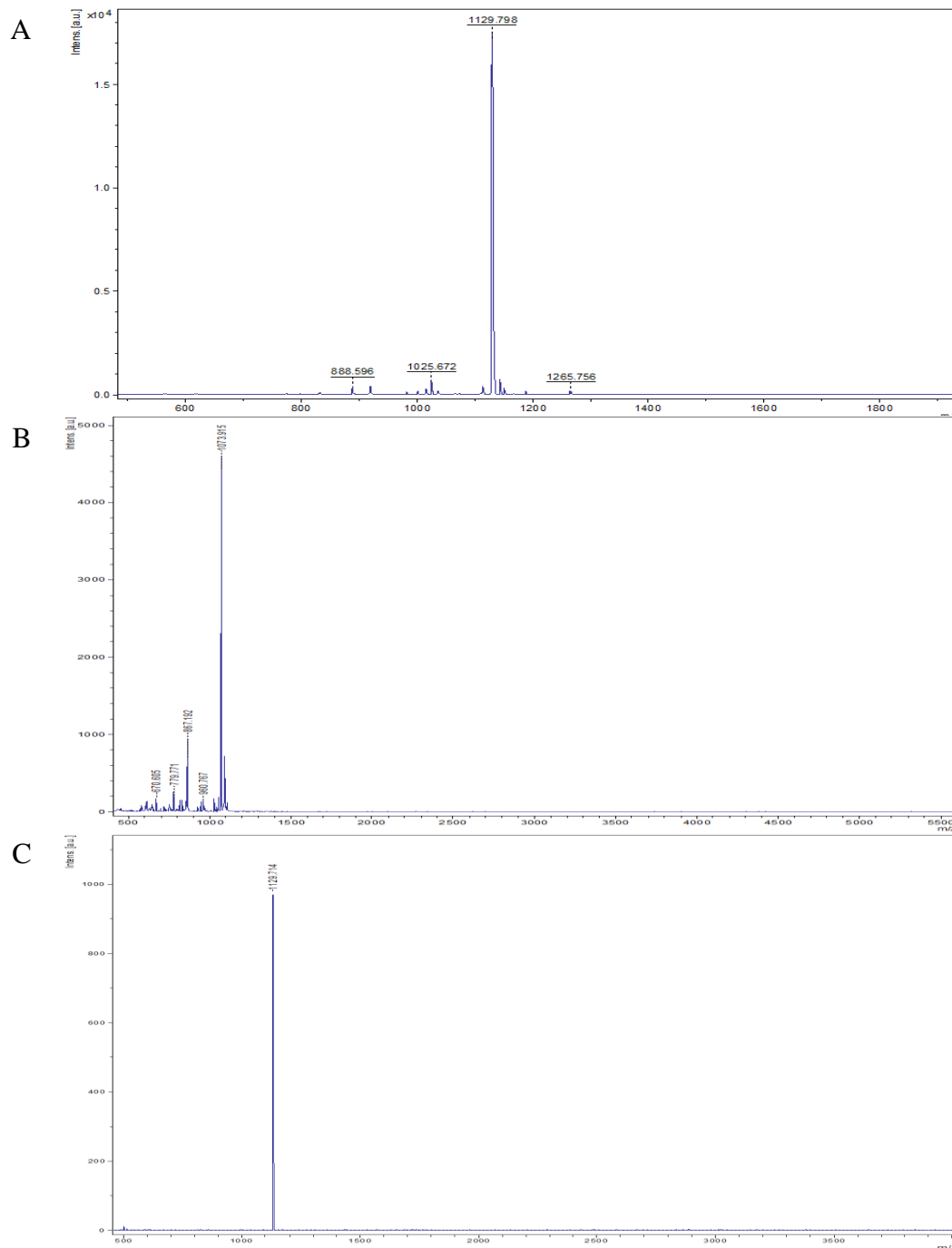


**Figure 4.6** MALDI-TOF mass spectrometry was used to confirm that the purified peptoid mass matched the theoretical mass. A) Peptoid JPT1 theoretical mass was 1130.48 Da, B) Peptoid JPT1a theoretical mass was 1073.4 Da, and C) peptoid JPT1s theoretical mass was 1130.48 Da.

to be >98% pure (Figure 4.5) via analytical HPLC (Waters 2695 Separations Module) equipped with a Duragel G C18 150 x 2.1 mm column (Peeke Scientific) using a linear gradient of 5 to

95% solvent D in C (solvent D: acetonitrile, 0.1% TFA; solvent C: water, 0.1% TFA) over 30 min. MALDI-TOF mass spectrometry was used to confirm that the purified peptoid mass matched the theoretical mass (Figure 4.6). Purified peptoid solutions were dried to powder using a Labconco lyophilizer (Kansas City, MO) and stored at -20 °C.

#### *4.4.3 Preparation of A $\beta$ Peptide Solution*

A $\beta$ 40 was dissolved in cold 1,1,1,3,3-hexafluoro-2-propanol (HFIP) to create a 1 mM solution and was incubated on ice for 60 min. After incubation, the solution was separated into individual non-stick vials and allowed to evaporate overnight at room temperature resulting in the creation of thin peptide films. The resulting peptide film was stored with desiccant at -80 °C until use. Prior to experimentation, peptide films were rehydrated with 5 mM NaOH on ice for 5 min and then 40 mM Tris-HCl (pH 8.0) was added for 10 min on ice. Finally, 150 mM NaCl was added along with either 5% DMSO (v/v) or peptoid inhibitor (dissolved in DMSO) to a final concentration of 20  $\mu$ M.

#### *4.4.4 A $\beta$ 40 Aggregation Assay*

Aggregation assays were performed with 20  $\mu$ M rehydrated A $\beta$ 40 peptide films in 5 mM NaOH, 40 mM Tris-HCl (pH 8.0), and 150 mM NaCl. Peptoids were dissolved in DMSO and added at 100  $\mu$ M such that the final DMSO concentration was 5% (v/v). Assays were performed at 25 °C under agitation on an orbital shaker at 800 rpm. For ThT measurements, an aliquot was taken at varying time points and combined with ThT at a 5:1 molar ratio (ThT to A $\beta$ ). Samples were well mixed for 8 s and then scanned with a Shimadzu RF-150 mini fluorometer (excitation at 440  $\pm$  10 nm and emission at 490  $\pm$  10 nm) with an average scan time of 4 seconds. ThT fluorescence with background (ThT alone) subtraction was normalized for the fluorescence detected at equilibrium for the control reaction and plotted against time. Lag time was noted for

both the control and peptoids as the time point before a significant increase in fluorescence was observed (5% of the plateau). Lag extension was calculated as the ratio of the lag time for peptoids to that of the control. Equilibrium plateau was determined for both the control and peptoids and percent inhibition was calculated as the percentage decrease of the plateau relative to the control.

#### *4.4.5 Transmission Electron Microscopy*

Monomer aggregation reactions were gridded for transmission electron microscopy (TEM) at time points after which the control reaction reached plateau. A 3  $\mu$ L sample was placed onto a wax substrate and a 300 square mesh formvar-carbon supported nickel grid was inverted onto the sample. After 1 min, the sample was wicked away from the bottom side of the grid using a piece of filter paper. A 3  $\mu$ L sample of 2% uranyl acetate was then placed onto the wax substrate and the grid was inverted onto the solution for a period of 45 seconds. Excess stain was wicked away with a piece of filter paper and the grids were allowed to dry for a period of 24 h. Imaging was performed using a JEOL-1011 (JEOL Ltd., Tokyo, Japan) with an accelerating voltage of 110 kV. Blinded observation of samples with random selection of grid areas was implemented to reduce bias during imaging. Images are the representative of 3 repeated experiments and 3 random sections of the grids.

## **Chapter 5 The Effects of Incorporating Charged Side Chain Groups within KLVFF-based Peptoid Mimics on A $\beta$ 42 Aggregation Species and Morphology**

### **Abstract**

Alzheimer's disease (AD) is a growing concern as the baby boomer generation approaches the average age of diagnosis. AD is characterized by the buildup of insoluble aggregated amyloid beta proteins (A $\beta$ ) fibrils in the brain. These fibrils eventually clump together to form plaques that accumulate between the neural cells in the brain. The small intermediate stages of aggregation of A $\beta$  are widely believed to exhibit the cytotoxic effects that result in the deterioration of neuronal cells. Researchers have focused on developing small molecules and peptides to modulate A $\beta$ ; however, little progress has been made. We previously reported a peptoid-based mimic of the peptide KLVFF (residues 16-20 of A $\beta$ ), referred to as JPT1, that shows promise as a potential new therapeutic agent for AD. Specifically, JPT1 modulates A $\beta$ 40 aggregation, reduces  $\beta$ -sheet aggregate formation, reduces the total number of fibrillar structured aggregates formed, and alters the morphology of aggregates present at equilibrium. In this study, we further investigate the effects of incorporating positively or negatively charged side chains at position 6 in JPT1. The peptoids were found to modulate A $\beta$ 42 while reducing total  $\beta$ -sheet and fibrillar aggregates. However, the different charged peptoids resulted in differing amounts of aggregation. These results suggest that incorporation of side chain charge within peptoid and peptide sequences alters the interaction with A $\beta$ , thus possibly indicating a potential aggregation mechanism associated with charge.

### **5.1 Introduction**

The progression of Alzheimer's disease (AD) is widely believed to be associated with the aggregation of the amyloid beta protein (A $\beta$ ).<sup>2,34</sup> A $\beta$  occurs in a range of isoforms from 37-43

amino acids in length.<sup>19,20</sup> However, the two most common isoforms of A $\beta$  associated with AD are the 40-residue and 42-residue forms of A $\beta$ , A $\beta$ 40 and A $\beta$ 42 respectively, are most commonly associated with AD progression. A $\beta$ 40 is typically associated with fibrillation, whereas A $\beta$ 42 is more pathogenic.

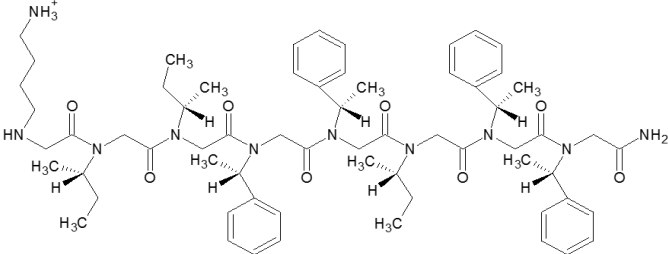
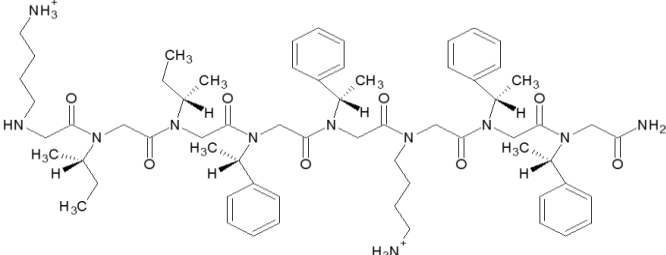
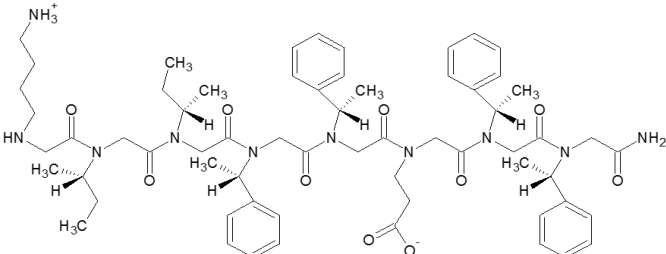
Though the specific causes of AD are still unknown, many research groups have focused on utilizing small molecules and peptidomimetics as a means to modulate or inhibit A $\beta$  aggregation.<sup>54,55,60,98,101,104,148</sup> These compounds have shown great promise at altering A $\beta$  kinetics, morphology, and aggregation pathways. Interestingly, many of these compounds affect A $\beta$  aggregation by different mechanisms, thus creating a degree of complexity associated with identifying a potential therapeutic agent. Tjernberg et al. identified the hydrophobic sequence KLVFF (residues 16-20 of A $\beta$ ) as the key recognition element within A $\beta$  that is responsible for aggregation.<sup>86,87</sup> By utilizing this hydrophobic core, researchers were able to create variants of the KLVFF peptide, bind to A $\beta$  like all peptides and inhibit aggregation *in vitro*.<sup>59,78,87-91,96</sup> Unfortunately, KLVFF variants are susceptible to proteolysis, resulting in rapid degradation *in vivo*.<sup>141</sup>

We have previously published the design and characterization of a protease-resistant peptoid-based mimics of KLVFF (JPT1; Table 5.1).<sup>53</sup> Peptoids are a unique class of peptidomimetics that are resistant to protease degradation and elicit a low immune response, making them ideal candidates for use as therapeutics and detection agents in protein misfolding diseases.<sup>97</sup> Peptoids and peptides have a structurally similar backbone, except the location of the side chain is appended to the amide nitrogen in peptoids rather than the alpha-carbon. Even though peptoids have an achiral backbone, the inclusion of chiral side chains within the sequence allows for the formation of a helical secondary structure.<sup>106,113,114,116,122</sup> The inclusion of chiral, aromatic side

chains results in peptoids that adopt a polyproline type-I like helix that has a helical pitch of ~6 Å and 3 monomers per turn.<sup>106</sup> Peptoid helices are extremely stable and can withstand denaturation in 8 M urea at 70°C.<sup>122</sup> Furthermore, the change in backbone structure allows peptoids to have an increased bioavailability compared to peptides that can improve therapeutics.<sup>2</sup>

Peptoids have only recently begun to be investigated for use in therapeutics and diagnostics in the neurodegenerative field. Specifically, peptoids have been designed as a potential therapeutic agent for Huntington's disease (HD).<sup>139</sup> Specifically, the peptoid HQP09 was capable of binding to expanded polyglutamine proteins to inhibit aggregation of Htt-N-53Q *in vitro* and shows promise *in vivo* by exerting Ca<sup>2+</sup> stabilizing and neurprotective effects in HD mice.<sup>139</sup> Peptoids have been designed from both a combinatorial library approach and a rationally designed approach to inhibit Aβ40 aggregation.<sup>53,140</sup> Peptoids have also been used to create an AD blood test that can sense antibodies that are specific to AD patients.<sup>136,137</sup> Finally, peptoids have been demonstrated to bypass the blood-brain barrier (BBB) to allow for a new route of drug delivery for the peptoid class of drugs.<sup>99</sup> Peptoids are ideal therapeutic candidates for neurodegenerative disease, such as AD, due to increased bioavailability compared to peptides<sup>97,105,107</sup> and improved membrane permeability compared to small molecules.<sup>97,143,145</sup> In this present study, we present the effects of incorporating positively or negatively charged residues at the 6 position within a rationally designed KLVFF-based peptoid mimic (Table 1) to modulate Aβ42 aggregation.

**Table 5.1** Peptoid structures, molecular weights (MW), and percent acetonitrile elution from analytical HPLC (% elution).

	Structure	MW (Da)	% Elution
JPT1		1130	72
JPT1+		1146	67
JPT1-		1146	74

## 5.2 Results

### 5.2.1 Circular Dichroism Spectroscopy

Circular dichroism (CD) spectroscopy was used to determine the secondary structure of JPT1+ and JPT1-. The CD spectra for both peptoids (Figure 5.1) in methanol exhibited a maxima near 190 nm and two minima near 205 and 220 nm.

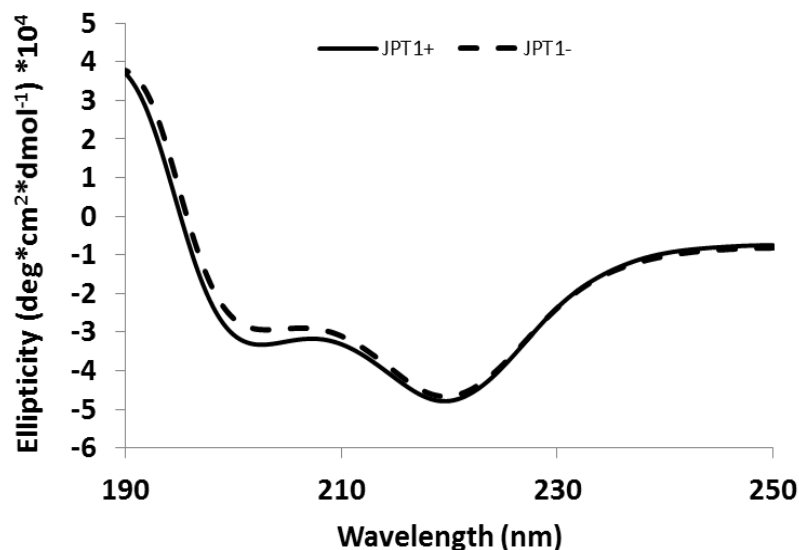
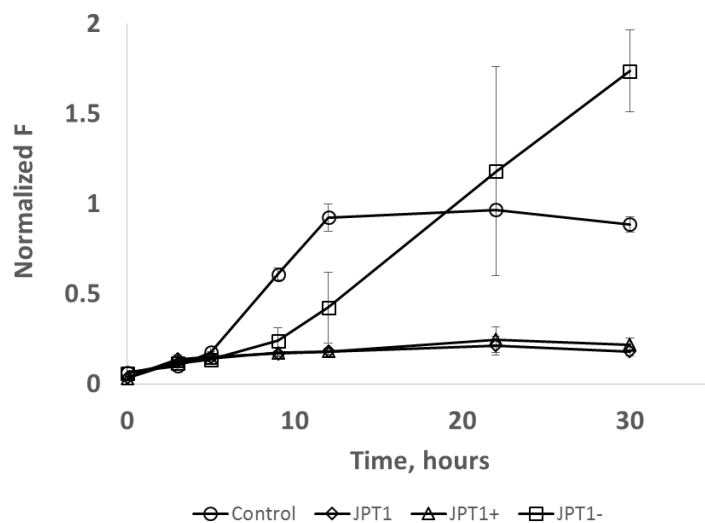


**Figure 5.1** Circular dichroism spectra for JPT1+ and JPT1-. The spectra depicts a polyproline type-I-like helical secondary structure in methanol.

### 5.2.2 ThT Aggregation Assays

Thioflavin T (ThT) aggregation assays were used to assess the ability of peptoids JPT1, JPT1+, and JPT1- to prevent the formation of  $\beta$ -sheet aggregates. Assays were performed using 20  $\mu$ M A $\beta$ 42 monomer in the absence (control) and presence of 100  $\mu$ M JPT1, JPT1+, or JPT1-. Aggregation was initiated via orbital shaker at 200 RPM and 25°C in the presence of 50 mM NaCl. ThT fluorescence measurements (excitation at 440 $\pm$ 10 nm and emission at 490 $\pm$ 10 nm) were taken at specific time points to monitor  $\beta$ -sheet formation. In the absence of peptoid, the formation of  $\beta$ -sheet aggregates began to occur at 5 h and the total number of  $\beta$ -sheets continued to increase until 9 h at which the fluorescent signal stayed consistent until 30 h. This represents a typical A $\beta$  aggregation curve that has been reported multiple times.<sup>29,33,53,77,148,149</sup> In the presence of JPT1 and JPT1+, the plateau intensity is drastically reduced compared to the control (78.7  $\pm$  3.4 % and 76.4  $\pm$  4.7 %, respectively) which indicates the formation of fewer  $\beta$ -sheet aggregates at equilibrium (Figure 5.2). In contrast, JPT1- enhanced  $\beta$ -sheet formation compared to JPT1 and JPT1+, as well as the control.





	JPT1	JPT1+	JPT1-
<b>% Inhibition</b>	78.7 ± 3.4	76.4 ± 4.7	-59.7 ± 66.6
<b>Lag Extension</b>	ND	ND	2.0 ± 0.2

**Figure 5.2** ThT analysis shows that peptoid JPT1, JPT1+, and JPT1- modulate A $\beta$ 42 aggregation. Peptoids JPT1 and JPT1+ reduce the formation of  $\beta$ -sheet aggregates, whereas JPT1- enhances the formation of  $\beta$ -sheet containing aggregates. Peptoids were added to 20  $\mu$ M A $\beta$ 42 monomer at concentrations of 100  $\mu$ M and  $\beta$ -sheet aggregates were detected via ThT fluorescence. Normalized fluorescence values are calculated as the percentage of the control plateau. Parameters are expressed as mean  $\pm$  SEM, n = 3.

### 5.2.3 Dot Blot Analysis

To assess the presence of fibrillar species of A $\beta$ 42, dot blot analysis was performed in conjunction with the A $\beta$ 42 monomer aggregation assays. A $\beta$  aggregates can be detected via antibodies that are either sequence-specific or conformation-specific. The sequence-specific antibody 6E10 recognizes residues 1-16 of A $\beta$ , allowing for detection of multiple conformations.<sup>62</sup> Conformation-specific antibodies such as A11, OC, and LOC, recognize only specific species of A $\beta$ . Specifically, OC and LOC have both been shown to bind to fibrillar A $\beta$  species.<sup>61</sup>

In the presence of 100  $\mu$ M JPT1, JPT1+, and JPT1-, OC detection resulted in 55.7 $\pm$ 12.2%, 52.4 $\pm$ 6.9%, and -49.5 $\pm$ 11.0%, respectively (Figure 5.3A). Detection with LOC resulted in

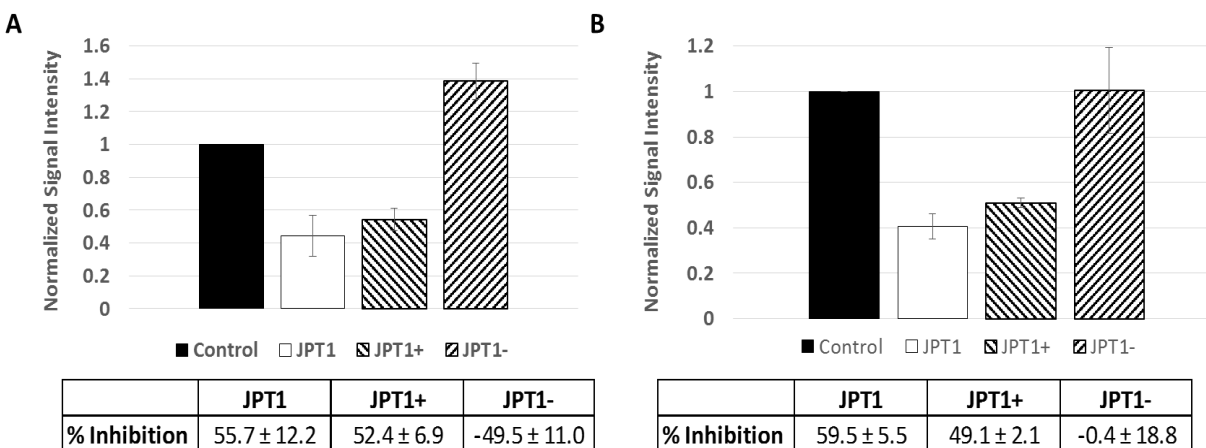


**Figure 5.3** Dot blot analysis confirms peptoids JPT1, JPT1+, and JPT1- modulate A $\beta$ 42 aggregation. A) Dot blot analysis with the primary antibody OC, which has been shown to bind to both fibrils and higher order A $\beta$  aggregates.<sup>63</sup> JPT1 and JPT1+ both reduce signal intensity as compared to the control. JPT1- does not decrease signal intensity compared to the control, indicating no reduction in higher ordered A $\beta$  aggregates. Parameters are expressed as mean  $\pm$  SEM, n = 3. B) Dot blot analysis with the primary antibody LOC, which has been shown to be more specific to A $\beta$  fibrils than OC.<sup>63</sup> Both JPT1 and JPT1+ have a significant reduction in signal intensity compared to the control, indicating a drastic reduction in fibrillar aggregates. Interestingly, JPT1- increases signal intensity for fibrillar aggregate detection, which corroborates ThT data. Parameters are expressed as mean  $\pm$  SEM, n = 2.

59.5 $\pm$ 5.5%, 49.1 $\pm$ 2.1%, and -0.4 $\pm$ 18.8%, respectively (Figure 5.3B). LOC has been reported as being more specific to fibril detection than OC.<sup>63</sup> Although the percent inhibition of the plateau for JPT1 and JPT1+ were similar for both OC and LOC primary antibodies, a significant difference was noted for JPT1-. This indicates that even though we see an increased production of  $\beta$ -sheet and higher ordered aggregates by ThT fluorescence and OC dot blot analysis, JPT1- does not contain more fibril species than the control. The increased detection by OC indicates the increased production of oligomers that are conformationally similar to fibrils.

The primary antibody 6E10 recognizes the N-terminus is commonly used as a positive control to ensure A $\beta$  is present (Figure 5.4). The positioning of the N-terminus has been correlated to playing a role in conformational changes during aggregation.<sup>98,146</sup> For JPT1 and JPT1+, the 6E10 signal intensity decreased beginning at the 5 h time point. This data indicates

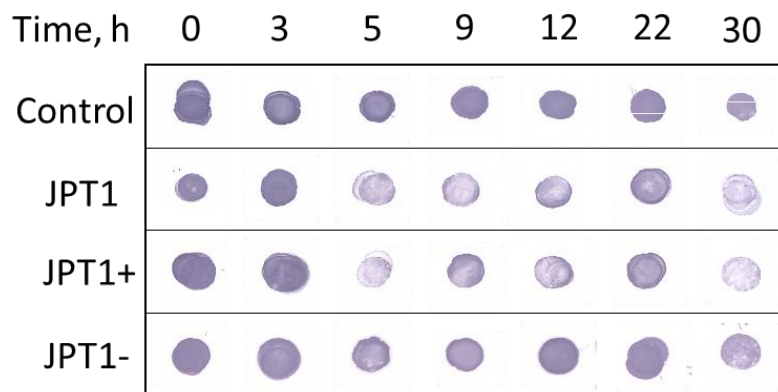


**Figure 5.4** Representative figure of dot blot analysis with primary antibody 6E10. 20  $\mu\text{M}$   $\text{A}\beta\text{42}$  was incubated in the presence and absence of 100  $\mu\text{M}$  peptoids. The amino terminus is widely believe to play a role in conformational changes during oligomerization.<sup>13,46</sup> JPT1 and JPT1+ result in a decreased signal intensity compared to the control and JPT1-, indicating a JPT1- does not alter the  $\text{A}\beta$  conformational state.

that the binding site for 6E10 in the presence of JPT1 and JPT1+ is not as readily available compared to the control and JPT1-. This phenomenon has been observed in other studies with other  $\text{A}\beta$  inhibitors.<sup>98,146</sup>

#### 5.2.4 TEM Studies

To confirm modulation of  $\text{A}\beta\text{42}$  aggregation in the presence of peptoids, transmission electron microscopy (TEM) images were acquired at various time points. In the absence of peptoids,  $\text{A}\beta\text{42}$  aggregates form high ordered aggregates to a vast fibrillar network (Figure 5.5 A-E). This fibrillar network has been observed previously.<sup>33,77,149</sup> The addition of JPT1, JPT1+, and JPT1- resulted in a morphological change to the aggregation of  $\text{A}\beta\text{42}$ . JPT1 and JPT1+ still allowed the formation of fibrils at 30 hours, but drastically reduced the expanded network of fibrils. JPT1 did allow for the formation of fibrils to develop; however, these fibrils were significantly reduced in size compared to that of the control (Figure 5.5, F-J). JPT1+ greatly

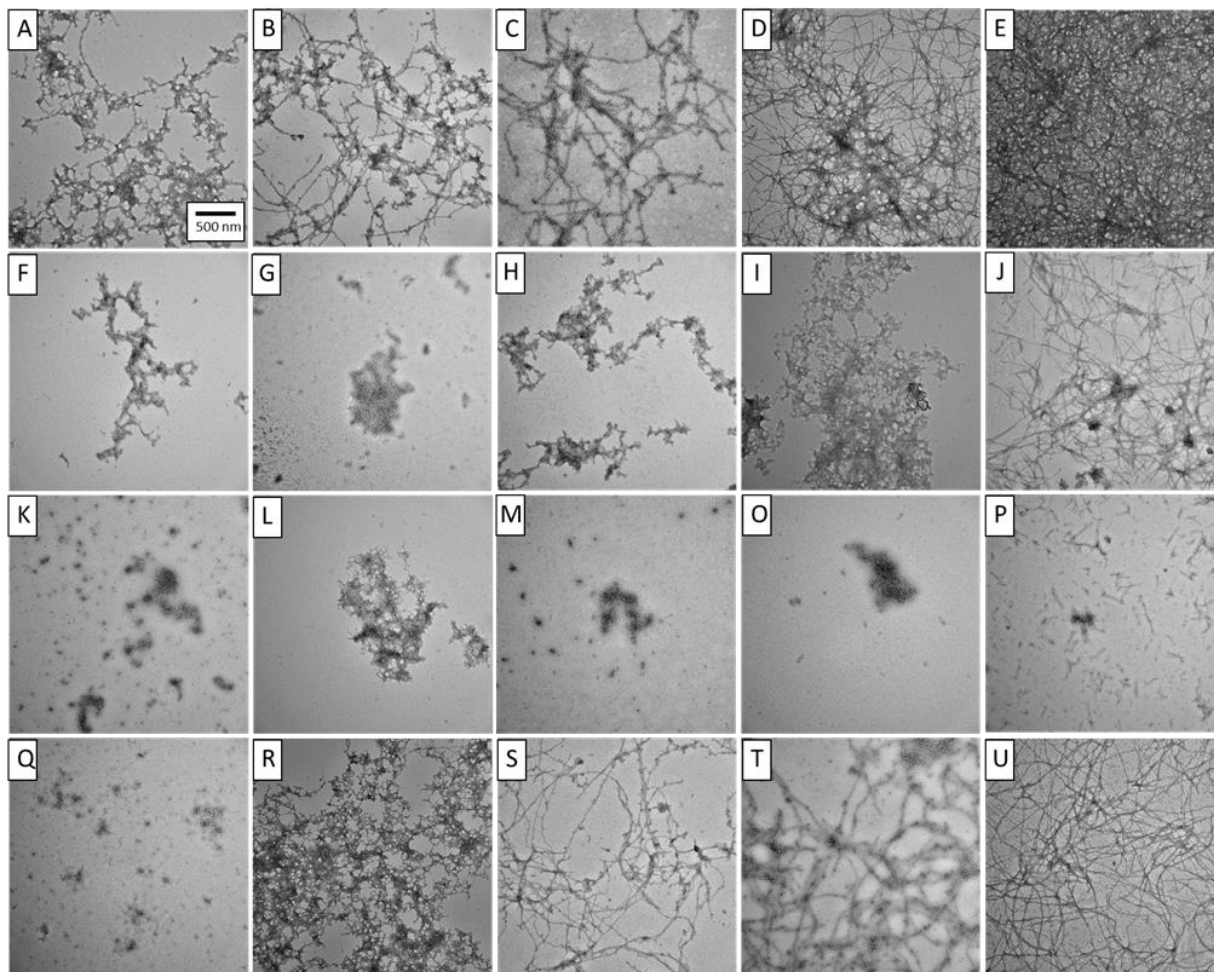


**Figure 5.5** Morphology of A $\beta$ 42 aggregates formed in the presence and absence of peptoid with varying side chain charge. 20  $\mu$ M A $\beta$ 42 monomer in 40 mM Tris-HCl (pH 8.0) was aggregated alone (control, A-E) or in the presence of 100  $\mu$ M peptoid (F-J) JPT1, (K-P) JPT1+, or (Q-U) JPT1-. Samples were gridded at 3, 5, 9, 12, and 30 h time points (right to left) and visualized by TEM. Results are representative of 3 independent experiments and imaged grids were randomly selected.

reduced the length of the aggregates formed and may potentially be a ‘off-pathway’ aggregate species as previously reported (Figure 5.5, K-P).<sup>18,151</sup> JPT1- reduced the branching and accumulation of fibrils compared to the control. JPT1- formed fibrils share a similar morphology to that of the control, but delayed the formation of fibrils by 9 h (Figure 5.5, Q-U). This suggests that even though JPT1- allows for the formation of A $\beta$  fibrils, aggregation is modulated compared to that of the control.

#### 5.2.4 AFM Studies

To better investigate the formation of A $\beta$ 42 oligomers, atomic force microscopy (AFM) was performed at specific time points. In the absence of peptoids, A $\beta$ 42 has low molecular weight aggregates present at 3 h (Figure 5.6A), higher molecular weight aggregates at 12 h (Figure 5.6B), and fibrils at 30 h (Figure 5.6C). The addition of JPT1 results in the formation of ordered aggregates at 3 h (Figure 5.6D), aggregates to form off pathway sphere-like aggregates at 12 h (Figure 5.6E), and the formation of higher ordered aggregates at 30 h (Figure 5.6F) that do not appear fibrillar in conformation. The addition JPT1+ results in the formation of ordered aggregates at 3 h (Figure 5.6G), aggregates to form higher ordered aggregates at 12 h (Figure 5.6H) and 30 h (Figure 5.6I). The addition of JPT1- resulted in no aggregate species at 3 h (Figure 5.6J), aggregates to form similar high molecular weight aggregates at 12 h with reduced size compared to the control (Figure 5.6K), and low and high molecular weight aggregates at 30 h with no visible fibrils (Figure 5.6L).

### 5.3 Discussion

The peptoids JPT1, JPT1+, and JPT1- (Table 5.1) were designed to have a similar sequence to that of the peptide KLVFF. They exhibit a helical secondary structure in methanol (Figure 5.1). The peptoids were designed such that the chiral, aromatic F-like groups align on two faces of the helix with  $\sim 6$  Å spacing between. The spacing between the F-like groups on the face of the helix corresponds to the spacing of a  $\beta$ -sheet between the backbone carbons  $i$  and  $i+2$ . This is hypothesized to help facilitate pi-pi stacking between the aromatic groups within the peptoid and A $\beta$  aggregates.

Previous work on KLVFF peptide variants show an increase in inhibitor activity when positively or negatively charged side chains are incorporated at the C-terminus.<sup>59,88</sup> To better

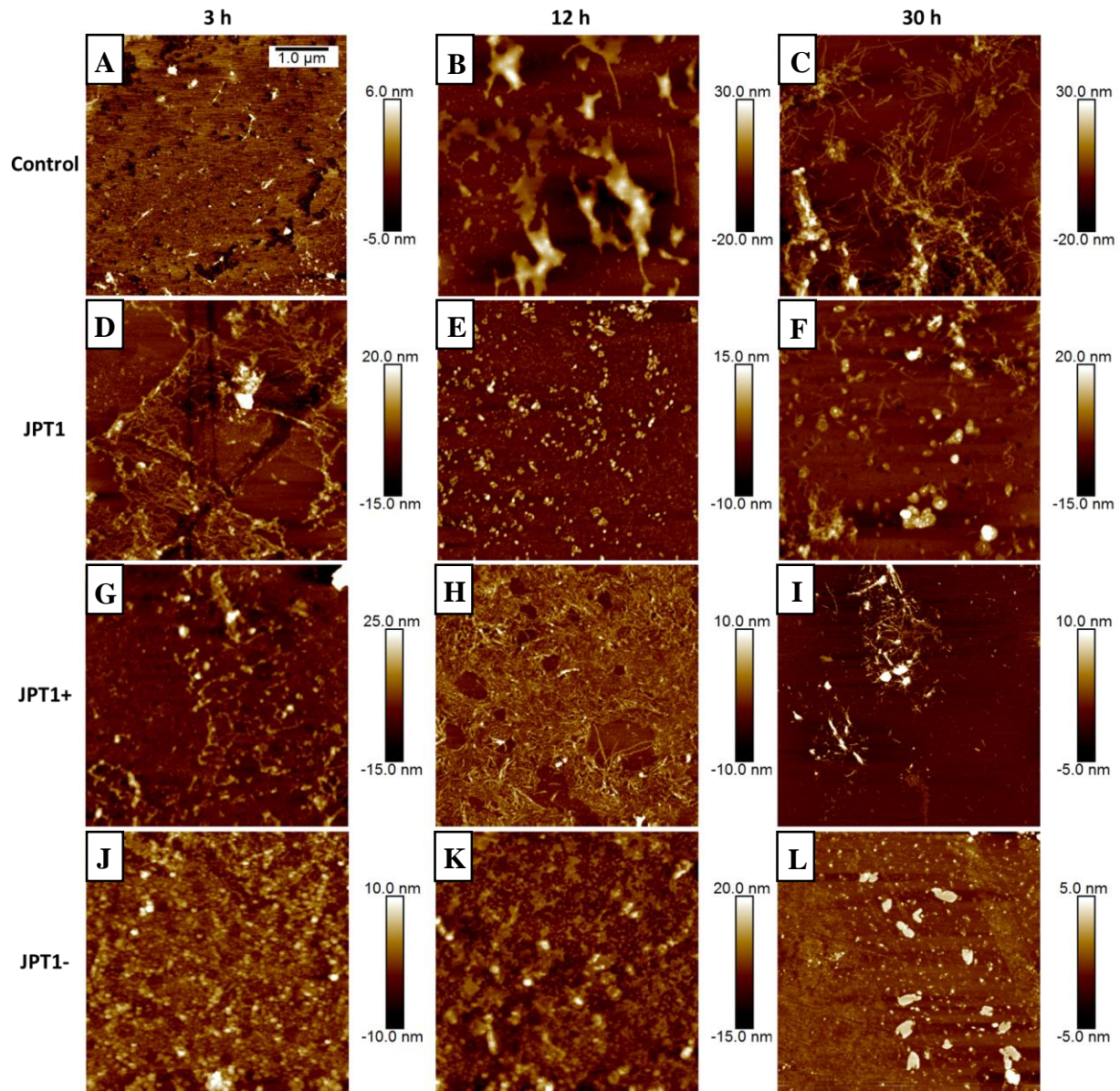


**Figure 5.6** 20  $\mu\text{M}$  A $\beta$ 42 monomer was aggregated at 200 RPM at 25  $^{\circ}\text{C}$  in 40 mM Tris HCl buffer with 50 mM NaCl. Samples were taken at 3, 12, and 30 h and incubated on ruby muscovite mica for 10 min and was then rinsed with 0.2  $\mu\text{m}$  filtered water and then dried under nitrogen for 3 h. Control groups (A-C) display a typical A $\beta$ 42 aggregation that contains: A) low molecular weight species, B) large aggregates, C) fibrils. In the presence of JPT1 (D-F), A $\beta$ 42 aggregates to form: D) ordered branched aggregates, E) small, circular aggregates, and F) off pathway aggregates. In the presence of JPT1+ (G-I), A $\beta$ 42 aggregates to form: G) ordered aggregates, H) packed aggregates, and I) high ordered aggregates. In the presence of JPT1- (J-L), A $\beta$ 42 aggregates to form J) small molecular weight oligomers, K) low molecular weight species, and L) small and large aggregates.

understand the effects of side chain charge, the charge of the side chain at position 6 was varied (JPT1+ and JPT1-, Table 5.1). This position is equivalent to the C-terminus of KLVFF. Previous

studies have shown that charged small molecules inhibit A $\beta$  aggregation by disrupting protein folding via electrostatic disruptions.<sup>152–156</sup> More specifically, peptide KLVFF variants that include positively charged residues on the C-terminus have been shown to decrease A $\beta$  aggregates formed.<sup>59,157</sup> However, when positively charged residues are added to either the N-terminus or both termini, then the ability of these charged KLVFF peptides to decrease A $\beta$  aggregates decreases.<sup>157</sup> Finally, the addition of negatively charged residues to the C-terminus of peptide KLVFF variants has shown to either have no effect on A $\beta$  aggregation or even slightly promoting fibrillar growth.<sup>88</sup> Based on these studies, we hypothesized our peptoid KLVFF mimics would have a similar effect on A $\beta$ 42 aggregation.

The studies reported here show that all three peptoids designed to mimic the sequence of the peptide KLVFF modulate A $\beta$ 42 aggregation. We have previously published that JPT1 was designed for optimal interaction with the hydrophobic regions of the A $\beta$  cross  $\beta$ -sheet structure.<sup>53</sup> The incorporation of varying charges at the sixth side chain location resulted in altered morphologies and  $\beta$ -sheet content in the presence of all three peptoids. ThT aggregation assays confirm all three peptoids modulate A $\beta$ 42 aggregation. JPT1 and JPT1+ both reduced the formation of  $\beta$ -sheet aggregates, whereas JPT1- enhanced the formation of  $\beta$ -containing aggregates. Dot blot analysis with OC and LOC agreed with ThT data. JPT1 and JPT1+ reduced fibrillar aggregates compared to the control. OC detection has been linked to binding to oligomers that are conformationally similar to fibrils.<sup>63</sup> Dot blot analysis with both OC and LOC provide similar results with JPT1 and JPT1+, indicating no presence of oligomers that are conformationally similar to fibrils. However, JPT1- had varying results with OC and LOC. While both antibodies indicate JPT1- does not reduce fibrillar aggregates, the increased signal

intensity for OC over LOC indicates the presence of oligomers that are conformationally similar to fibrils.

Our results are in agreement with charge modified KLVFF peptides that interfered with A $\beta$ 40 aggregation. Bett *et al.* investigated KLVFF peptides with N- and C-terminus charge additions to inhibit A $\beta$ 40 aggregation.<sup>157</sup> Similar to JPT1+, the addition of a positively charged R group to the C-terminus of KLVFF significantly reduced A $\beta$ 40 aggregation. Lowe *et al.* reported that a KLVFF variant containing four E groups promoted fibrillar aggregate promotion, similar to the promoted fibrillar growth observed by JPT1-.<sup>88</sup> Thus, our results agree with prior findings regarding KLVFF peptide mimics that contain positively or negatively charged groups, specifically at the C-terminus.

The N-terminus has been correlated to playing a role in conformational changes during A $\beta$  aggregation.<sup>98,146</sup> Interestingly, the ability for peptoids to reduce  $\beta$ -sheet containing aggregates and fibrillar aggregates corresponded to 6E10 signal intensity. The 6E10 signal for the control and A $\beta$ 42 in the presence of JPT1- was higher than the signal for A $\beta$ 42 in the presence of JPT1 and JPT1+. This indicates JPT1- is not altering the conformation of the amino terminus. Thus, N-terminus masking may play a pivotal role in assessing small molecules ability to reduce the formation of fibrillar aggregates.

To further examine the effects of charged peptoids on A $\beta$ 42 aggregation, TEM and AFM were employed to evaluate the morphological states. Our results indicate that JPT1 and JPT1+ are capable of significantly reducing the size and structure of A $\beta$ 42 oligomers and fibrils. In contrast, JPT1- appears to have reduced the amount of fibrils compared to the control, but seem to have increased the amount of oligomers present at 30 h. These results agree with dot blot analysis with primary antibodies OC and LOC. Unlike JPT1 and JPT1+, JPT1- modulates A $\beta$ 42



aggregation in a way that promotes aggregate growth. This is consistent with the KLVFF-E<sub>4</sub> peptide variant that was previously reported.<sup>88</sup> Overall, these results demonstrate the role of charged groups within KLVFF-based peptoid mimics that modulate A $\beta$ 42 aggregation.

## 5.4 Conclusions

Development of a treatment for AD is imperative. Many small molecules and peptides have been developed to target A $\beta$  aggregation as a therapeutic intervention. In this study, we demonstrated the effects of utilizing positively and negatively charged residues within KLVFF-based peptoid mimics to act as novel modulators of A $\beta$  aggregation.

JPT1 and JPT1+ proved to be more effective A $\beta$ 42 modulators compared to JPT1-. As previously mentioned, positively and negatively charged KLVFF variants at the C-terminus have a similar effect on A $\beta$  aggregation as presented here.<sup>88,157</sup> Further studies will focus on modifying the placement of positively and negatively charged residues within KLVFF-based peptoids. In addition, evaluating the effects of peptoids on AD mouse models will help determine the capabilities of these novel compounds as a therapeutic option for AD.

## 5.5 Materials and Methods

### 5.5.1 Materials

(N)-(S)-*sec*-Butylamine (I-like side chain), (S)-(-)- $\alpha$ -methylbenzylamine (F-like side chain), and Thioflavin T (ThT) were purchased from Sigma-Aldrich (St. Louis, MO). *tert*-Butyl N-(4-aminobutyl) carbate (Boc protected K-like side chain) was purchased from CNH Technologies, Inc. (Woburn, MA). H-Ala-OtBu-HCl was purchased from BACHEM (Torrance, CA), which underwent a free-base reaction before amine coupling during synthesis. MBHA rink amide resin was purchased from NovaBiochem (Gibbstown, NJ). A $\beta$ 42 was purchased from Anaspec, Inc. (Freemont, CA). Primary antibody OC and LOC was purchased from EMD Millipore (Billerica,

MA). Primary antibody 6E10, alkaline phosphatase-conjugated anti-mouse IgG, and alkaline phosphatase-conjugated anti-rabbit IgG were purchased from Thermo Scientific (Rockford, IL). All other reagents used during synthesis, purification, and sample preparation were purchased from VWR or Fisher. All chemicals were used without further modification unless otherwise indicated.

### 5.5.2 Peptoid Synthesis and Purification

Peptoids were synthesized *via* a two-step process using an Applied Biosystems 433A automated peptide synthesizer (Carlsband, CA) that was refurbished from a 431A synthesizer.<sup>110</sup> Rink amide resin was swelled with dimethylformamide (DMF) and the Fmoc protecting group was removed using 20% piperidine in DMF. The secondary amine was acylated by adding 1.2 M bromoacetic acid in DMF and diisopropylcarbodiimide at a ratio of 5.3:1 and vortexing for 60 min. Side chain amines were added to the resin *via* an S<sub>N</sub>2 reaction mechanism. The peptoid was removed from the resin by bathing it in a cleavage cocktail consisting of 95% trifluoroacetic acid (TFA), 2.5% triisopropylsilane, and 2.5% water for 5 min. The acid was removed using a Heidolph Laborota 4001 rotating evaporator (Elk Grove Village, IL) and the peptoid was diluted

to a concentration of  $\sim 3 \text{ mg mL}^{-1}$  in a 50:50 solution of acetonitrile-water. Peptoids were purified using a Waters Delta 600 preparative high performance liquid chromatography unit (HPLC;

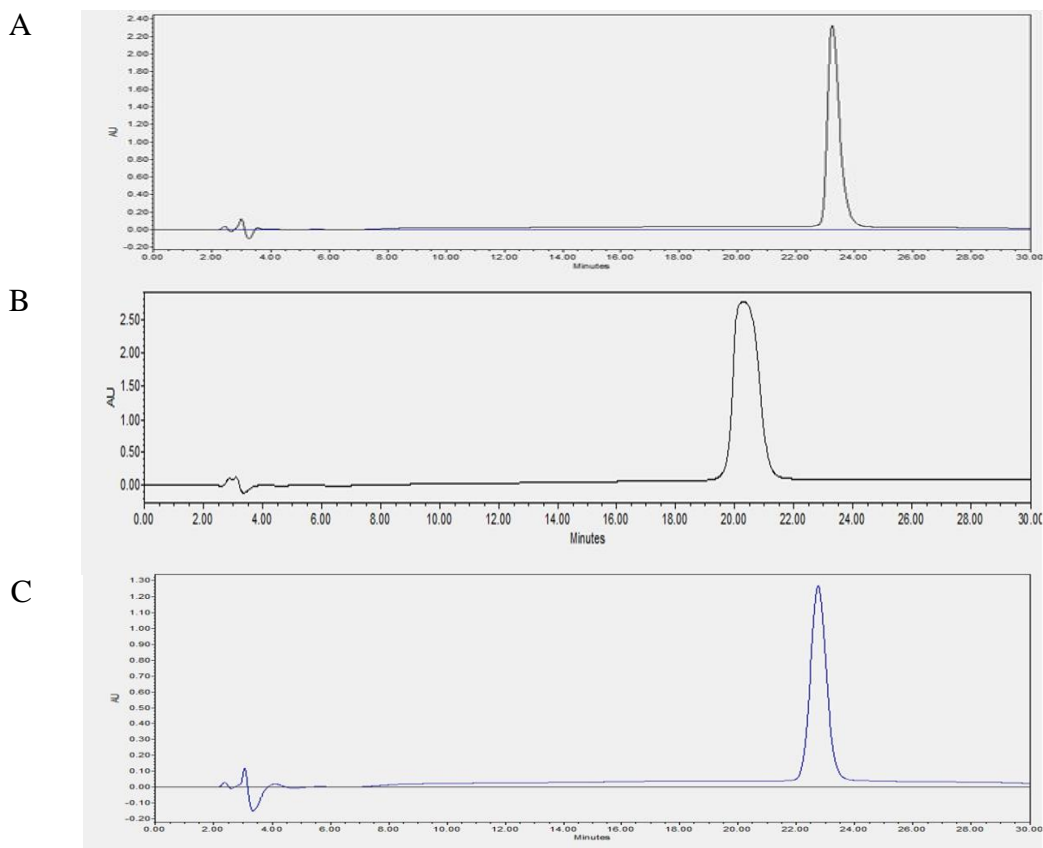


**Figure 5.7** Peptoids ( A: JPT1, B: JPT1a, and C: JPT1s) were confirmed to be >98% pure via analytical HPLC (Waters 2695 Separations Module) equipped with a Duragel G C18 150 x 2.1 mm column (Peeke Scientific) using a linear gradient of 5 to 95% solvent D in C (solvent D: acetonitrile, 0.1% TFA; solvent C: water, 0.1% TFA) over 30 min.

Milford, MA) with a Duragel G C18 150 x 20 mm column (Peeke Scientific, Novato, CA).

Gradients were run at  $\sim 1\%$  per minute with 5-95% solvent B in A (solvent A: water, 5%

acetonitrile, 0.1% TFA; solvent B: acetonitrile, 5% water, 0.1% TFA). Peptoids were confirmed

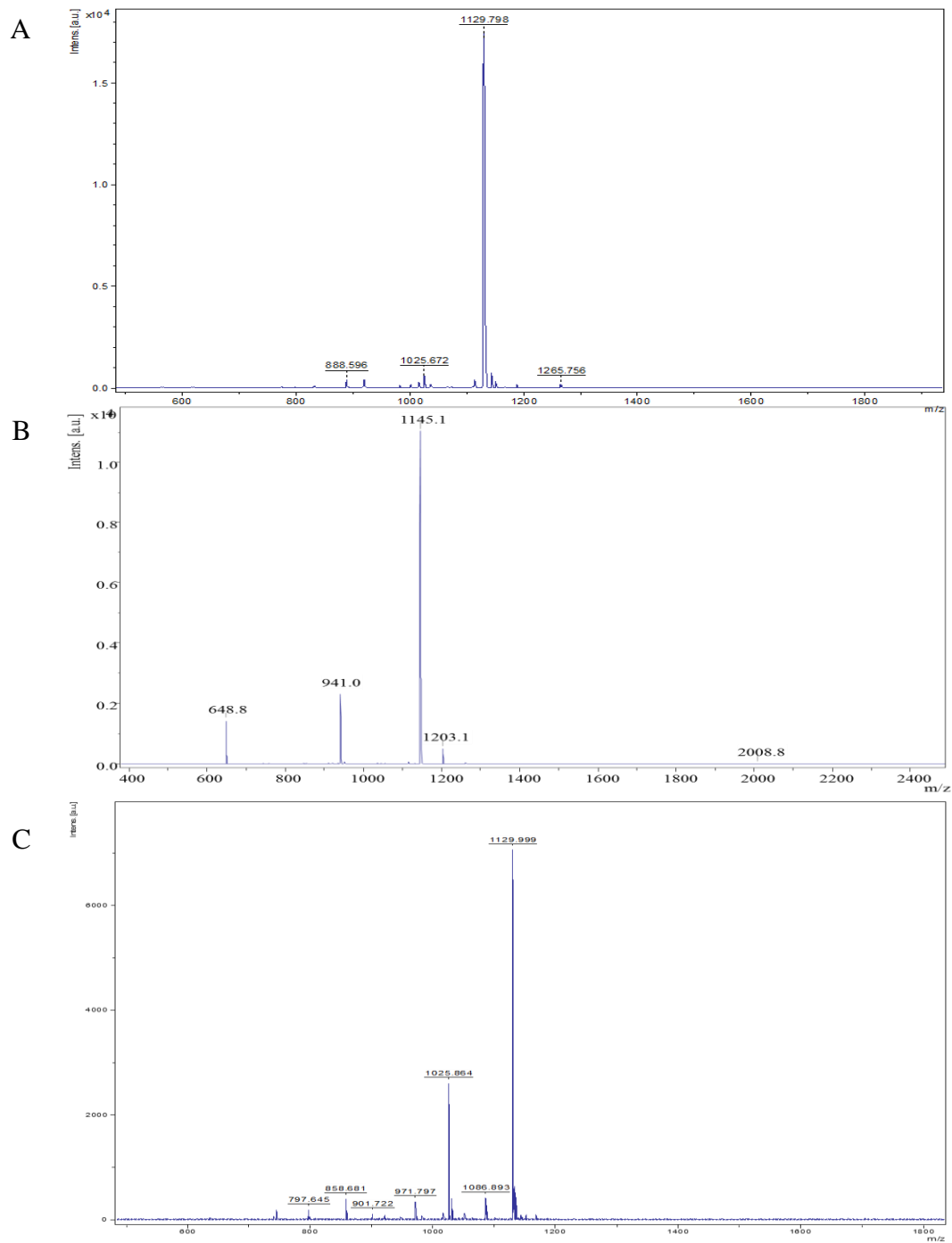


**Figure 5.8** MALDI-TOF mass spectrometry was used to confirm that the purified peptoid mass matched the theoretical mass. A) Peptoid JPT1 theoretical mass was 1130.5 Da, B) Peptoid JPT1+ theoretical mass was 1145.1 Da, and C) peptoid JPT1-theoretical mass was 1130.5 Da.

to be >98% pure (Figure 5.7) via analytical HPLC (Waters 2695 Separations Module) equipped with a Duragel G C18 150 x 2.1 mm column (Peeke Scientific) using a linear gradient of 5 to

95% solvent D in C (solvent D: acetonitrile, 0.1% TFA; solvent C: water, 0.1% TFA) over 30 min. MALDI-TOF mass spectrometry was used to confirm that the purified peptoid mass matched the theoretical mass (Figure 5.8). Purified peptoid solutions were dried to powder using a Labconco lyophilizer (Kansas City, MO) and stored at -20 °C.

### 5.5.3 Preparation of A $\beta$ 42 Peptide Solution

A $\beta$ 40 was dissolved in cold HFIP to create a 1 mM solution and was incubated on ice for 60 min. After incubation, the solution was separated into individual non-stick vials and allowed to evaporate overnight at room temperature resulting in the creation of thin peptide films. The resulting peptide film was stored with desiccant at -80 °C until use. Prior to experimentation, peptide films were rehydrated with 5 mM NaOH on ice for 5 min and then 40 mM Tris-HCl (pH 8.0) was added for 10 min on ice. Finally, 150 mM NaCl was added along with either 5% DMSO (v/v) or peptoid inhibitor (dissolved in DMSO) to a final concentration of 20  $\mu$ M.

### 5.5.4 A $\beta$ 42 Aggregation Assay

Aggregation assays were performed with 20  $\mu$ M rehydrated A $\beta$ 42 peptide films in 5 mM NaOH, 40 mM Tris-HCl (pH 8.0), and 150 mM NaCl. Peptoids were dissolved in DMSO and added at 100  $\mu$ M such that the final DMSO concentration was 5% (v/v). Assays were performed at 25 °C under agitation on an orbital shaker at 800 rpm. For ThT measurements, an aliquot was taken at varying time points and combined with ThT at a 5:1 molar ratio (ThT to A $\beta$ ). Samples were well mixed for 8 s and then scanned with a Shimadzu RF-150 mini fluorometer (excitation at 440  $\pm$  10 nm and emission at 490  $\pm$  10 nm) with an average scan time of 4 seconds. ThT fluorescence with background (ThT alone) subtraction was normalized for the fluorescence detected at equilibrium for the control reaction and plotted against time. Lag time was noted for both the control and peptoids as the time point before a significant increase in fluorescence was

observed (5% of the plateau). Lag extension was calculated as the ratio of the lag time for peptoids to that of the control. Equilibrium plateau was determined for both the control and peptoids and percent inhibition was calculated as the percentage decrease of the plateau relative to the control.

#### *5.5.5 Transmission Electron Microscopy*

Monomer aggregation reactions were gridded for transmission electron microscopy (TEM) at time points after which the control reaction reached plateau. A 3  $\mu$ L sample was placed onto a wax substrate and a 300 square mesh formvar-carbon supported nickel grid was inverted onto the sample. After 1 min, the sample was wicked away from the bottom side of the grid using a piece of filter paper. A 3  $\mu$ L sample of 2% uranyl acetate was then placed onto the wax substrate and the grid was inverted onto the solution for a period of 45 seconds. Excess stain was wicked away with a piece of filter paper and the grids were allowed to dry for a period of 24 h. Imaging was performed using a JEOL-1011 (JEOL Ltd., Tokyo, Japan) with an accelerating voltage of 110 kV. Blinded observation of samples with random selection of grid areas was implemented to reduce bias during imaging. Images are the representative of 3 repeated experiments and 3 random sections of the grids.

#### *5.5.6 Atomic Force Microscopy*

Samples were taken at 3, 12, and 30 h for atomic force microscopy (AFM) studies. A 10  $\mu$ L sample was incubated onto freshly cleaved ruby musconite mica for 10 min and was then triple rinsed with 0.2  $\mu$ m filtered DI water. Samples were then allowed to dry under gentle nitrogen flow for 3 h. AFM studies were performed on a Bunker AFM Dimension 3100 (Billerica, MA) in standard tapping mode with HQ:NSC15/AL BS tip probes (MicroMasch USA, Lady's Island,

SC). Samples were scanned with a rate of 1.0 Hz. Images are the representative of 3 repeated experiments.

## **Chapter 6 Future Directions and Conclusion**

### **6.1 Future Directions**

#### *6.1.1 In-Vivo Studies in Transgenic Mouse Models*

Thus far, all studies involving peptoids and AD have been *in-vitro*. To better understand how peptoids can serve as a therapeutic agent, future work needs to revolve around testing the efficacy of peptoid-based KLVFF mimics in AD mouse models. Many of these models allow for A $\beta$  plaque clearing and the measurement of improved cognitive effects. Specifically, investigating the impact on A $\beta$  plaque clearing may prove insightful. Though plaques are no longer believed to be the main cause of AD, improved cognitive effects in AD mouse models have been noted.<sup>49,158</sup> Clearing of plaques does show premise that a compound has the potential to break down aggregates, similar to a class III compound that has been previously reported.<sup>80</sup> These studies would demonstrate the overall capabilities of peptoids, thus allowing for future testing of peptoids in human clinical trials. Overall, these studies would help determine the therapeutic benefits of peptoids for patients with AD.

#### *6.1.2 Peptoid Biocompatibility*

Though peptoids resistance to proteolysis is promising for therapeutic applications, the increased half-life *in-vivo* could pose potential problems, especially in the neuronal environment. However, one peptoid has been delivered via intranasal administration through the olfactory nerve and into the neuronal environment.<sup>99</sup> CHIR5585 demonstrated a clearing mechanism similar to peptides and was noted to have a presence in the kidneys. This was the one of the first indications that peptoids can still clear biological systems without proteolysis. Though

CHIR5585 is of similar size compared to the peptoids proposed here, studies should still focus on both associated toxicity and clearing mechanisms of peptoid-based KLVFF mimics.

### *6.1.3 Investigation of peptoids creating unique pathways of A $\beta$ aggregation*

Small molecules, such as rhodamine B and congo red, have shown to act on A $\beta$  aggregation via unique pathways. This has led to the organization of three classes that can act on A $\beta$  aggregation very differently.<sup>80</sup> It was also postulated that many more unique aggregation pathways may be in existence that have not yet been identified. This creates an interesting opportunity to investigate the potential of peptoids acting on new, mechanistic A $\beta$  aggregation pathways. Specifically, several known small molecules have already been organized within classes of compounds that act on dependent and independent A $\beta$  aggregation pathways.<sup>65</sup> Prior to investigating the effects of peptoid helicity and side chain placement (Chapter 4), testing for any possible synergistic effects with peptoid JPT1, Congo Red, Orange G, and Rhodamine B was conducted (Appendix C). Congo Red, Orange G, and Rhodamine B each represent a unique and distinct pathway that acts on A $\beta$  aggregation. By investigating these small molecules with JPT1, we had hoped to determine if JPT1 could be organized within the same class as one of these small molecules. The potential for synergistic effects when mixing these small molecules with JPT1 on A $\beta$  aggregation was also hypothesized. Investigation within this area would be interesting to see if peptoid-based KLVFF mimics act on unique A $\beta$  aggregation pathways.

## **6.2 Conclusion**

AD is a growing concern as the aging baby boomer generation approaches the typical age of diagnosis. There is still no cure for this debilitating disease; however, great strides have been made at finding a potential therapeutic option. Still, there are concerns as many of these technologies have shortcomings associated with poor bioavailability, short half-life *in-vivo*, and



potential problems crossing the BBB. Recent studies have identified the hydrophobic core of A $\beta$  (residues 16-20 of A $\beta$ ; KLVFF) as the key recognition element.<sup>86,87</sup> Many variants of this peptide sequence have been investigated for potential use as a therapeutic option for AD.<sup>59,78,88-91,96</sup> However, as with all peptides, KLVFF based peptide are susceptible to proteolysis.

Here, we designed a novel class of peptoid-based KLVFF mimics to overcome the issues KLVFF peptides have faced. Peptoids are structurally similar to peptides; however, by attaching the side chain groups to the amide nitrogen rather than the  $\alpha$ -carbon, a protease resistant structure is formed. This allows for improved bioavailability compared to peptides.<sup>97,107</sup> Our peptoid analogs have utilized aromatic structures that may help facilitate pi-pi stacking with the aromatic structures in A $\beta$ . Pi-pi stacking has been hypothesized to help stabilize A $\beta$  oligomer aggregates, thus reducing the associated toxicity.<sup>80</sup> Peptoids have significant potential for use as a therapeutic treatment for AD due to ease of synthesis, increased bioavailability, and the endless combination of commercially available side chain amines.

Within Chapter 3, we examined the ability of a rationally designed peptoid-based KLVFF variant to modulate A $\beta$ 40 aggregation. Peptoid JPT1 demonstrated capabilities of reducing  $\beta$ -sheet containing aggregates up to ~84% in a 5-fold molar excess of A $\beta$ 40 monomer. We noted significant lag time reductions compared to the control, indicating JPT1 may be acting on a unique pathway of A $\beta$ 40 aggregation similar to the effects of fibrillar seeds propagating A $\beta$ 40 aggregation from monomer to fibril while bypassing intermediate stages of oligomerization.<sup>44</sup> The results presented here demonstrate the peptoid-based KLVFF mimics have similar, if not better capabilities at modulating A $\beta$  aggregation *in vitro* compared to peptide-based KLVFF variants.<sup>59,78,88,89,96</sup>

In Chapter 4, we investigated the effect of peptoid secondary structure and side chain placement within peptoid-based KLVFF mimics. We removed side chain chirality to create JPT1a, a peptoid that did not have a helical secondary structure. This peptoid reduced a similar number of  $\beta$ -sheets compared to JPT1; however, immunoblotting studies demonstrated that JPT1a was superior at reducing fibrillar aggregates. Further analysis with TEM demonstrated a significant morphological changes to A $\beta$ 40 aggregation with JPT1a compared to JPT1. We hypothesized JPT1a had improved interaction and modulation activity to that of JPT1 due to the increased backbone flexibility. By rationally scrambling JPT1, JPT1s was designed so that only one face of the helix contained two F-like groups to investigate if spacing of the F-like groups was essential to A $\beta$  modulation activity. Immunoblotting suggested a slight increased ability of JPT1s to reduce fibrillar aggregates; however, TEM revealed the two peptoids had a similar number of fibrillar aggregates at equilibrium. Thus, we rationalized that the positioning of the F-like groups on peptoid-based KLVFF mimics that are 8 side chain residues in length may not be as essential as originally thought.

In Chapter 5, we investigated the inclusion of positively or negatively charged residues at the 6 position. Inclusion of a positively K-like group (peptoid JPT1+) resulted in a slight decrease in modulation activity when compared to JPT1 with immunoblotting techniques. Morphology studies suggested the aggregates formed in the presence of JPT1+ were reduced in size compared to those observed with JPT1. In contrast, the inclusion of a negatively charged E-like group (JPT1-) enhanced the formation of  $\beta$ -sheets and oligomers that have a conformation similar to fibrils. TEM studies did not indicate promoted growth of fibrils or high molecular weight aggregates compared to the control; however, AFM studies did indicate the presence of smaller aggregates after 30 h compared to the control. These results are in agreement with negatively

charged peptide-based KLVFF variants, suggesting an underlying mechanism that is occurring to propagate A $\beta$  aggregation.<sup>157</sup> This study demonstrates the effectiveness of four unique peptoid sequences (JPT1, JPT1a, JPT1s, and JPT1+) that were rationally derived from the peptide KLVFF at modulating both A $\beta$ 40 and A $\beta$ 42 aggregation. Specifically, morphology studies indicated three distinct morphological alterations to A $\beta$  aggregates between these sequences. This may indicate unique and independent A $\beta$  aggregation pathways. Overall, this work has demonstrated the potential use of peptoids as a therapeutic agent for AD. Further investigation with these peptoid sequences may help determine a viable cure for AD.

## REFERENCES

- (1) What Is Alzheimer's? [http://www.alz.org/alzheimers\\_disease\\_what\\_is\\_alzheimers.asp](http://www.alz.org/alzheimers_disease_what_is_alzheimers.asp) (accessed Oct 22, 2014).
- (2) Selkoe, D. J. Amyloid Protein and Alzheimer's Disease. *Sci. Am.* **1991**, *265*, 68–78.
- (3) Hardy, J.; Selkoe, D. J. The Amyloid Hypothesis of Alzheimer's Disease: Progress and Problems on the Road to Therapeutics. *Science*. **2002**, *297*, 353–356.
- (4) Orpiszewski, J.; Schormann, N.; Kluge-Beckerman, B.; Liepnieks, J. J.; Benson, M. D. Protein Aging Hypothesis of Alzheimer Disease. *FASEB* **2000**, *14*, 1255–1263.
- (5) Walsh, D. M.; Selkoe, D. J. Deciphering the Molecular Basis of Memory Failure in Alzheimer's Disease. *Neuron*. **2004**, *44*, 181–193.
- (6) Selkoe, D. J. Amyloid Beta-Protein and the Genetics of Alzheimer's Disease. *J. Biol. Chem.* **1996**, *271*, 18295–18298.
- (7) Castillo-Carranza, D. L.; Sengupta, U.; Guerrero-Munoz, M. J.; Lasagna-Reeves, C. A.; Gerson, J. E.; Singh, G.; Estes, D. M.; Barrett, A. D. T.; Dineley, K. T.; Jackson, G. R.; Kaye, R. Passive Immunization with Tau Oligomer Monoclonal Antibody Reverses Tauopathy Phenotypes without Affecting Hyperphosphorylated Neurofibrillary Tangles. *J. Neurosci.* **2014**, *34*, 4260–4272.
- (8) Rapoport, M.; Dawson, H. N.; Binder, L. I.; Vitek, M. P.; Ferreira, A. Tau Is Essential to Beta-Amyloid-Induced Neurotoxicity. *Proc. Natl. Acad. Sci. U. S. A.* **2002**, *99*, 6364–6369.
- (9) Hardy, J. A.; Higgins, G. A. Alzheimer's Disease: The Amyloid Cascade Hypothesis. *Science*. **1992**, *256*, 184–185.
- (10) Ramírez-Alvarado, M.; Merkel, J. S.; Regan, L. A Systematic Exploration of the Influence of the Protein Stability on Amyloid Fibril Formation in Vitro. *Proc. Natl. Acad. Sci. U. S. A.* **2000**, *97*, 8979–8984.
- (11) Chiang, P. K.; Lam, M. A.; Luo, Y. The Many Faces of Amyloid Beta in Alzheimer's Disease. *Curr. Mol. Med.* **2008**, *8*, 580–584.
- (12) Irvine, G. B.; El-Agnaf, O. M.; Shankar, G. M.; Walsh, D. M. Protein Aggregation in the Brain: The Molecular Basis for Alzheimer's and Parkinson's Diseases. *Mol. Med.* **2008**, *14*, 451–464.
- (13) Ferreira, S. T.; Vieira, M. N. N.; De Felice, F. G. Soluble Protein Oligomers as Emerging Toxins in Alzheimer's and Other Amyloid Diseases. *IUBMB Life*. **2007**, *59*, 332–345.

- (14) Haataja, L.; Gurlo, T.; Huang, C. J.; Butler, P. C. Islet Amyloid in Type 2 Diabetes, and the Toxic Oligomer Hypothesis. *Endocr. Rev.* **2008**, *29*, 303–316.
- (15) Höppener, J. W.; Ahrén, B.; Lips, C. J. Islet Amyloid and Type 2 Diabetes Mellitus. *N. Engl. J. Med.* **2000**, *343*, 411–419.
- (16) More than Just Mad Cow Disease. *Nat. Struct. Biol.* **2001**, *8*, 281.
- (17) Dobson, C. M. Protein Misfolding, Evolution and Disease. *Trends Biochem. Sci.* **1999**, *24*, 329–332.
- (18) Ehrnhoefer, D. E.; Bieschke, J.; Boeddrich, A.; Herbst, M.; Masino, L.; Lurz, R.; Engemann, S.; Pastore, A.; Wanker, E. E. EGCG Redirects Amyloidogenic Polypeptides into Unstructured, off-Pathway Oligomers. *Nat. Struct. Mol. Biol.* **2008**, *15*, 558–566.
- (19) Glenner, G. G.; Wong, C. W. Alzheimer's Disease: Initial Report of the Purification and Characterization of a Novel Cerebrovascular Amyloid Protein. *Biochem. Biophys. Res. Commun.* **1984**, *120*, 885–890.
- (20) Masters, C. L.; Simms, G.; Weinman, N. A.; Multhaup, G.; McDonald, B. L.; Beyreuther, K. Amyloid Plaque Core Protein in Alzheimer Disease and Down Syndrome. *Proc. Natl. Acad. Sci. U. S. A.* **1985**, *82*, 4245–4249.
- (21) Götz, J.; Eckert, A.; Matamales, M.; Ittner, L. M.; Liu, X. Modes of A $\beta$  Toxicity in Alzheimer's Disease. *Cell. Mol. Life Sci.* **2011**, *68*, 3359–3375.
- (22) Edbauer, D.; Winkler, E.; Regula, J. T.; Pesold, B.; Steiner, H.; Haass, C. Reconstitution of Gamma-Secretase Activity. *Nat. Cell Biol.* **2003**, *5*, 486–488.
- (23) Wolfe, M. S.; Xia, W.; Ostaszewski, B. L.; Diehl, T. S.; Kimberly, W. T.; Selkoe, D. J. Two Transmembrane Aspartates in Presenilin-1 Required for Presenilin Endoproteolysis and Gamma-Secretase Activity. *Nature* **1999**, *398*, 513–517.
- (24) De Strooper, B.; Saftig, P.; Craessaerts, K.; Vanderstichele, H.; Guhde, G.; Annaert, W.; Von Figura, K.; Van Leuven, F. Deficiency of Presenilin-1 Inhibits the Normal Cleavage of Amyloid Precursor Protein. *Nature* **1998**, *391*, 387–390.
- (25) Vassar, R.; Bennett, B. D.; Babu-khan, S.; Kahn, S.; Mendiaz, E. A.; Denis, P.; Teplow, D. B.; Ross, S.; Amarante, P.; Loeloff, R.; Luo, Y.; Fisher, S.; Fuller, J.; Edenson, S.; Lile, J.; Jarosinski, M. A.; Biere, A. L.; Curran, E.; Burgess, T.; Louis, J.; Collins, F.; Treanor, J.; Rogers, G.; Citron, M. Beta-Secretase Cleavage of Alzheimer's Amyloid Precursor Protein by the Transmembrane Aspartic Protease BACE. *Science (80-. )*. **1999**, *286*, 735–741.
- (26) Götz, J.; Ittner, L. M. Animal Models of Alzheimer's Disease and Frontotemporal Dementia. *Nat. Rev. Neurosci.* **2008**, *9*, 532–544.

- (27) Etienne, M. A.; Edwin, N. J.; Aucoin, J. P.; Russo, P. S.; McCarley, R. L.; Hammer, R. P. Beta-Amyloid Protein Aggregation. *Methods Mol. Biol.* **2007**, *386*, 203–225.
- (28) Giuffrida, M. L.; Caraci, F.; de, B. P.; Pappalardo, G.; Nicoletti, F.; Rizzarelli, E.; Copani, A. The Monomer State of B-Amyloid: Where the Alzheimer's Disease Protein Meets Physiology. *Rev. Neurosci.* **2010**, *21*, 83–93.
- (29) Nilsson, M. R. Techniques to Study Amyloid Fibril Formation in Vitro. *Methods* **2004**, *34*, 233–234.
- (30) Roychaudhuri, R.; Yang, M.; Hoshi, M. M.; Teplow, D. B. Amyloid Beta-Protein Assembly and Alzheimer's Disease. *J. Biol. Chem.* **2009**, *284*, 4749–4753.
- (31) Nichols, M. R.; Moss, M. A.; Reed, D. K.; Lin, W. L.; Mukhopadhyay, R.; Hoh, J. H.; Rosenberry, T. L. Growth of B-Amyloid (1-40) Protofibrils by Monomer Elongation and Lateral Association. Characterization of Distinct Products by Light Scattering and Atomic Force Microscopy. *Biochemistry* **2002**, *41*, 6115–6127.
- (32) Ahmed, M.; Davis, J.; Aucoin, D.; Sato, T.; Ahuja, S.; Aimoto, S.; Elliott, J. I.; Van Nostrand, W. E.; Smith, S. O. Structural Conversion of Neurotoxic Amyloid- $\beta$ 1-42 Oligomers to Fibrils. *Nat. Struct. Mol. Biol.* **2010**, *17*, 561–567.
- (33) Wu, J. W.; Breydo, L.; Isas, J. M.; Lee, J.; Kuznetsov, Y. G.; Langen, R.; Glabe, C. Fibrillar Oligomers Nucleate the Oligomerization of Monomeric Amyloid  $\beta$  but Do Not Seed Fibril Formation. *J. Biol. Chem.* **2010**, *285*, 6071–6079.
- (34) Walsh, D. M.; Klyubin, I.; Fadeeva, J. V.; Rowan, M. J.; Selkoe, D. J. Amyloid-  $\beta$  Oligomers: Their Production, Toxicity and Therapeutic Inhibition. *Biochem. Soc. Trans.* **2002**, *30*, 552–557.
- (35) Sabate, R.; Estelrich, J. Evidence of the Existence of Micelles in the Fibrillogenesis of  $\beta$  - Amyloid Peptide. *J. Phys. Chem.* **2005**, *109*, 11027–11032.
- (36) Catalano, S. M.; Dodson, E. C.; Henze, D. A.; Joyce, J. G.; Krafft, G. A.; Kinney, G. The Role of Amyloid-  $\beta$  Derived Diffusible Ligands (ADDLs) in Alzheimer's Disease. *Curr. Top. Med. Chem.* **2006**, *6*, 597–608.
- (37) Lambert, M. P.; Barlow, A. K.; Chromy, B. A.; Edwards, C.; Freed, R.; Liosatos, M.; Morgan, T. E.; Rozovsky, I.; Trommer, B.; Viola, K. L.; Wals, P.; Zhang, C.; Finch, C. E.; Krafft, G. A.; Klein, W. L. Diffusible, Nonfibrillar Ligands Derived from A $\beta$ 1-42 Are Potent Central Nervous System Neurotoxins. *Proc. Natl. Acad. Sci. United States Am.* **1998**, *95*, 6448–6453.
- (38) Westlind-Danielsson, A.; Amerup, G. Spontaneous in Vitro Formation of Supramolecular  $\beta$ -Amyloid Structures, “ $\beta$ amy Balls,” by  $\beta$ -Amyloid 1-40 Peptide. *Biochemistry* **2001**, *40*, 14736–14747.

- (39) Matsumura, S.; Shinoda, K.; Yamada, M.; Yokojima, S.; Inoue, M.; Ohnishi, T.; Shimada, T.; Kikuchi, K.; Masui, D.; Hashimoto, S. Two Distinct Amyloid  $\beta$ -Protein ( $A\beta$ ) Assembly Pathways Leading to Oligomers and Fibrils Identified by Combined Fluorescence Correlation Spectroscopy, Morphology, and Toxicity Analyses. *J. Biol. Chem.* **2011**, *286*, 11555–11562.
- (40) Hartley, D. M.; Walsh, D. M.; Ye, C. P.; Diehl, T.; Vasquez, S.; Vassilev, P. M.; Teplow, D. B.; Selkoe, D. J. Protofibrillar Intermediates of Amyloid Beta-Protein Induce Acute Electrophysiological Changes and Progressive Neurotoxicity in Cortical Neurons. *J. Neurosci.* **1999**, *19*, 8876–8884.
- (41) Ward, R.; Jennings, K.; Howlett, D. Fractionation and Characterization of Oligomeric, Protofibrillar and Fibrillar Forms of  $\beta$  -Amyloid Peptide. *Biochemistry* **2000**, *348*, 137–144.
- (42) Ahmad, A.; Millett, I. Partially Folded Intermediates in Insulin Fibrillation. *Biochemistry* **2003**, *42*, 11404–11416.
- (43) Yu, C.; Chin, C. In Situ Probing of Insulin Aggregation in Chromatography Effluents with Spectroturbidimetry. *J. Colloid Interface Sci.* **2006**, *299*, 733–739.
- (44) Wu, W.; Liu, Q.; Sun, X.; Yu, J.; Zhao, D.; Yu, Y.; Luo, J.; Hu, J.; Yu, Z.; Zhao, Y.; Li, Y. Fibrillar Seeds Alleviate Amyloid- $\beta$  Cytotoxicity by Omitting Formation of Higher-Molecular-Weight Oligomers. *Biochem. Biophys. Res. Commun.* **2013**, *439*, 321–326.
- (45) Caughey, B.; Lansbury, P. T. Protofibrils, Pores, Fibrils, and Neurodegeneration: Separating the Responsible Protein Aggregates from the Innocent Bystanders. *Annu. Rev. Neurosci.* **2003**, *26*, 267–298.
- (46) Glabe, C. G. Common Mechanisms of Amyloid Oligomer Pathogenesis in Degenerative Disease. *Neurobiol. Aging* **2006**, *27*, 570–575.
- (47) Gonzalez-Velasquez, F. J.; Kotarek, J. A.; Moss, M. A. Soluble Aggregates of the Amyloid-Beta Protein Selectively Stimulate Permeability in Human Brain Microvascular Endothelial Monolayers. *J. Neurochem.* **2008**, *107*, 466–477.
- (48) Lesné, S.; Koh, M. T.; Kotilinek, L.; Kaye, R.; Glabe, C. G.; Yang, A.; Gallagher, M.; Ashe, K. H. A Specific Amyloid-Beta Protein Assembly in the Brain Impairs Memory. *Nature* **2006**, *440*, 352–357.
- (49) Westerman, M. A.; Cooper-Blacketer, D.; Mariash, A.; Kotilinek, L.; Kawarabayashi, T.; Younkin, L. H.; Carlson, G. A.; Younkin, S. G.; Ashe, K. H. The Relationship between  $A\beta$  and Memory in the Tg2576 Mouse Model of Alzheimer's Disease. *J. Neurosci.* **2002**, *22*, 1858–1867.

- (50) Busciglio, J. A.; Lorenzo, A.; Yankner, A. B. Methodological Variables in the Assessment of Beta Amyloid Neurotoxicity. *Neurobiol. Aging* **1992**, *13*, 609–612.
- (51) Shen, C. L.; Murphy, R. M. Solvent Effects on Self-Assembly of  $\beta$ -Amyloid Peptide. *Biophys. J.* **1995**, *69*, 640–651.
- (52) Teplow, D. B. Preparation of Amyloid Beta-Protein for Structural and Functional Studies. *Methods Enzymol.* **2006**, *413*, 20–33.
- (53) Turner, J. P.; Lutz-Rechtin, T.; Moore, K. A.; Rogers, L.; Bhave, O.; Moss, M. A.; Servoss, S. L. Rationally Designed Peptoids Modulate Aggregation of Amyloid-Beta 40. *ACS Chem. Neurosci.* **2014**, *5*, 552–558.
- (54) Luo, J.; Otero, J. M.; Yu, C. H.; Wärmländer, S. K. T. S.; Gräslund, A.; Overhand, M.; Abrahams, J. P. Inhibiting and Reversing Amyloid- $\beta$  Peptide (1-40) Fibril Formation with Gramicidin S and Engineered Analogues. *Chemistry.* **2013**, *19*, 17338–17348.
- (55) Kroth, H.; Ansaloni, A.; Varisco, Y.; Jan, A.; Sreenivasachary, N.; Rezaei-Ghaleh, N.; Giriens, V.; Lohmann, S.; López-Deber, M. P.; Adolfsson, O.; Pihlgren, M.; Paganetti, P.; Froestl, W.; Nagel-Steger, L.; Willbold, D.; Schrader, T.; Zweckstetter, M.; Pfeifer, A.; Lashuel, Hilal, A.; Muhs, A. Discovery and Structure Activity Relationship of Small Molecule Inhibitors of Toxic  $\beta$ -Amyloid-42 Fibril Formation. *J. Biol. Chem.* **2012**, *287*, 34786–34800.
- (56) Ban, T.; Hamada, D.; Hasegawall, K.; Naiki, H.; Goto, Y. Direct Observation of Amyloid Fibril Growth Monitored by Thioflavin T Fluorescence. *J. Biol. Chem.* **2003**, *278*, 16462–16465.
- (57) Hudson, S. A.; Ecroyd, H.; Kee, T. W.; Carver, J. A. The Thioflavin T Fluorescence Assay for Amyloid Fibril Detection Can Be Biased by the Presence of Exogenous Compounds. *FEBS J.* **2009**, *276*, 5960–5972.
- (58) Davis, T. J.; Soto-Ortega, D. D.; Kotarek, J. A.; Gonzalez-Velasquez, F. J.; Sivakumar, K.; Wu, L.; Wang, Q.; Moss, M. A. Comparative Study of Inhibition at Multiple Stages of Amyloid-Beta Self-Assembly Provides Mechanistic Insight. *Mol. Pharmacol.* **2009**, *76*, 405–413.
- (59) Moss, M. A.; Nichols, M. R.; Reed, D. K. I. M.; Hoh, J. A. N. H.; Rosenberry, T. L. The Peptide KLVFF-K6 Promotes  $\beta$ -Amyloid (1–40) Protofibril Growth by Association but Does Not Alter Protofibril Effects on Cellular Reduction of 3-(4,5-Dimethylthiazol-2-yl)-2,5-Diphenyltetrazolium Bromide (MTT). *Mol. Pharmacol.* **2003**, *64*, 1160–1168.
- (60) Moss, M. A.; Varvel, N. H.; Nichols, M. R.; Reed, D. K.; Rosenberry, T. L. Nordihydroguaiaretic Acid Does Not Disaggregate Beta-Amyloid (1-40) Protofibrils but Does Inhibit Growth Arising from Direct Protofibril Association. *Mol. Pharmacol.* **2004**, *66*, 592–600.



- (61) Rosenman, D. J.; Connors, C. R.; Chen, W.; Wang, C.; García, A. E. A $\beta$  Monomers Transiently Sample Oligomer and Fibril-like Configurations: Ensemble Characterization Using a Combined MD/NMR Approach. *J. Mol. Biol.* **2013**, *425*, 3338–3359.
- (62) Pike, C. J.; Overman, M. J.; Cotman, C. W. Amino-Terminal Deletions Enhance Aggregation of Beta-Amyloid Peptides in Vitro. *J. Biol. Chem.* **1995**, *270*, 23895–23898.
- (63) Kaye, R.; Head, E.; Sarsoza, F.; Saing, T.; Cotman, C. W.; Necula, M.; Margol, L.; Wu, J.; Breydo, L.; Thompson, J. L.; Rasool, S.; Gurlo, T.; Butler, P.; Glabe, C. G. Fibril Specific, Conformation Dependent Antibodies Recognize a Generic Epitope Common to Amyloid Fibrils and Fibrillar Oligomers That Is Absent in Prefibrillar Oligomers. *Mol. Neurodegener.* **2007**, *2*, 18.
- (64) Cardoso, I.; Pereira, P. J. B.; Damas, A. M.; Saraiva, M. J. M. Aprotinin Binding to Amyloid Fibrils. *Eur. J. Biochem.* **2000**, *267*, 2307–2311.
- (65) Necula, M.; Kaye, R.; Milton, S.; Glabe, C. G. Small Molecule Inhibitors of Aggregation Indicate That Amyloid  $\beta$  Oligomerization and Fibrillization Pathways Are Independent and Distinct. *J. Biol. Chem.* **2007**, *14*, 10311–10324.
- (66) Bartolini, M.; Naldi, M.; Fiori, J.; Valle, F.; Biscarini, F.; Nicolau, D. V.; Andrisano, V. Kinetic Characterization of Amyloid-Beta 1-42 Aggregation with a Multimethodological Approach. *Anal. Biochem.* **2011**, *414*, 215–225.
- (67) Pryor, N. E.; Moss, M. a.; Hestekin, C. N. Unraveling the Early Events of Amyloid- $\beta$  Protein (A $\beta$ ) Aggregation: Techniques for the Determination of A $\beta$  Aggregate Size. *Int. J. Mol. Sci.* **2012**, *13*, 3038–3072.
- (68) Sabella, S.; Quaglia, M.; Lanni, C.; Racchi, M.; Govoni, S.; Caccialanza, G.; Calligaro, A.; Bellotti, V.; D, L. E. Capillary Electrophoresis Studies on the Aggregation Process of  $\beta$ -Amyloid 1-42 and 1-40 Peptides. *Electrophoresis* **2004**, *25*, 3186–3194.
- (69) Syme, C. D.; Nadal, R. C.; Rigby, S. E. J.; Viles, J. H. Copper Binding to the Amyloid-Beta (A $\beta$ ) Peptide Associated with Alzheimer's Disease: Folding, Coordination Geometry, pH Dependence, Stoichiometry, and Affinity of A $\beta$ (1-28): Insights from a Range of Complementary Spectroscopic Techniques. *J. Biol. Chem.* **2004**, *279*, 18169–18177.
- (70) Austen, B. M.; Paleologou, K. E.; Ali, S. A. E.; Qureshi, M. M.; Allsop, D.; El-Agnaf, O. M. A. Designing Peptide Inhibitors for Oligomerization and Toxicity of Alzheimer's. *Biochemistry* **2008**, *47*, 1984–1992.
- (71) Wu, C.; Murray, M. M.; Bernstein, S. L.; Condrón, M. M.; Bitan, G.; Shea, J.-E.; Bowers, M. T. The Structure of A $\beta$ 42 C-Terminal Fragments Probed by a Combined Experimental and Theoretical Study. *J. Mol. Biol.* **2009**, *387*, 492–501.

- (72) Breitner, J. C. S. The Role of Anti-Inflammatory Drugs in the Prevention and Treatment of Alzheimer's. *Annu. Rev. Med.* **1996**, *47*, 401–411.
- (73) Aisen, P. S. The Potential of Anti-Inflammatory Drugs for the Treatment of Alzheimer's Disease. *Lancet Neurol.* **2002**, *1*, 279–284.
- (74) Liu, B.; Hong, J.-S. Role of Microglia in Inflammation-Mediated Neurodegenerative Diseases: Mechanisms and Strategies for Therapeutic Intervention. *J. Pharmacol. Exp. Ther.* **2003**, *304*, 1–7.
- (75) Refolo, L. M.; Pappolla, M. A.; LaFrancois, J.; Malester, B.; Schmidt, S. D.; Thomas-Bryant, T.; Tint, G. S.; Wang, R.; Mercken, M.; Petanceska, S. S.; Duff, K. E. A Cholesterol-Lowering Drug Reduces Beta-Amyloid Pathology in a Transgenic Mouse Model of Alzheimer's Disease. *Neurobiol. Dis.* **2001**, *8*, 890–899.
- (76) Puglielli, L.; Konopka, G.; Pack-Chung, E.; Ingano, L. A.; Berezovska, O.; Hyman, B. T.; Chang, T. Y.; Tanzi, R. E.; Kovacs, D. M. Acyl-Coenzyme A: Cholesterol Acyltransferase Modulates the Generation of the Amyloid Beta-Peptide. *Nat. Cell Biol.* **2001**, *3*, 905–912.
- (77) Rajasekhar, K.; Suresh, S. N.; Manjithaya, R.; Govindaraju, T. Rationally Designed Peptidomimetic Modulators of A $\beta$  Toxicity in Alzheimer's Disease. *Sci. Rep.* **2015**, *5*, 8139.
- (78) Pallitto, M. M.; Ghanta, J.; Heinzelman, P.; Kiessling, L. L.; Murphy, R. M. Recognition Sequence Design for Peptidyl Modulators of Beta-Amyloid Aggregation and Toxicity. *Biochemistry* **1999**, *38*, 3570–3578.
- (79) Bohrmann, B.; Adrian, M.; Dubochet, J.; Kuner, P.; Müller, F.; Huber, W.; Nordstedt, C.; Döbeli, H. Self-Assembly of Beta-Amyloid 42 Is Retarded by Small Molecular Ligands at the Stage of Structural Intermediates. *J. Struct. Biol.* **2000**, *130*, 232–246.
- (80) Reza, A.; Ladiwala, A.; Dordick, J. S.; Tessier, P. M. Aromatic Small Molecules Remodel Toxic Soluble Oligomers of Amyloid  $\beta$  through Three Independent Pathways. *J. Biol. Chem.* **2011**, *286*, 3209–3218.
- (81) Gazit, E. A Possible Role for  $\pi$ -Stacking in the Self-Assembly of Amyloid Fibrils. *FASEB J.* **2002**, *16*, 77–83.
- (82) Lee, S.; Fernandez, E. J.; Good, T. A. Role of Aggregation Conditions in Structure, Stability, and Toxicity of Intermediates in the A $\beta$  Fibril Formation Pathway. *Protein Sci.* **2007**, *16*, 723–732.
- (83) Latham, P. W. Therapeutic Peptides Revisited. *Nat. Biotechnol.* **1999**, *17*, 755–757.

- (84) Hilbich, C.; Kisters-Woike, B.; Reed, J.; Masters, C. L.; Beyreuther, K. Substitutions of Hydrophobic Amino Acids Reduce the Amyloidogenicity of Alzheimer's Disease  $\beta$ A4 Peptides. *J. Mol. Biol.* **1992**, *228*, 460–473.
- (85) Esler, W. P.; Stimson, E. R.; Ghilardi, J. R.; Lu, Y. A.; Felix, A. M.; Vinters, H. V.; Mantyh, P. W.; Lee, J. P.; Maggio, J. E. Point Substitution in the Central Hydrophobic Cluster of a Human Beta-Amyloid Congener Disrupts Peptide Folding and Abolishes Plaque Competence. *Biochemistry* **1996**, *35*, 13914–13921.
- (86) Tjernberg, L. O.; Näslund, J.; Lindqvist, F.; Johansson, J.; Karlström, A. R.; Thyberg, J.; Terenius, L.; Nordstedt, C. Arrest of Beta-Amyloid Fibril Formation by a Pentapeptide Ligand. *J. Biol. Chem.* **1996**, *271*, 8545–8548.
- (87) Tjernberg, L. O.; Lilliehöök, C.; Callaway, D. J.; Näslund, J.; Hahne, S.; Thyberg, J.; Terenius, L.; Nordstedt, C. Controlling Amyloid Beta-Peptide Fibril Formation with Protease-Stable Ligands. *J. Biol. Chem.* **1997**, *272*, 12601–12605.
- (88) Lowe, T. L.; Strzelec, A.; Kiessling, L. L.; Murphy, R. M. Structure-Function Relationships for Inhibitors of Beta-Amyloid Toxicity Containing the Recognition Sequence KLVFF. *Biochemistry* **2001**, *40*, 7882–7889.
- (89) Watanabe, K.; Nakamura, K.; Akikusa, S.; Okada, T.; Kodaka, M.; Konakahara, T.; Okuno, H. Inhibitors of Fibril Formation and Cytotoxicity of Beta-Amyloid Peptide Composed of KLVFF Recognition Element and Flexible Hydrophilic Disrupting Element. *Biochem. Biophys. Res. Commun.* **2002**, *290*, 121–124.
- (90) Hamley, I. W.; Castelletto, V.; Moulton, C. M.; Rodríguez-Pérez, J.; Squires, A. M.; Eralp, T.; Held, G.; Hicks, M. R.; Rodger, A. Alignment of a Model Amyloid Peptide Fragment in Bulk and at a Solid Surface. *J. Phys. Chem. Biol.* **2010**, *114*, 8244–8254.
- (91) Arai, T.; Sasaki, D.; Araya, T.; Sato, T.; Sohma, Y. A Cyclic KLVFF-Derived Peptide Aggregation Inhibitor Induces the Formation of Less-Toxic Off-Pathway Amyloid-B Oligomers. *ChemBioChem* **2014**, *15*, 2577–2583.
- (92) Soto, C.; Sigurdsson, E. M.; Morelli, L.; Kumar, R. A.; Castaño, E. M.; Frangione, B. Beta-Sheet Breaker Peptides Inhibit Fibrillogenesis in a Rat Brain Model of Amyloidosis: Implications for Alzheimer's Therapy. *Nat. Med.* **1998**, *4*, 822–826.
- (93) Sigurdsson, E. M.; Permanne, B.; Soto, C.; Wisniewski, T.; Frangione, B. In Vivo Reversal of Amyloid-Beta Lesions in Rat Brain. *J. Neuropathol. Exp. Neurol.* **2000**, *59*, 11–17.
- (94) Poduslo, J.; Curran, G.; Kumar, A.; Frangione, B.; Soto, C. Beta-Sheet Breaker Peptide Inhibitor of Alzheimer's Amyloidogenesis with Increased Blood-Brain Barrier Permeability and Resistance to Proteolytic Degradation in Plasma. *J. Neurobiol.* **1999**, *39*, 371–382.

- (95) Ghanta, J.; Shen, C. L.; Kiessling, L. L.; Murphy, R. M. A Strategy for Designing Inhibitors of Beta-Amyloid Toxicity. *J. Biol. Chem.* **1996**, *271*, 29525–29528.
- (96) Chafekar, S. M.; Malda, H.; Merckx, M.; Meijer, E. W.; Viertl, D.; Lashuel, H. A.; Baas, F.; Scheper, W. Branched KLVFF Tetramers Strongly Potentiate Inhibition of  $\beta$ -Amyloid Aggregation. *ChemBioChem* **2007**, *8*, 1857–1864.
- (97) Miller, S. M.; Simon, R. J.; Ng, S.; Zuckermann, R. N.; Kerr, J. M.; Moos, W. H. Comparison of the Proteolytic Susceptibilities of Homologous L-Amino Acid, D-Amino Acid, and N-Substituted Glycine Peptide and Peptoid Oligomers. *Drug Dev. Res.* **1995**, *35*, 20–32.
- (98) Wong, H. E.; Qi, W.; Choi, H. M.; Fernandez, E. J.; Kwon, I. A Safe, Blood-Brain Barrier Permeable Triphenylmethane Dye Inhibits Amyloid-B Neurotoxicity by Generating Nontoxic Aggregates. *ACS Chem. Neurosci.* **2011**, *2*, 645–657.
- (99) Ross, T. M.; Zuckermann, R. N.; Reinhard, C.; Frey, W. H. Intranasal Administration Delivers Peptoids to the Rat Central Nervous System. *Neurosci. Lett.* **2008**, *439*, 30–33.
- (100) Sato, A. K.; Viswanathan, M.; Kent, R. B.; Wood, C. R. Therapeutic Peptides: Technological Advances Driving Peptides into Development. *Curr. Opin. Biotechnol.* **2006**, *17*, 638–642.
- (101) Vagner, J.; Qu, H.; Hruby, V. J. Peptidomimetics, a Synthetic Tool of Drug Discovery. *Curr. Opin. Chem. Biol.* **2008**, *12*, 292–296.
- (102) Seebach, D.; Matthews, J. L. Peptides: A Surprise at Every Turn. *Chem. Commun.* **1997**, *1*, 2015–2022.
- (103) Appella, D. H.; Christianson, L. A.; Karle, I. L.; Powell, D. R.; Gellman, S. H. B-Peptide Foldamers: Robust Helix Formation in a New Family of  $\beta$ -Amino Acid Oligomers. *J. Am. Chem. Soc.* **1996**, *7863*, 13071–13072.
- (104) Smith, A.B., III, Keenan, T.P., Holcomb, R.C., Sprengeler, P.A., Guzman, M.C., Wood, J.L., Carrol, P.J., & Hirschmann, R. Design, Synthesis, and Crystal-Structure of a Pyrrolinone-Based Peptidomimetic Possessing the Conformation of a Beta-Strand - Potential Application to the Design of Novel Inhibitors of Proteolytic-Enzymes. *J. Am. Chem. Soc.* **1992**, *114*, 10672–10674.
- (105) Simon, R. J.; Kania, R. S.; Zuckermann, R. N.; Huebner, V. D.; Jewell, D. A.; Banville, S.; Ng, S.; Wang, L.; Rosenberg, S.; Marlowe, C. K. Peptoids: A Modular Approach to Drug Discovery. *Proc. Natl. Acad. Sci. U. S. A.* **1992**, *89*, 9367–9371.
- (106) Kirshenbaum, K.; Barron, A. E.; Goldsmith, R. A.; Armand, P.; Bradley, E. K.; Truong, K. T. V; Dill, K. A.; Cohen, F. E.; Zuckermann, R. N. Sequence-Specific Polypeptoids: A

- Diverse Family of Heteropolymers with Stable Secondary Structure. *Proc. Natl. Acad. Sci. U. S. A.* **1998**, *95*, 4303–4308.
- (107) Miller, S. M.; Simon, R. J.; NG, S.; Zuckermann, R. N.; Kerr, J. M.; Moos, W. H. Proteolytic Studies of Homologous Peptide and N-Substituted Glycine Peptoid Oligomers. *Bioorganic Med. Chem. Lett.* **1994**, *4*, 2657–2662.
- (108) Chongsiriwatana, N. P.; Patch, J. A.; Czyzewski, A. M.; Dohm, M. T.; Ivankin, A.; Gidalevitz, D.; Zuckermann, R. N.; Barron, A. E. Peptoids That Mimic the Structure, Function, and Mechanism of Helical Antimicrobial Peptides. *Proc. Natl. Acad. Sci. U. S. A.* **2008**, *105*, 2794–2799.
- (109) Gibbons, J. A.; Hancock, A. A.; Vitt, C. R.; Knepper, S.; Buckner, S. A.; Brune, M. E.; Milicic, I.; Kerwin, J. F.; Richter, L. S.; Taylor, E. W.; Spear, K. L.; Zuckermann, R. N.; Spellmeyer, D. C.; Braeckman, R. A.; Moos, W. H. Pharmacologic Characterization of CHIR2279, an N-Substituted Glycine Peptoid with High-Affinity Binding for  $\alpha(1)$ -Adrenoceptors. *J. Pharmacol. Exp. Ther.* **1996**, *277*, 885–899.
- (110) Zuckermann, R.N., Kerr, J.M., Kent, B.H., Moos, W. H. Efficient Method for the Preparation of Peptoids [Oligo(N-Substituted Glycines)] by Submonomer Solid-Phase Synthesis. *Journal Am. Chem. Soc.* **1992**, *114*, 10646–10647.
- (111) Kirshenbaum, K.; Zuckermann, R. N.; Dill, K. A. Designing Polymers That Mimic Biomolecules. *Curr. Opin. Struct. Biol.* **1999**, *9*, 530–535.
- (112) Barron, A. E.; Zuckermann, R. N. Bioinspired Polymeric Materials: In-between Proteins and Plastics. *Curr. Opin. Chem. Biol.* **1999**, *3*, 681–687.
- (113) Armand, P.; Kirshenbaum, K.; Falicov, A.; Dunbrack, R. L.; Dill, K. A.; Zuckermann, R. N.; Cohen, F. E. Chiral N-Substituted Glycines Can Form Stable Helical Conformations. *Fold. Des.* **1997**, *2*, 369–375.
- (114) Armand, P.; Kirshenbaum, K.; Goldsmith, R. A.; Farr-Jones, S.; Barron, A. E.; Truong, K. T. V.; Dill, K. A.; Mierke, D. F.; Cohen, F. E.; Zuckermann, R. N.; Bradley, E. K. NMR Determination of the Major Solution Conformation of a Peptoid Pentamer with Chiral Side Chains. *Proc. Natl. Acad. Sci. U. S. A.* **1998**, *95*, 4309–4314.
- (115) Wu, C. W.; Sanborn, T. J.; Zuckermann, R. N.; Barron, A. E. Peptoid Oligomers with Alpha-Chiral, Aromatic Side Chains: Effects of Chain Length on Secondary Structure. *J. Am. Chem. Soc.* **2001**, *123*, 2958–2963.
- (116) Wu, C. W.; Sanborn, T. J.; Huang, K.; Zuckermann, R. N.; Barron, A. E. Peptoid Oligomers with Alpha-Chiral, Aromatic Side Chains: Sequence Requirements for the Formation of Stable Peptoid Helices. *J. Am. Chem. Soc.* **2001**, *123*, 6778–6784.

- (117) Mohle, K.; Hofmann, H. Secondary Structure Formation in N-Substituted Peptides. *J. Pept. Res.* **1998**, *1*, 19–28.
- (118) Patch, J. A.; Kirshenbaum, K.; Seuryneck, S. L.; Zuckermann, R. N.; Barron, A. E. Versatile Oligo(N-Substituted) Glycines : The Many Roles of Peptoids in Drug Discovery. *Pseudo-Peptides in Drug Development*; 2005.
- (119) Hebert, M. L.; Shah, D. S.; Blake, P.; Turner, J. P.; Servoss, S. L. Tunable Peptoid Microspheres: Effects of Side Chain Chemistry and Sequence. *Org. Biomol. Chem.* **2013**, *11*, 4459–4464.
- (120) Hebert, M.; Shah, D.; Blake, P.; Servoss, S. L. Uniform and Robust Peptoid Microsphere Coatings. *Coatings* **2013**, *3*, 98–107.
- (121) Stringer, J. R.; Crapster, J. A.; Guzei, I. a.; Blackwell, H. E. Extraordinarily Robust Polyproline Type I Peptoid Helices Generated via the Incorporation of A-Chiral Aromatic N-1-Naphthylethyl Side Chains. *J. Am. Chem. Soc.* **2011**, *133*, 15559–15567.
- (122) Sanborn, T. J.; Wu, C. W.; Zuckermann, R. N.; Barron, A. E. Extreme Stability of Helices Formed by Water-Soluble Poly-N-Substituted Glycines (polypeptoids) with Alpha-Chiral Side Chains. *Biopolymers* **2002**, *63*, 12–20.
- (123) Dong, D. Y.; Wetzler, M. Faster and Greener: One Minute Reactions for Synthesis of Peptoid Oligomers and Polymers. *Annual ACS Meeting*; 2014.
- (124) Tran, H., Gael, S.L., Connolly, M.D., & Zuckermann, R. N. Solid-Phase Submonomer Synthesis of Peptoid Polymers and Their Self-Assembly into Highly-Ordered Nanosheets. *J. Vis. Exp.* **2011**, *8*, 2–7.
- (125) Seo, J.; Barron, A. E.; Zuckermann, R. N. Novel Peptoid Building Blocks: Synthesis of Functionalized Aromatic Helix-Inducing Submonomers. *Org. Lett.* **2010**, *12*, 492–495.
- (126) Wu, C. W.; Kirshenbaum, K.; Sanborn, T. J.; Patch, J. A.; Huang, K.; Dill, K. A.; Zuckermann, R. N.; Barron, A. E. Structural and Spectroscopic Studies of Peptoid Oligomers with Alpha-Chiral Aliphatic Side Chains. *J. Am. Chem. Soc.* **2003**, *125*, 13525–13530.
- (127) Seuryneck-Servoss, S. L.; Dohm, M. T.; Barron, A. E. Effects of Including an N-Terminal Insertion Region and Arginine-Mimetic Side Chains in Helical Peptoid Analogues of Lung Surfactant Protein B. *Biochemistry* **2006**, *45*, 11809–11818.
- (128) Dohm, M. T.; Seuryneck-Servoss, S. L.; Seo, J.; Zuckermann, R. N.; Barron, A. E. Close Mimicry of Lung Surfactant Protein B by “Clicked” Dimers of Helical, Cationic Peptoids. *Biopolymers* **2009**, *92*, 538–553.

- (129) Wu, C. W.; Seurnyck, S. L.; Lee, K. Y. C.; Barron, A. E. Helical Peptoid Mimics of Lung Surfactant Protein C. *ACS Chem. Biol.* **2003**, *10*, 1057–1063.
- (130) Seurnyck, S. L.; Patch, J. A.; Barron, A. E. Simple, Helical Peptoid Analogs of Lung Surfactant Protein B. *Chem. Biol.* **2005**, *12*, 77–88.
- (131) Brown, N. J.; Wu, C. W.; Seurnyck-Servoss, S. L.; Barron, A. E. Effects of Hydrophobic Helix Length and Side Chain Chemistry on Biomimicry in Peptoid Analogues of SP-C. *Biochemistry* **2008**, *47*, 1808–1818.
- (132) Brown, N. J.; Johansson, J.; Barron, A. E. Biomimicry of Surfactant Protein C. *Acc. Chem. Res.* **2008**, *41*, 1409–1417.
- (133) Huang, C.; Uno, T.; Murphy, J. E.; Lee, S.; Hamer, J. D.; Escobedo, J. A.; Cohen, F. E.; Radhakrishnan, R.; Dwarki, V.; Zuckermann, R. N. Lipitoids-Novel Cationic Lipids for Cellular Delivery of Plasmid DNA in Vitro. *Chem. Biol.* **1998**, *5*, 345–354.
- (134) Gondi, C.; Lakka, S.; Yanamandra, N.; Siddique, K.; Dinh, D.; Olivero, W.; Gujrati, M.; Rao, J. Expression of Antisense uPAR and Antisense uPA from Bicistronic Adenoviral Construct Inhibits Glioma Cell Invasion, Tumor Growth, and Angiogenesis. *Oncogene* **2003**, *22*, 5967–5975.
- (135) Mishima, K.; Mazar, A.; Gown, A.; Skelly, M.; Ji, X.; Wang, X.; Jones, T.; Cavenee, W.; Huang, H. A Peptide Derived from the Non-Receptor-Binding Region of Urokinase Plasminogen Activator Inhibits Glioblastoma Growth and Angiogenesis in Vivo in Combination with Cisplatin. *Proc. Natl. Acad. Sci. U. S. A.* **2000**, *97*, 8484–8489.
- (136) Gao, C. M.; Yam, A. Y.; Wang, X.; Magdangal, E.; Salisbury, C.; Peretz, D.; Zuckermann, R. N.; Connolly, M. D.; Hansson, O.; Minthon, L.; Zetterberg, H.; Blennow, K.; Fedynyshyn, J. P.; Allauzen, S. A $\beta$ 40 Oligomers Identified as a Potential Biomarker for the Diagnosis of Alzheimer's Disease. *PLoS One* **2010**, *5*, e15725.
- (137) Yam, A. Y.; Wang, X.; Gao, C. M.; Connolly, M. D.; Zuckermann, R. N.; Bleu, T.; Hall, J.; Fedynyshyn, J. P.; Allauzen, S.; Peretz, D.; Salisbury, C. M.; Bleua, T.; Halla, J.; Fedynyshyn, J. P.; Allauzen, S.; Peretz, D.; Salisbury, C. M. A Universal Method for Detection of Amyloidogenic Misfolded Proteins. *Biochemistry* **2011**, *50*, 4322–4329.
- (138) Greenwaldiek, J.; Riek, R. Biology of Amyloid: Structure, Function, and Regulation. *Structure* **2010**, *18*, 1244–1260.
- (139) Chen, X.; Wu, J.; Luo, Y.; Liang, X.; Supnet, C.; Kim, M. W.; Lotz, P.; Yang, G.; Muchowski, P. J.; Kodadek, T.; Bezprozvanny, I. Expanded Polyglutamine-Binding Peptoid as a Novel Therapeutic Agent for Treatment of Huntington's Disease. *J. Biol. Chem.* **2012**, *18*, 1113–1125.

- (140) Luo, Y.; Vali, S.; Sun, S.; Chen, X.; Liang, X.; Drozhzhina, T.; Popugaeva, E.; Bezprozvanny, I. A $\beta$ 42-Binding Peptoids as Amyloid Aggregation Inhibitors and Detection Ligands. *ACS Chem. Neurosci.* **2013**, *6*, 952–962.
- (141) Aileen Funke, S.; Willbold, D. Peptides for Therapy and Diagnosis of Alzheimer's Disease. *Curr. Pharm. Des.* **2012**, *18*, 755–767.
- (142) Adessi, C.; Frossard, M. J.; Boissard, C.; Fraga, S.; Bieler, S.; Ruckle, T.; Vilbois, F.; Robinson, S. M.; Mutter, M.; Banks, W. A.; Soto, C. Pharmacological Profiles of Peptide Drug Candidates for the Treatment of Alzheimer's Disease. *J. Biol. Chem.* **2003**, *278*, 13905–13911.
- (143) Zuckermann, R. N.; Kodadek, T. Peptoids as Potential Therapeutics. *Curr. Opin. Mol. Ther.* **2009**, *11*, 299–307.
- (144) Utku, Y.; Rohatgi, A.; Yoo, B.; Kirshenbaum, K. Rapid Multistep Synthesis of a Bioactive Peptidomimetic Oligomer for the Undergraduate Laboratory. *J. Chem. Educ.* **2010**, *87*, 637–639.
- (145) Cho, S.; Choi, J.; Kim, A.; Lee, Y.; Kwon, Y. U. Efficient Solid-Phase Synthesis of a Series of Cyclic and Linear Peptoid-Dexamethasone Conjugates for the Cell Permeability Studies. *J. Comb. Chem.* **2010**, *12*, 321–326.
- (146) Irwin, J. A.; Wong, H. E.; Kwon, I. Different Fates of Alzheimer's Disease Amyloid- $\beta$  Fibrils Remodeled by Biocompatible Small Molecules. *Biomacromolecules* **2013**, *14*, 264–274.
- (147) Findeis, M. A.; Musso, G. M.; Arico-Muendel, C. C.; Benjamin, H. W.; Hundal, A. M.; Lee, J. J.; Chin, J.; Kelley, M.; Wakefield, J.; Hayward, N. J.; Molineaux, S. M. Modified-Peptide Inhibitors of Amyloid Beta-Peptide Polymerization. *Biochemistry* **1999**, *38*, 6791–6800.
- (148) Churches, Q. I.; Caine, J.; Cavanagh, K.; Epa, V. C.; Waddington, L.; Tranberg, C. E.; Meyer, A. G.; Varghese, J. N.; Streltsov, V.; Duggan, P. J. Naturally Occurring Polyphenolic Inhibitors of Amyloid Beta Aggregation. *Bioorganic Med. Chem. Lett.* **2014**, *24*, 3108–3112.
- (149) Goldsbury, C.; Frey, P.; Olivieri, V.; Aebi, U.; Müller, S. A. Multiple Assembly Pathways Underlie Amyloid-B Fibril Polymorphisms. *J. Mol. Biol.* **2005**, *352*, 282–298.
- (150) Laursen, J. S.; Engel-Andreasen, J.; Fristrup, P.; Harris, P.; Olsen, C. A. Cis-Trans Amide Bond Rotamers in  $\beta$ -Peptoids and Peptoids: Evaluation of Stereoelectronic Effects in Backbone and Side Chains. *J. Am. Chem. Soc.* **2013**, *135*, 2835–2844.
- (151) Bellesia, G.; Shea, J. E. Diversity of Kinetic Pathways in Amyloid Fibril Formation. *J. Chem. Phys.* **2009**, *131*, 111102.

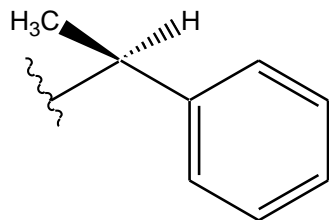


- (152) Lorenzo, A.; Yankner, B. Beta-Amyloid Neurotoxicity Requires Fibril Formation and Is Inhibited by Congo Red. *Proc. Natl. Acad. Sci. U. S. A.* **1994**, *91*, 12243–12247.
- (153) Kisilevsky, R.; Lemieux, L.; Fraser, P.; Kong, X.; Hultin, P.; Szarek, W. Arresting Amyloidosis in-Vivo Using Small-Molecule Anionic Sulfonates or Sulfates - Implications for Alzheimer's Disease. *Nat. Med.* **1995**, *1*, 143–148.
- (154) Bose, P.; Chatterjee, U.; Xie, L.; Johansson, J.; Gothelid, E.; Arvidsson, P. Effects of Congo Red on A beta(1-40) Fibril Formation Process and Morphology. *ACS Chem. Neurosci.* **2010**, *1*, 315–324.
- (155) Podlisny, M.; Walsh, D.; Amarante, P.; Ostaszewski, B.; Stimson, E. Oligomerization of Endogenous and Synthetic Amyloid Beta-Protein at Nanomolar Levels in Cell Culture and Stabilization of Monomer by Congo Red. *Biochemistry* **1998**, *37*, 3602-3611.
- (156) Wood, S.; MacKenzie, L.; Maleeff, B.; Hurle, M.; Wetzel, R. Selective Inhibition of A Beta Fibril Formation. *J. Biol. Chem.* **1996**, *271*, 4086–4092.
- (157) Bett, C. K.; Serem, W. K.; Fontenot, K. R.; Hammer, R. P.; Garno, J. C. Effects of Peptides Derived from Terminal Modifications of the A Beta Central Hydrophobic Core on A Beta Fibrillization. *ACS Chem. Neurosci.* **2010**, *1*, 661–678.
- (158) Permanne, B.; Adessi, C.; Saborio, G.; Fraga, S.; Frossard, M.; Van Dorpe, J.; Dewachter, I.; Banks, W.; Van Leuven, F.; Soto, C. Reduction of Amyloid Load and Cerebral Damage in a Transgenic Mousemodel of Alzheimer's Disease by Treatment with a  $\beta$ -Sheet Breaker Peptide. *FASEB J.* **2002**, *16*, 860–862.
- (159) Karran, E.; Mercken, M.; Strooper, B. De. The Amyloid Cascade Hypothesis for Alzheimer's Disease: An Appraisal for the Development of Therapeutics. *Nat. Rev. Drug Discov.* **2011**, *10*, 698–712.
- (160) Xu, W. File: APP cleavage produce toxic Abeta.png  
[http://commons.wikimedia.org/wiki/File:APP\\_cleavage\\_produce\\_toxic\\_Abeta.png](http://commons.wikimedia.org/wiki/File:APP_cleavage_produce_toxic_Abeta.png)  
(accessed Apr 3, 2015).
- (161) Moore, K. A. Gold Nanoparticles and Peptoids as Novel Inhibitors of Amyloid Beta Aggregation in Alzheimer's Disease, University of South Carolina, 2013, pp. 1–103.

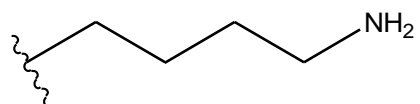
## Chapter 2 Appendices

### Appendix A: Submonomer structures

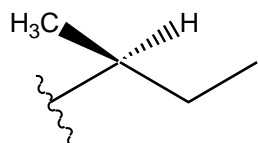
*Nspe*: (S)-*N*-(1-phenylethyl)glycine



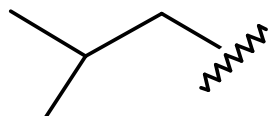
*NLys*:



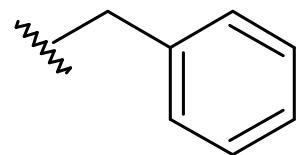
*Nssb*: (S)-*N*-(2-butyl)glycine



*Nleu*: 2-methylbutane



*Nphe*: ethylbenzene



## Appendix B: Effects of Reduced Peptoid Length on A $\beta$ 40 Aggregation

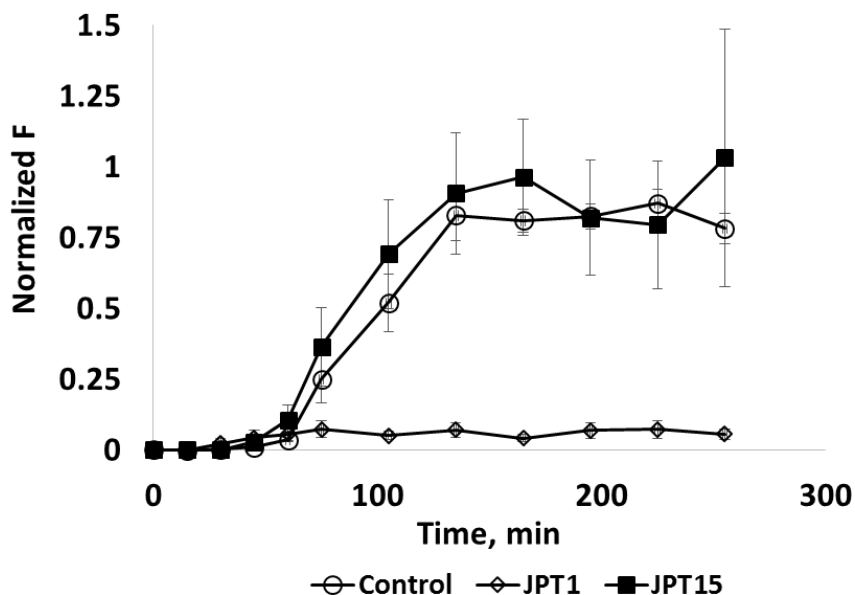
Peptoid JPT1 was initially designed to mimic the peptide KLVFF with the inclusion of an aliphatic I-like side chain to help induce a helical secondary structure. To allow for better interaction with the cross  $\beta$ -sheet structure of A $\beta$ , an additional turn of the helix (IFF in corresponding amino acids) was added to the peptoid. The capabilities of JPT1 to modulate A $\beta$ 40 and A $\beta$ 42 aggregation have been outlined in Chapters 3, 4, and 5. However, JPT1 has a molecular mass of 1130.5 Da and may have difficulty bypassing the BBB without the use of techniques such as intranasal administration. To circumvent this problem, we designed a reduced length variant of JPT1 (Table B.1). This peptoid was designed to only have five side chain monomers attached to the backbone. The side chains selected were solely based on the hydrophobic core (KLVFF; residues 16-20 of A $\beta$ ). Similar to JPT1, JPT1<sub>5</sub> utilized aliphatic I-like groups to help induce a helical secondary structure.

**Table B.1** Peptoids corresponding 1 letter amino acid code and molecular weight.

JPT15	KIIFF	694.9 Da
JPT1	KIIFFIFF	1130.5 Da

Peptoid helical length has been linked to biological activity.<sup>108</sup> We had hypothesized the reduced helical length of JPT1<sub>5</sub> would result in a decrease in activity in regards to modulating A $\beta$ 40 aggregation. To test this hypothesis, we utilized a standard ThT aggregation assay with A $\beta$ 40 that was monomerized by organic dissolution with HFIP (Chapter 2 for reference). A $\beta$ 40 monomer was agitated at 800 RPM in 40 mM Tris-HCl buffer (pH 8.0) in the presence of 150 mM NaCl. Aggregation assays were performed in the absence (control) and presence of peptoids on an orbital shaker at 25 °C. Aliquots were taken periodically to measure the presences of  $\beta$ -sheet containing aggregates with ThT fluorescence. The results of the assay are presented in

Figure B.1. When A $\beta$ 40 monomer was incubated in the presence of JPT1, the formation of  $\beta$ -sheets was reduced by  $83.07 \pm 4.84$  %. In the presence of JPT1<sub>5</sub>, the overall change in  $\beta$ -sheet containing aggregates is  $-15.31 \pm 22.39$  %. This indicates JPT1<sub>5</sub> does not have an effect on A $\beta$ 40 aggregation.



	JPT1	JPT1 <sub>5</sub>
<b>% Inhibition</b>	<b>83.07 ± 4.84</b>	<b>-15.31 ± 22.39</b>

**Figure B.1** ThT analysis shows that peptoid JPT1 modulates A $\beta$ 40 aggregation. JPT1<sub>5</sub> did not reduce the formation of  $\beta$ -sheet aggregates. Peptoids were added to 20  $\mu$ M A $\beta$ 40 monomer at concentrations of 100  $\mu$ M and  $\beta$ -sheet aggregates were detected via ThT fluorescence. Normalized fluorescence values are calculated as the percentage of the control plateau. Parameters are expressed as mean  $\pm$  SEM, n = 7.

When compared to JPT1, JPT1<sub>5</sub> did not reduce the formation of  $\beta$ -sheet aggregates and resulted in no change in the reduction of  $\beta$ -sheet containing aggregates. However, these results are surprising considering a JPT1<sub>5</sub> still contains the KIIF sequence. Peptoid helical length has been shown to play a correlation with biological activity in antimicrobial peptoids.<sup>108</sup> The reduction of the IFF side chain groups most likely reduced the ability of JPT1<sub>5</sub> to specifically

bind to A $\beta$ 40. Another possible explanation for the promoted growth of  $\beta$ -sheets is the reduced number of aromatics within the peptoid sequence. It has been hypothesized that the aromatics in small molecule inhibitors and A $\beta$  interact to yield pi-pi stacking that is believed to help stabilize A $\beta$  oligomers, thus reducing toxicity.<sup>80</sup>

The results in this study indicate peptoid helical length is important; however, previous work with the peptide iA $\beta$ 5 (5mer peptide) indicates inhibitor length may not be the important factor.<sup>86</sup> Pi-pi stacking has been implicated in stabilizing A $\beta$  oligomers.<sup>80</sup> Further studies should focus on utilizing short chain peptoid oligomers that include a varying number of aromatic side chains to better understand if pi-pi stacking with A $\beta$  is more important.

## Appendix C: Investigation of Unique Pathways Associated with Peptoid-Based KLVFF Mimics

Previous work with small molecules containing aromatics have demonstrated that there are classes of molecules that act on varying A $\beta$  aggregation pathways.<sup>55,65,80</sup> Many of these compounds have been shown to block specific pathways such as A $\beta$  oligomerization or fibrillation.<sup>65,80</sup> Other compounds have shown the ability to dissociate A $\beta$  fibrils or stabilizing oligomers so that they do not become toxic in cellular studies.<sup>80</sup> These small molecules are believed to act on A $\beta$  aggregation due to pi-pi stacking between the aromatics in the small molecules and the aromatics in A $\beta$ .

Early work with peptoid-based KLVFF mimics have demonstrated the potential of these molecules as a therapeutic option for AD. We have demonstrated the capability of peptoid JPT1 to modulate A $\beta$ 40 aggregation previously.<sup>53</sup> While we were the first group to report the benefits of utilizing a peptoid-based KLVFF mimic, we were not the first group to utilize peptoids as a potential modulator or inhibitor of A $\beta$  aggregation. IAM1 was the first peptoid that had been investigated as a potential inhibitor of A $\beta$ 40 and A $\beta$ 42 aggregation.<sup>140</sup> However, IAM1 and its dimer, (IAM1)<sub>2</sub>, were not as effective at inhibiting A $\beta$ 40 aggregation as JPT1. This is most likely due to the placement of the aromatics within IAM1 and (IAM1)<sub>2</sub>.

In Chapter 4, we demonstrated via immunoblotting techniques that the placement of the F-like groups did result in a change in the amount of fibrillar aggregates present. This indicates pi-pi stacking between peptoids and A $\beta$  can impact the mechanistic aggregation pathway. To investigate this phenomenon, we utilized peptoid JPT1 and three small molecule inhibitors of A $\beta$ . These small molecule inhibitors have each been demonstrated to act on various mechanistic pathways of A $\beta$  aggregation.<sup>65</sup> Table C.1 represents the small molecules selected for this

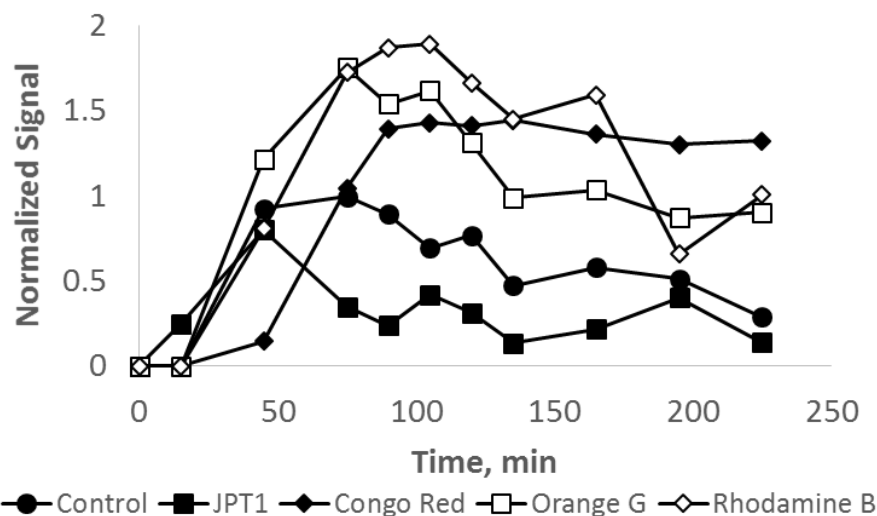
experiment. Class I compounds are known for inhibiting oligomerization, but not fibrillation. Class II compounds inhibit both oligomerization and fibrillation, whereas Class III compounds inhibit fibrillation, but not oligomerization.

**Table C.1** Small compounds and their respective class of compound.

	<b>Class of Compound</b>
<b>Congo Red</b>	Class I
<b>Rhodamine B</b>	Class II
<b>Orange G</b>	Class III
<b>JPT1</b>	?

Aggregation assays were used to compare JPT1 to Congo Red (Class I), Rhodamine B (Class II), and Orange G (Class III). Assays were performed by agitating 20  $\mu\text{M}$  A $\beta$ 40 monomer at 800 RPM on an orbital shaker at 25  $^{\circ}\text{C}$  in 40 mM Tris-HCl (pH 8.0) with 150 mM NaCl. ThT aggregation assays were not used due to potential competitive binding between ThT and small molecules. Dot blot analysis was performed by using primary antibody OC to detect the formation of fibrillar aggregates (Figure C.1).

The addition of 100  $\mu\text{M}$  JPT1 resulted in a  $57.6 \pm 4.6\%$  reduction of fibrillar aggregates. Surprisingly, the addition of 100  $\mu\text{M}$  Congo Red, Rhodamine B, and Orange G resulted in  $-92.4 \pm 23.8\%$ ,  $-77.9 \pm 50.0\%$ , and  $-117.2 \pm 84.5\%$  reduction of fibrillar aggregates. These small molecules have previously been linked to potential therapeutic agents for AD due to reduction of A $\beta$  aggregates.<sup>65</sup> However, while spotting A $\beta$ 40 samples on the nitrocellulose membrane for dot blot analysis, it was noted that the small molecules did appear to leave a dyed residue on the membrane (data not shown). It was hypothesized that this could adversely affect the analysis mean densitometry analysis with imageJ software during quantification.



	JPT1	Congo Red	Orange G	Rhodamine B
<b>% Inhibition</b>	57.6±4.6%	-92.4±23.8%	-77.9±50.0%	-117.2±84.5%

**Figure C.1** Dot blot analysis of known small molecules that work on unique A $\beta$  aggregation pathways. Peptoid JPT1 and small molecules were added to 20  $\mu$ M A $\beta$ 40 monomer at concentrations of 100  $\mu$ M and fibrillar aggregates were detected via primary antibody OC. Normalized values are calculated as a percentage of the control plateau. Parameters are expressed as mean  $\pm$  SEM, n = 2. Data above is a graphical representation of all experiments.

To better compare JPT1 to the small molecules listed in Table C.1, TEM was utilized to observe the growth of larger aggregates. Aggregation assays were conducted with 20  $\mu$ M A $\beta$ 40 monomer in the presence or absence (control) of 100  $\mu$ M small molecules or JPT1 in 40 mM Tris-HCl (pH 8.0). Assays were initiated by adding 150 mM NaCl and agitating at 800 RPM on an orbital shaker at 25  $^{\circ}$ C. Assays were monitored via ThT fluorescence (control) until the plateau was observed at which point samples were gridded onto 300 square mesh formvar-carbon supported nickel grids. Following sample incubation on grids, a 2% solution of uranyl acetate was placed on the grid for 45 seconds and then gently wicked away with a piece of filter paper. Results are presented in Figure C.2.



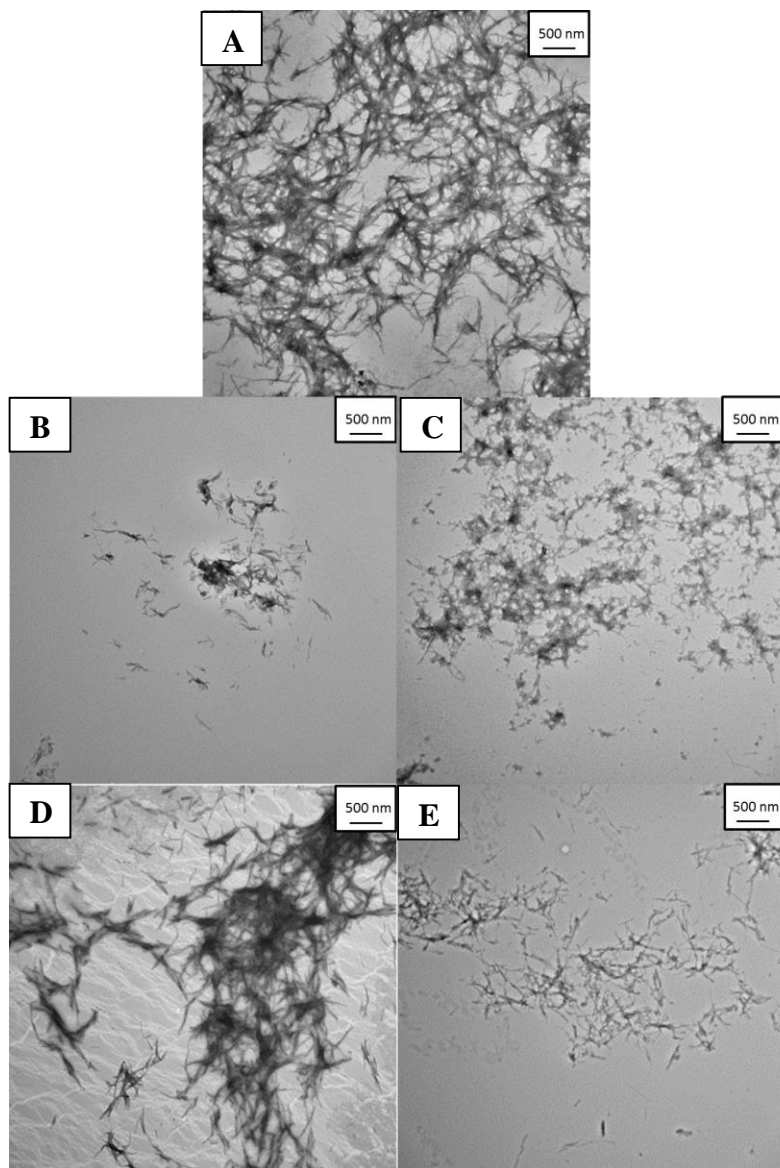


**Figure C.2** Morphology studies of A $\beta$ 40 aggregates formed in the presence (control; A) and absence of B) JPT1, C) Congo Red, D) Orange G, and E) Rhodamine B. 20  $\mu$ M A $\beta$ 40 monomer was aggregated in the presence and absence of 100  $\mu$ M small molecules at 800 RPM in 40 mM Tris-HCl (pH 8.0) in the presence of 150 mM NaCl.

In the absence of peptoid or small molecules, A $\beta$ 40 aggregates to form a branched fibrillar network (Figure C.2 A). In the presence of JPT1, A $\beta$ 40 has a significant reduction of fibrillar aggregates is observed compared to the control (Figure C.2 B). The addition of Congo Red to A $\beta$ 40 results in a reduction of aggregates and changes the morphology to where they no longer

appear fibrillar (Figure C.2 C). This is interesting considering Congo Red is a Class I compound, meaning that it is capable of inhibiting oligomerization, but not fibrillation. This change in fibrillar aggregate morphology is most likely due to unique aggregation pathway that Class I compounds inflict on A $\beta$ 40 aggregation.

In the presence of Orange G, A $\beta$ 40 still adopts fibrillar like aggregates, but in a reduced quantity compared to the control (Figure C.2 D). Similar to Congo Red, these results were surprising considering Orange G is a Class III compound and inhibits fibrillation but not oligomerization. The addition of Rhodamine B had the most profound effect on A $\beta$ 40 aggregation among the small molecule inhibitors (Figure C.2 E). In the presence of Rhodamine B, A $\beta$ 40 aggregates have a reduced quantity of aggregates compared to the control and exhibit reduced branching. Class II compounds are known for inhibiting both oligomerization and fibrillation. Surprisingly, the presence of small molecule inhibitors reduces the number of fibrillar aggregates in comparison to dot blot data. As mentioned before, during the immunoblotting process, it was noted that the small molecules left a color residue on the nitrocellulose membrane. TEM results prove immunoblotting results were skewed.

Based on the work presented here, JPT1 appears to be acting on a different pathway than the small molecules represented here. Further investigation is warranted here. Significant issues with ThT and immunoblotting assays did not allow for a full determination of these small molecules capabilities. TEM results demonstrate that JPT1 had a far superior effect on A $\beta$ 40 aggregation than the small molecules presented here. However, to determine if JPT1 is acting on a unique aggregation pathway, synergistic effects need to be observed. By utilizing the IC<sub>50</sub> of the small molecules presented here and observing A $\beta$ 40 aggregation when mixing small molecules with JPT1, a defined aggregation pathway may be observed.